THE OHIO STATE UNIVERSITY

Final Report on Adaptive Antenna Arrays for Satellite Communication

Inder J. Gupta

The Ohio State University
ElectroScience Laboratory

Department of Electrical Engineering
Columbus, Ohio 43212

Technical Report 716111-9
Grant No. NAG3-536
September 1989

National Aeronautics and Space Administration
Lewis Research Center
21000 Brookpark Road
Cleveland, Ohio 44135

NOTICES

When Government drawings, specifications, or other data are used for any purpose other than in connection with a definitely related Government procurement operation, the United States Government thereby incurs no responsibility nor any obligation whatsoever, and the fact that the Government may have formulated, furnished, or in any way supplied the said drawings, specifications, or other data, is not to be regarded by implication or otherwise as in any manner licensing the holder or any other person or corporation, or conveying any rights or permission to manufacture, use, or sell any patented invention that may in any way be related thereto.

50272-101

REPORT DOCUMENTATION PAGE	1. REPORT NO.	2.	3. Recipient's Accession No.

4. Title and Subtitle
Final Report on Adaptive Antenna Arrays for Satellite Communication

5. Report Date
September 1989

6.

7. Author(s)
Inder J. Gupta

8. Performing Org. Rept. No.
716111-9

9. Performing Organization Name and Address
The Ohio State University
ElectroScience Laboratory
1320 Kinnear Road
Columbus, OH 43212

10. Project/Task/Work Unit No.

11. Contract(C) or Grant(G) No.
(C)
(G) NAG3-536

12. Sponsoring Organization Name and Address
National Aeronautics and Space Administration
Lewis Research Center, 21000 Brookpark Road
Cleveland, Ohio 44135

13. Report Type/Period Covered
Technical Report

14.

15. Supplementary Notes

16. Abstract (Limit: 200 words)

This is the final report on the project entitled "Adaptive Antenna Arrays for Satellite Communication". This project was supported by a grant from NASA Lewis Research Center, Cleveland, Ohio to The Ohio State University. Under this project, the feasibility of using adaptive antenna arrays to provide interference protection in satellite communications was studied. The study included the feedback loops as well as the SMI algorithm for weight control. Appropriate modifications in the two were made to achieve the required interference suppression. An experimental system was built to test the modified feedback loops and the modified SMI algorithm. The performance of the experimental system was evaluated using bench generated signals and signals received from TVRO geosynchronous satellites. This report summarizes the research effort. Some suggestions for the future work are also presented.

17. Document Analysis a. Descriptors

b. Identifiers/Open-Ended Terms

c. COSATI Field/Group

18. Availability Statement	19. Security Class (This Report)	21. No. of Pages
A. Approved for public release; Distribution is unlimited.	Unclassified	137
	20. Security Class (This Page) Unclassified	22. Price

(See ANSI-Z39.18) *See Instructions on Reverse* OPTIONAL FORM 272 (4-77) Department of Commerce

Acknowledgement

The experimental results included in this report were generated by Ron Dilsavor, Karl Steadman and Jim Ward, three graduate students in the Electrical Engineering Department. Jim Ward built the experimental system with the signal simulator and the array simulator. Karl Steadman built the ground station to receive signals from geosynchronous satellites and Ron Dilsavor implemented the SMI algorithm on the experimental system. Other personnel involved at the various stages of this research project include Prof. A.A. Ksienski, Prof. R.L. Moses, Dr. W.G. Swarner, Dr. E.K. Walton, and Mr. Bob Evans and Mr. Don Henry. Dr. Walton was the co-principal investigator.

Contents

List of Figures

List of Tables

Chapter 1

Introduction

A major problem in satellite communications is the interference caused by transmission from adjacent satellites whose signals inadvertently enter the receiving system and interfere with the communication link. The same problem arises in the earth to satellite part of the link where transmissions from nearby ground stations enter the satellite receivers through their antenna sidelobes. The problem has recently become more serious because of the crowding of the geostationary orbit. Indeed this interference prevents the inclusion of additional satellite which could have been allowed if methods to suppress such interference were available. The interference may be suppressed at the originating station, either space or earth, by lowering the sidelobes of the transmitting antenna. Alternatively, the interference may be suppressed at the receiving site. A study of the use of adaptive antenna arrays to provide interference suppression at the receiving site was carried out under this Grant (NAG3-536) at The Ohio State University during March 1984-October 1985. The results of the study indicated that adaptive array technology can, in principle, provide the required interfer-

ence protection to satellite communication systems. However, a significant modification in the adaptive array configuration would be required to accommodate the specified signal and interference conditions prevalent in the satellite communications systems under consideration [1]–[3].

A thorough analysis of the modified adaptive arrays for the receiving site was carried out. The effect of various parameters such as noise decorrelation, gain of auxiliary antennas and errors in the steering vector, on the interference suppression provided by various adaptive arrays was studied. The possibility of using offset feeds of a reflector antenna as auxiliary antennas was also studied [4]. In situations where the main antenna is an array of small elements, it was shown that one can use subarrays of the main antenna as auxiliary elements [5]. An experimental system was designed to verify the theoretical analysis. During the period November 1985-June 1987, the experimental system was built and tested for various signal scenarios [6,7]. The experimental system can suppress two weak (5-10 dB below thermal noise level) interfering signals by 20-30 dB. In the experimental system, instead of actual antennas, an array simulator was used to generate the signals that would have been received by the various antenna elements. This permits one to evaluate the performance of the modified adaptive array for the various signal scenarios considered in the theoretical work. Next, during the period July 1987-August 1989, to study the performance of the experimental system in a more realistic signal and noise environment, the array simulator was replaced by actual antennas, RF amplifiers and down converters [8]. The testing of the experimental system with the signals received from various communication satellites in

the geosynchronous orbit has shown that one can suppress the interfering signals entering a ground station through the sidelobes of its antenna. In this report, a brief description of the above mentioned research is given and some suggestions for the future work are presented.

Under this grant (NAG3-536), the feasibility of using sample matrix inversion (SMI) adaptive arrays [9], [10] for suppression of weak interfering signals was also studied. A modification [11,12] to the conventional SMI algorithm was found so that the required interference suppression can be obtained. In the modified SMI algorithm, the sample covariance matrix [9],[10] is redefined to reduce the effect of thermal noise on the weights of the adaptive array. This is accomplished by subtracting a fraction of the smallest eigenvalue of the original covariance matrix from its diagonal terms. A thorough analysis of the modified SMI adaptive array was also carried out [13,14]. The effect of the number of samples used to estimate the covariance matrix on the performance of the modified SMI was studied. The modified SMI algorithm was implemented on the existing experimental system [15] and its performance using bench generated signals as well as signals received from geosynchronous satellites was tested. It was shown that the experimental SMI system can suppress a weak interfering signal by 20-25 dB. In this report, the research conducted on the SMI adaptive arrays is also summarized.

In the present application (satellite communication), the antenna array will consist of a main antenna and a few auxiliary antennas. The main antenna will be pointed towards the desired satellite while the auxiliary antennas will have either uniform coverage in the given field of view or

will be pointed in the general direction of interfering satellites. Thus, the auxiliary antennas may receive signals from satellites which are not visible to the main antenna. The signals from these satellites (additional interference) will affect the performance of the adaptive antennas. An analytical study of the effects of additional interfering signals was also carried out. It was shown that if the total number of interfering signals is less than the number of degrees of freedom of the adaptive array or the additional interfering signals are 10-15 dB below the interfering signals in the main antenna, the additional interfering signals will not affect the performance of the adaptive array. The results of this study are documented in technical report 716111-8 [16]. The rest of the report is organized as follows.

In Chapter II, modified feedback loops to suppress weak interfering signals are described. The selection and distribution of antenna elements to be used with modified feedback loops is also discussed there. The experimental system and its performance with bench generated signals is described in Chapter III. The ground station built to receive signals from various satellites is described in Chapter IV where the performance of the experimental adaptive array with TVRO satellite signals is discussed. Chapter V discusses modified SMI adaptive arrays. The implementation of the modified SMI algorithm on the experimental system is discussed in Chapter VI where its performance with bench generated signals as well as signals received from geosynchronous satellites are discussed. Finally, Chapter VII contains the general conclusions and some suggestion for future work.

Chapter 2

Modified Feedback Loops and Antenna Distribution

Under this grant, a study was carried out of the interference suppression provided by adaptive antenna arrays at the receiving site of a satellite communication system. It was found that the conventional feedback loops used to control the weights of adaptive arrays were unable to provide the desired interference suppression [1,2]. The reason for the lack of interference suppression is that in the satellite communication system under consideration, the interfering signals are relatively weak, occasionally even below thermal noise. Under such conditions, the thermal noise becomes the main source of degradation in the output signal-to-interference-plus-noise ratio (SINR) and thus it (thermal noise) dictates the adaptive array weights. The array adjusts its weights to minimize the thermal noise which in turn maximizes the output SINR. However, the interfering signals remain unsuppressed. To overcome this difficulty, one can either increase the interference signal level in the feedback loops by using high gain auxiliary antennas or modify the feedback loops controlling the array weights. Both approaches were

examined in detail.

When the directions of the sources radiating interfering signals are approximately known, one can use high gain auxiliary antennas and point their beams in those directions. The interfering signal level in the feedback loops will thus increase, enhancing the interference suppression. The larger the gain of the auxiliary antennas the higher the interference suppression. However, for very weak interfering signals, very high gain auxiliary antennas would be needed to achieve the desired interference suppressions. Since these antennas are highly directive, the interference arrival angle would have to be known to an accuracy which may not be met due to some uncertainty of the locations of the interfering signals sources. The limitations on the available antenna gains required a modification of the adaptive feedback loops which in combination with moderately high gain antennas can provide the required interference suppression.

In the modified feedback loops, the noise level in the feedback loops is reduced. The noise is reduced by reducing the correlation between the noise components of the two inputs to the correlator in the feedback loops (Figure 2.1). The higher the noise decorrelation, the stronger the interference suppression. However, for weak interfering signals, the noise should be almost completely decorrelated to achieve the desired interference suppression [2,3], which is impractical. A combination of the two techniques (noise decorrelation and high gain auxiliary antennas) is, therefore, recommended to provide the required interference suppression. Since directive auxiliary antennas will significantly increase the interfering signal levels in the feedback loops, the amount of noise decorrelation required to achieve

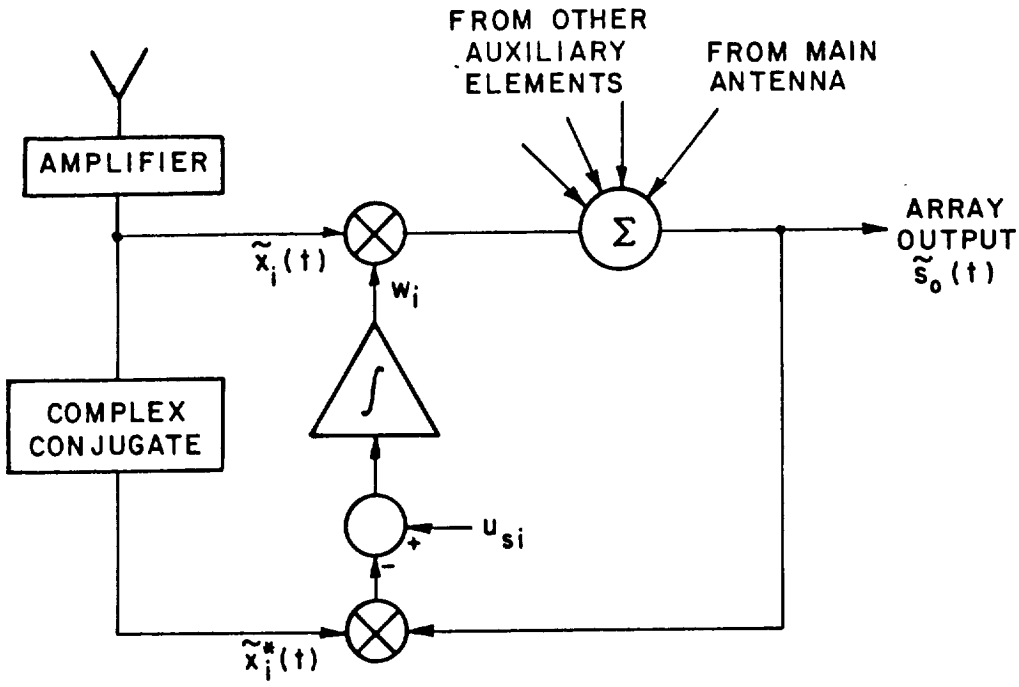

Figure 2.1: Steered beam adaptive array feedback loop.

the desired interference suppression will be within reasonable limits. A relationship between the amount of noise decorrelation required and the auxiliary antenna element gain was developed for the specified interference suppression [2,3].

The effects of noise decorrelation on the other signals (thermal noise and the desired signal) present in the communication system were also studied. It was shown that the desired signal level at the output port is maintained as long as an accurate steering vector [1] is used. The thermal noise at the output port, especially for low gain auxiliary antennas, increases with an increase in the noise decorrelation resulting in SINR degradation. A poor steering vector (error in the absolute amplitude) causes additional thermal noise as well as a degradation in the desired signal level at the array output. Thus, the output SINR degrades sharply. The SINR degradation increases with an increase in noise decorrelation. Therefore, for the optimum performance, one should use as accurate a steering vector as possible and the noise decorrelation should be kept to the minimum possible.

One way to avoid the degradation of the desired signal because of amplitude errors in the steering vector is to use a fully adaptive array. In the case of a fully adaptive array, in contrast to a sidelobe canceller [1], even the main antenna has an adaptive feedback loop. Thus, the total number of feedback loops is N + 1 (N is the number of auxiliary antennas). The performance of such fully adaptive arrays was also studied. It was shown that a fully adaptive array provides the same interference protection as a sidelobe canceller and has a better output SINR (the desired signal is not degraded).

Two techniques to decorrelate the noise in the two inputs to the feedback loop correlator were presented [1,2]. When the internal thermal noise is the main noise source, two different amplifiers (Figure 2.2) can be used in each feedback loop to decorrelate the noise. In situations where the external noise is significant, two separate antennas displaced from each other (Figure 2.3) should be used with each feedback loop. Though this scheme requires twice the number of auxiliary antennas and careful phase adjustments, it provides more noise decorrelation and applies to both external and internal noise. The two antennas should be located such that the phase of the signals incident on the two antennas is the same while the noise received by them is uncorrelated. Thus, the antenna patterns, particularly gain in the interfering signal direction and the spatial distribution of auxiliary antennas are quite important and should be carefully selected. Under this grant, the selection and distribution of antenna elements was also studied. A brief summary of our study is given below.

In the communication systems under consideration, the satellites are located in the geosynchronous orbit. Thus, the interfering signal sources are nearly coplanar with the desired signal source. Therefore, if two antennas are placed symmetrically along a line orthogonal to this plane, the signals received by the two antennas will be in phase while the separation between the two antennas will assure that the external noise in the two antennas is only partially correlated. These two antennas, however, should be directive and should be pointed in the general direction of interfering signal sources.

In the case of reflector antennas, the above requirement can be met by using defocussed feeds. By moving the feed away from the focus of a

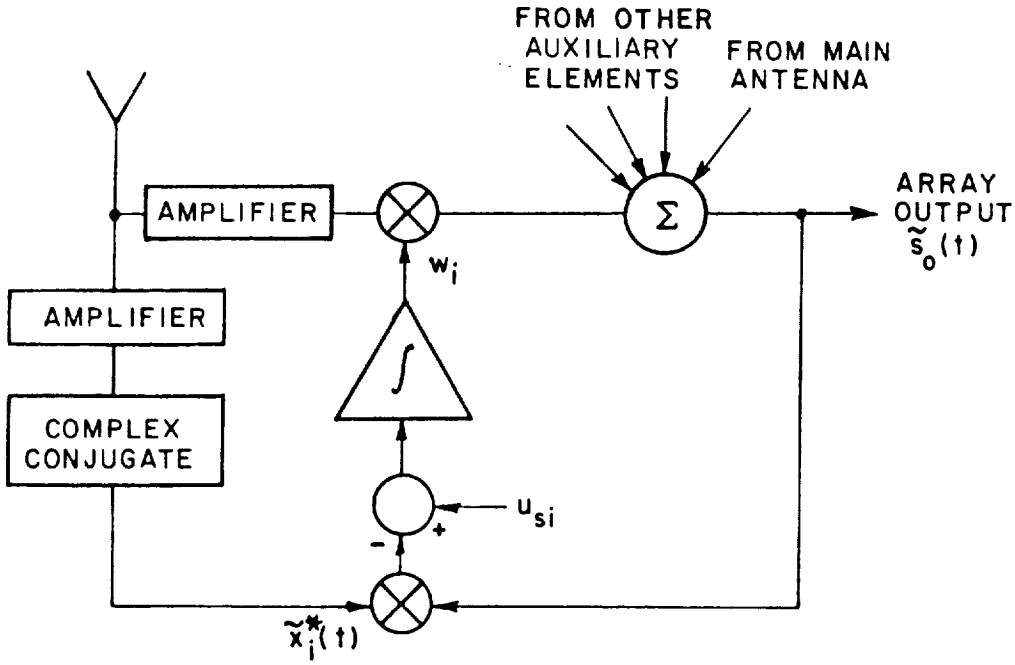

Figure 2.2: Modified feedback loop - two amplifiers.

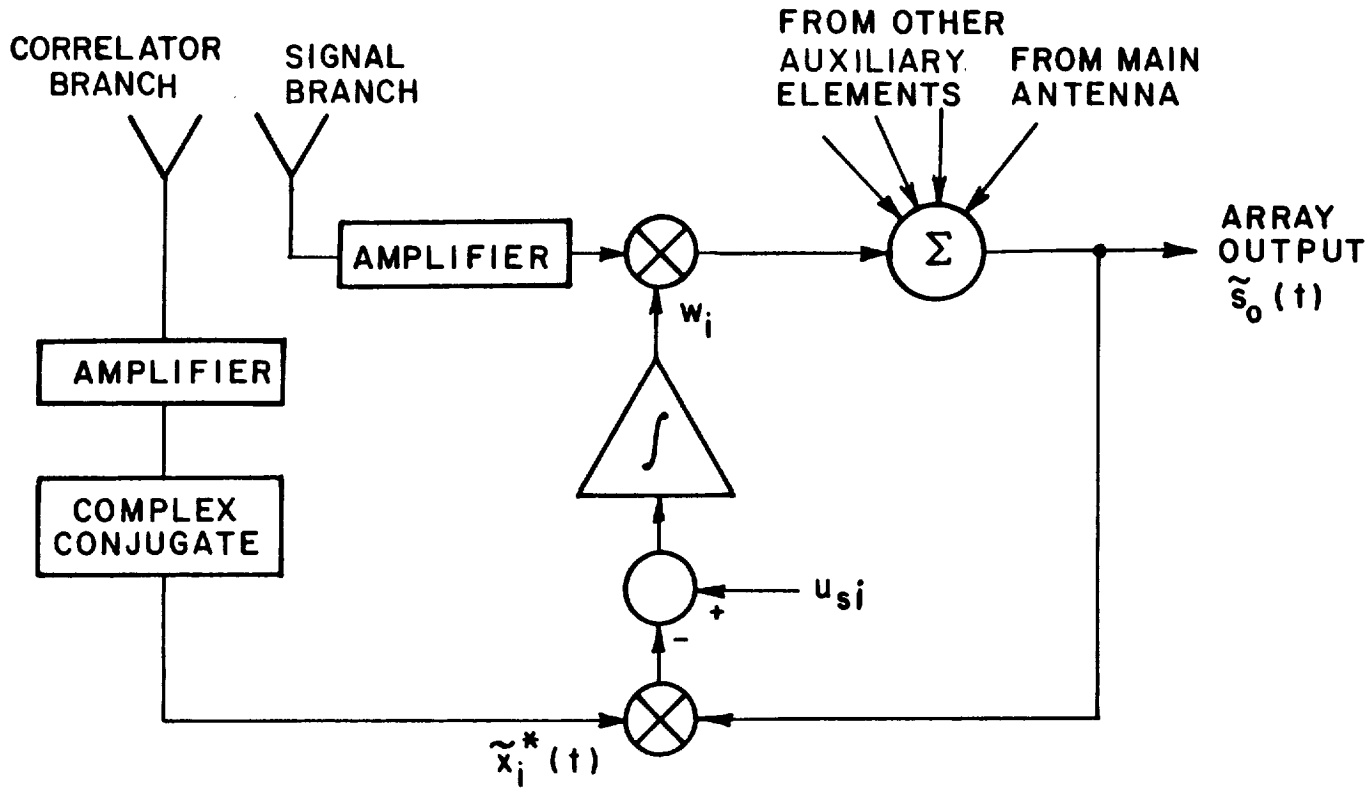

Figure 2.3: Modified feedback loop - two antennas.

reflector antenna, one can steer the beam of the antenna over a wide angular region. Thus, by proper selection of the feed location, one can steer the main beam in the general direction of interfering signals and by using an array of feeds, all signals (desired and undesired) can be received with high gain. One can also use defocussed feeds to achieve noise decorrelation [4]. Under the present grant, we have done a thorough study of the performance of adaptive arrays when defocussed feeds of a reflector antenna are used as auxiliary antennas. We have demonstrated that such auxiliary antennas can be used very effectively to suppress weak interfering signals.

The selection of the auxiliary antenna was also studied [5] when the main antenna is an array of small antennas. It was shown that subarrays of the main antenna can be used as auxiliaries. By adjusting the phases of the various elements in a subarray, its main beam can be steered in the general direction of an interfering signal. Thus, the interfering signal can be received with high gain. One can use two subarrays, displaced from each other, for each feedback loop to decorrelate the noise in the feedback loop. Since the two subarrays are displaced from each other and contain different antenna elements, noise entering them will be uncorrelated. However, to insure interference suppression, the phases of the various signals received by one of the subarrays should be equal to the phases of the corresponding signal received by the other subarray. It was shown that this condition can be met [5]. Thus, all the above mentioned requirements are met and the required interference suppression can be obtained.

Next, an experimental system was designed to demonstrate the interference suppression capabilities of an adaptive array with modified feedback

loops and to determine the performance limits which can be obtained in practical applications. The experimental system is discussed in the next chapter.

Chapter 3

The Experimental System

The experimental system [6,7] is a sidelobe canceller with two auxiliary antennas. The modified feedback loops are used to control the weights of the auxiliary channels. Two spatially separated antennas followed by their own individual amplifiers are used in the modified feedback loops. Thus, the experimental system uses five antenna elements, one for the main channel and two each for the two auxiliary channels. The main antenna is pointed in the desired signal direction, which is assumed to be known accurately. The auxiliary antennas are pointed in the general direction of the interfering signals. The auxiliary antennas are located such that the two antennas associated with a given auxiliary channel receive the directional signals nearly equal in phase, while the external noise received by the two antennas is only partially correlated.

In the first stage of the experimental system, instead of using actual antenna elements, the signals which would have been received by the five antennas were obtained using an array simulator. This enabled us to evaluate the performance of the system under a controlled environment. The

signal scenario was assumed to consist of a desired signal and as many as two interfering signals. These signals were bench generated pulse modulated sinusoidal signals.

Figure 3.1 shows a block diagram of the experimental system. The signal simulator generates the three signals assumed to be incident on the array. In the array simulator, these signals are combined with each other and with noise to form the signals that would be received by the five antenna elements. The array processor along with the system computer computes the array weights and sums the weighted auxiliary channels with the main channel to form the output signal. The system operates at 69 MHz with a bandwidth of 6 MHz. The system computer (PDP 11/23) is used to update the weights, control the various components and evaluate the system performance. A brief description of the individual system blocks is given below.

3.1 The Signal Simulator

The desired signal and the two interfering signals are bench generated in the signal simulator. In order to measure adaptive array performance characteristics such as interference suppression, output signal-to-noise ratio, and output signal-to-interference plus noise ratio, it is necessary to measure separately the desired signal power, the interference power, and the noise power present in each channel and at the array output. Pulse modulated sinusoids are used as the desired signals and the interfering signals to accomplish this objective. The modulation on one interfering signal is

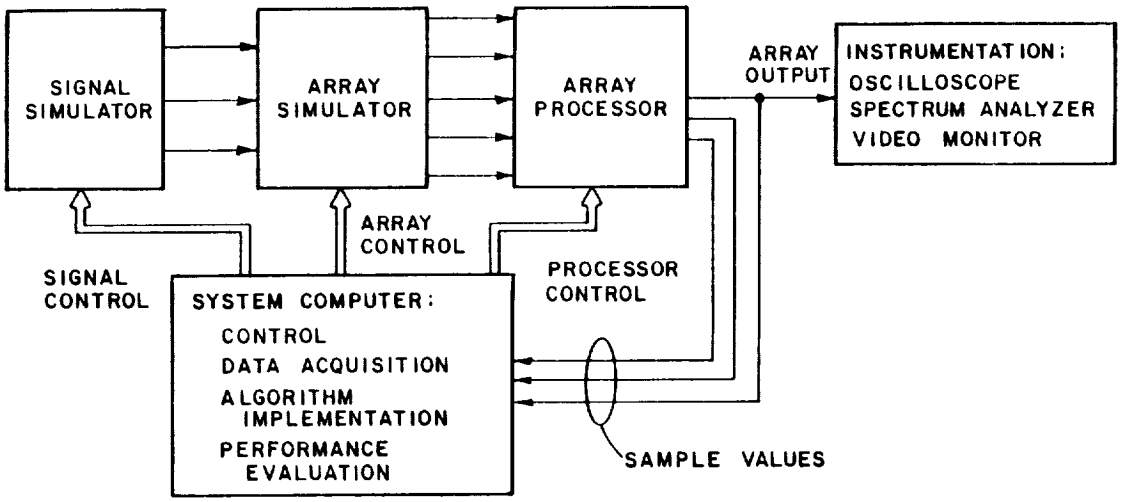

Figure 3.1: Block diagram of the experimental system

staggered from the modulation on the other interfering signal, and from the desired signal modulation, such that each signal occupies a different portion of the pulse repetition period. There is also a portion of each period when no signal (only noise) is present. The desired and interfering signals are therefore all uncorrelated with each other (for all interelement time delays of interest). Thus, a complete pulse modulated waveform contains the desired signal, the two interfering signals, and the additive noise. Figure 3.2 shows the envelope of a typical pulse modulated signal. The incident signals produced by the signal simulator are transferred to the array simulator which is described next.

3.2 The Array Simulator

Figure 3.3 shows a detailed block diagram of the array simulator. In the array simulator, the incident signals are combined and thermal noise is added to form the signals received at each array element, such that each element signal contains a component due to the desired signal, components due to both interfering signals, and additive thermal noise. Thus the array simulator has three inputs for the three incident signals, and five outputs corresponding to the five antenna elements of the array. The five elements are designated as the Main channel, Signal Branch 1 and correlator Branch 1 for auxiliary channel 1, and Signal Branch 2 and Correlator Branch 2 for auxiliary channel 2. The main channel output is the signal received at the main antenna. The other outputs are the signals received by the auxiliary antennas of the modified feedback loops of the two auxiliary channel

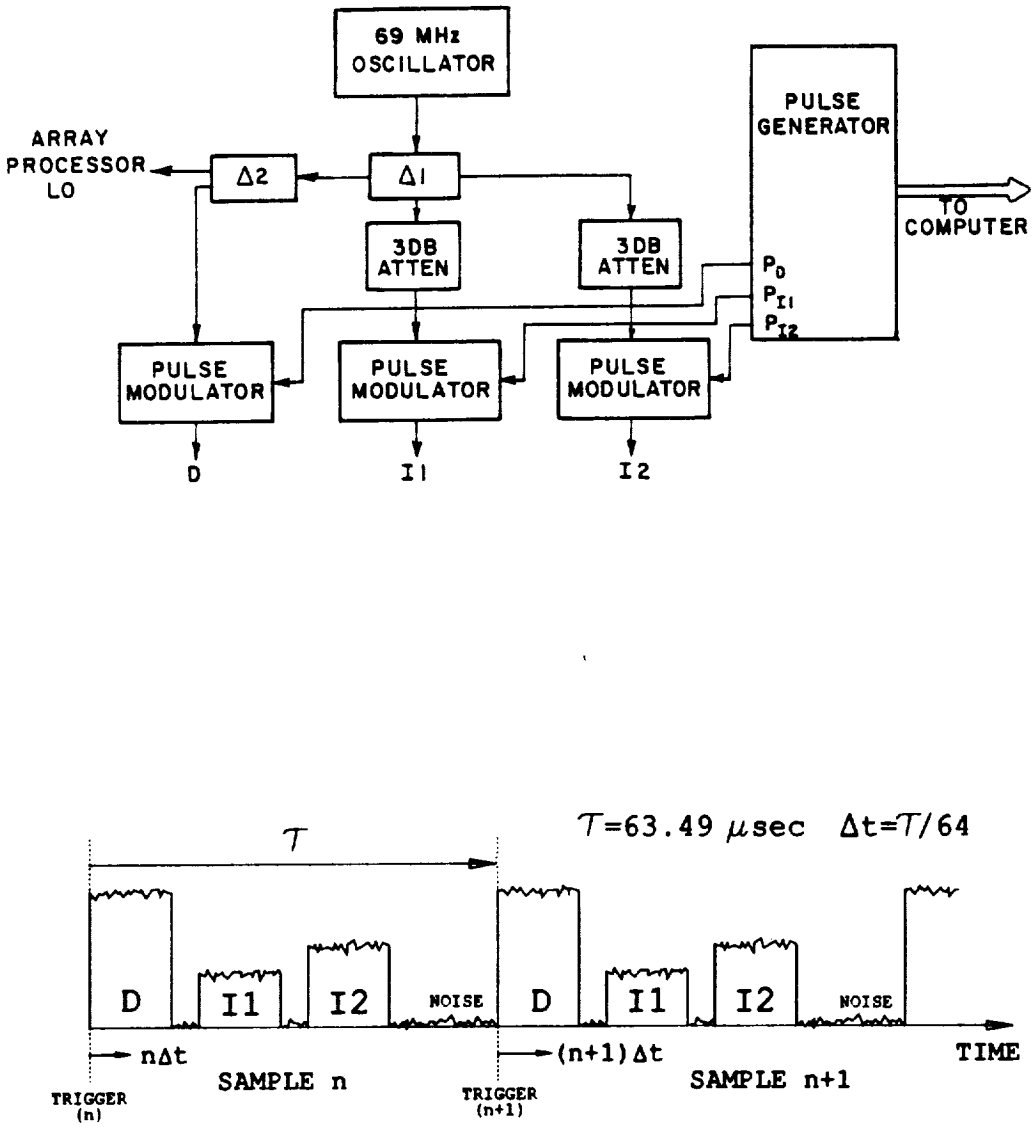

Figure 3.2: Signal simulator block diagram and staggered pulse modulation.

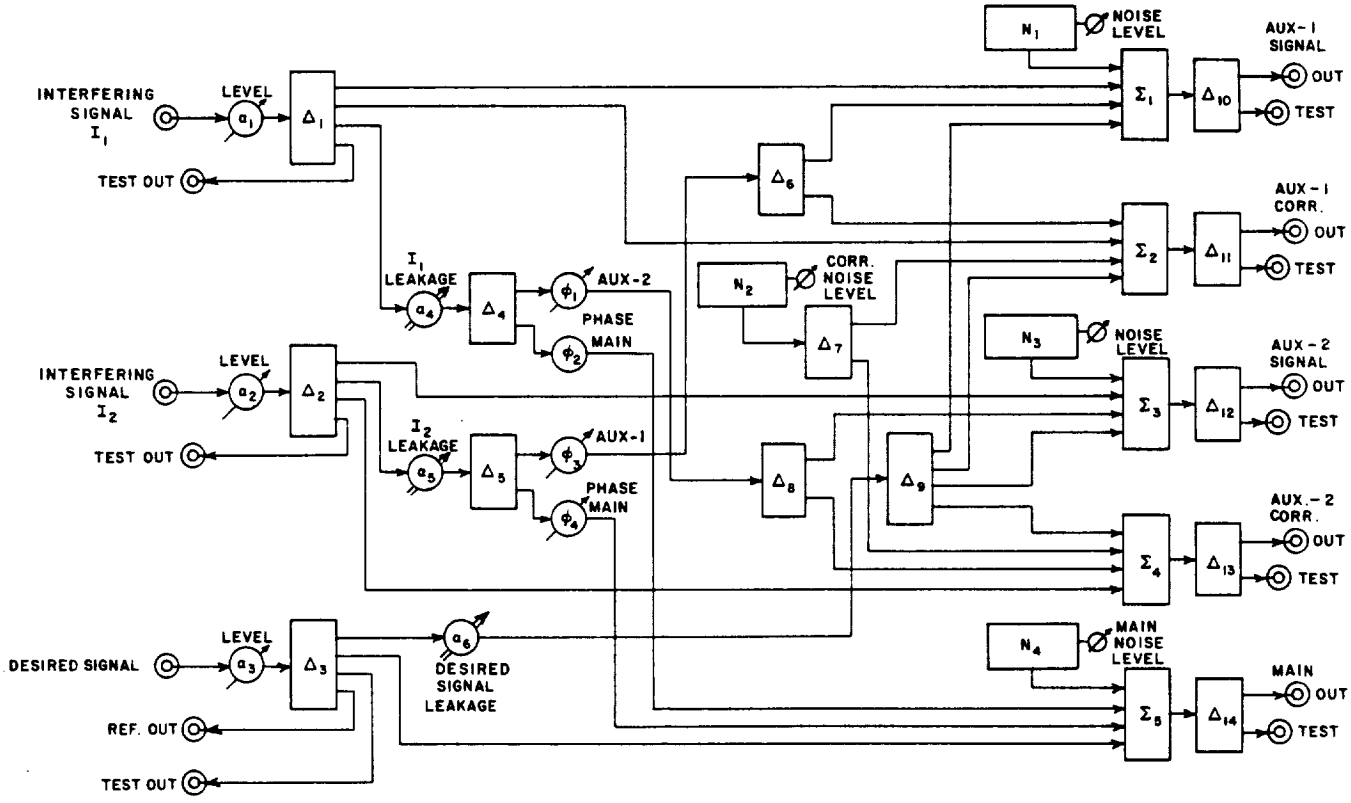

Figure 3.3: Array simulator detailed block diagram. Single arrows through a device indicate manual control, and double arrows indicate computer control.

sidelobe canceler. The blocks labeled N_1 through N_4 are the noise sources. Note that the noise components injected into the auxiliary signal branches and the main channel are all from different noise sources, and thus uncorrelated. Furthermore, the noise components in the auxiliary correlator branches originate from another noise source, and are therefore uncorrelated with the noise components of all the signal branches. In Figure 3.3, the Δ's are zero-phase power dividers. The Σ's represent summing junctions, which are zero-phase power dividers connected as summers. The α's are variable attenuators and the ϕ's denote variable phase shifters.

The phase shifters simulate variations of the interfering signal directions of arrival by varying the interelement phase shifts between interfering signal components of different array elements. There are no phase shifters associated with the desired signal because it is assumed to arrive from broadside and thus is received with the same phase at each array element. Variable attenuators are used to control the amount of each incident signal received at each output channel. This is analogous to varying the gains of the main and auxiliary antennas in the directions of incident signals. Once the desired scenario is set, the array simulator outputs are fed to the array processor, where the auxiliary channel weights are determined. The array processor is discussed next.

3.3 The Array Processor

A detailed block diagram of the array processor is shown in Figure 3.4. Note that the auxiliary channel correlator branch signals are downconverted to

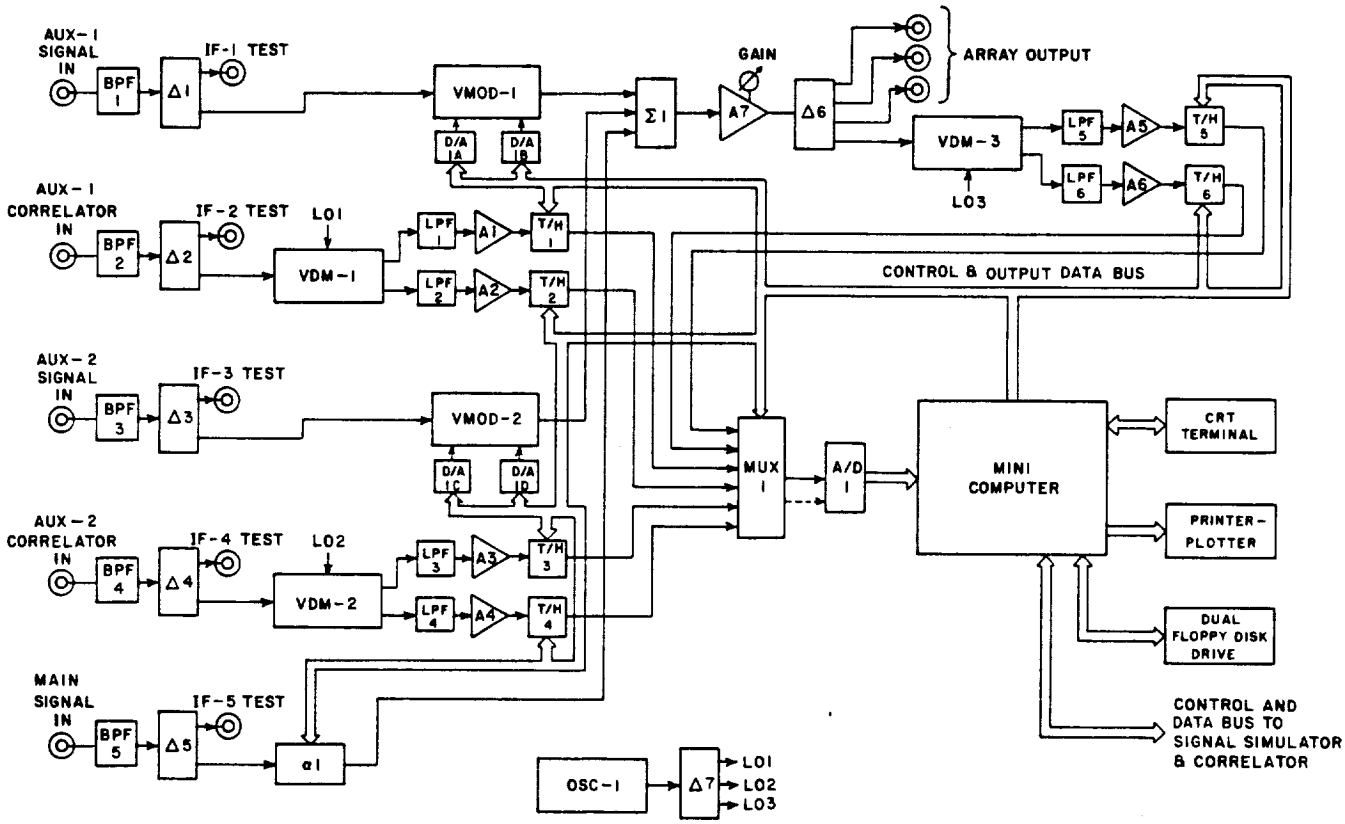

Figure 3.4: Detailed block diagram of the array processor.

baseband and quadrature detected by the vector demodulators (VDMs), as is the array output. These baseband voltages are simultaneously sampled, analog-to-digital (A/D) converted and read by the system computer, which implements the weight control equation and calculates the array weights. The new weights are then digital-to-analog (D/A) converted and applied to the auxiliary signal branches as I and Q control voltages of the two vector modulators (VMODs). The weighted auxiliary elements are summed with the main signal branch to form the array output. In the array processor, the I and Q outputs of each vector demodulator are processed prior to being sampled. A low pass filter first removes the second harmonic. The resultant baseband signals are then amplified to utilize the full dynamic range of the system A/D converter. Track and hold devices allow the multiplexing of all six VDM outputs to the single A/D converter, so that they can be sampled simultaneously. This preserves the signal and noise correlation between the samples of different branches. The track/hold devices of the array processor are triggered in synchronism with the pulse modulated signal envelope. Because of A/D conversion speed limitations, successive samples are not taken in the same pulse repetition period (τ), as can be seen in Figure 3.2. Instead, successive samples are from different pulse repetition periods, but separated by only a small time interval ($\Delta t \sim 1.0\mu$sec) from the start of a pulse repetition period. Thus, an effective sampling rate (1.0 MHz) much higher than the sampling rate possible in real time (15.75 KHz) is achieved. By varying the delay from the start of a period to the sampling instant, a sequence of samples covering the whole waveform is provided to the system computer. By averaging over a complete pulse modulated waveform period

(64 samples), as far as the adaptive array is concerned, the desired and interfering signals appear to be simultaneously present. Thus, the pulse modulation scheme is exploited solely for performance evaluation, and not used in determining the auxiliary channel weights.

Note that the system is a hybrid system. This is because analog weights are applied to analog signals, but the weights are calculated from discrete time samples of the element signals and the array output. The correlation between the correlator branch and the array output is estimated from the sampled data in software, which then updates the array weights. The discrete form of the modified feedback loop algorithm is described next.

3.4 The Modified Feedback Loop Algorithm

The I and Q weights of each auxiliary element are computed according to a discrete time form of the Applebaum control equation [17] and are given by

$$w_{iI}(n+1) = w_{iI}(n) - \gamma Re\,(c_i - u_{si}) \tag{3.1}$$

$$w_{iQ}(n+1) = w_{iQ}(n) + \gamma Im\,(c_i - u_{si}) \tag{3.2}$$

where w_{iI} and w_{iQ} are the in-phase and quadrature weights of the i^{th} auxiliary element, γ is the loop gain, u_{si} is the i^{th} component of the steering vector, and c_i is the correlation between the array output signal and the i^{th} auxiliary correlator branch signal. The loop gain, γ, determines the speed of response of the system. It is chosen as a compromise between response time and weight variance while ensuring that the weights remain stable.

The correlation, c_i is defined as

$$c_i = \frac{1}{N}\sum_{k=1}^{N} y_i(k)z^*(k) \tag{3.3}$$

where N is the number of samples used for the correlation estimate, and $y_i(k)$, $z(k)$ are, respectively the complex samples of the signals received by the i^{th} auxiliary correlator branch and the signals at the array output. Here, $*$ denotes the complex conjugate. Also,

$$y_i(k) = y_{iI}(k) + jy_{iQ}(k) \tag{3.4}$$

where $y_{ii}(k)$ and $y_{iQ}(k)$ are samples taken from the I and Q outputs of the I^{th} auxiliary element vector demodulator. Similarly for the array output

$$z(k) = z_I(k) + jz_Q(k) \tag{3.5}$$

The steering vector is defined as

$$u_{si} = \frac{1}{N}\sum_{k=1}^{N} y_{di}(k)z_d^*(k) \tag{3.6}$$

where N is the number of samples used for the correlation estimate, and $y_{di}(k)$, $z_d(k)$ are respectively the complex samples received in the i^{th} auxiliary element and the main channel due to the desired signal only. The steering vector components u_{si} prevent the array weights from adjusting to cancel the desired signal, and can be calculated using the angle of arrival of the desired signal which is assumed to be known exactly. The number of samples N is chosen so that the correlations are averages over several periods of the received signals. Also, note that the system noise at the array output is uncorrelated with the system noise in the auxiliary correlator

branches. Thus, if the number of samples is large enough, the weights will essentially be independent of the noise power in the various branches and the array will respond to the weak interfering signals.

By implementing the weight control equation in software, many problems often encountered with analog feedback loops, especially at low signal levels, are avoided. These include effects of DC offset voltages, stray coupling and feedthrough associated with the correlator multiplier, and leakage and DC offset voltages in analog integrators. Also, the use of a digital computer in the experimental system provides great flexibility, not only in algorithm implementation, but also in system calibration and quantitative performance evaluation. Some results obtained using the experimental system are given below.

3.5 System Performance Using Bench Generated Signals

Figures 3.5 and 3.6 show the performance of the adaptive array as the interference-to-noise ratio in the main channel (INR(main)) is varied by changing the interference level in the main channel. This corresponds to varying the sidelobe level of the main antenna in the directions of the interference. The SNR(main) is fixed at 13.6 dB.

In Figure 3.5 only one interfering signal is incident on the array. The INR(aux-1) is fixed at 8.8 dB. The noise level in the main channel is equal to the noise level in the auxiliary elements. Thus the auxiliary-1 channels represent moderately directive antennas (but less directive than the main

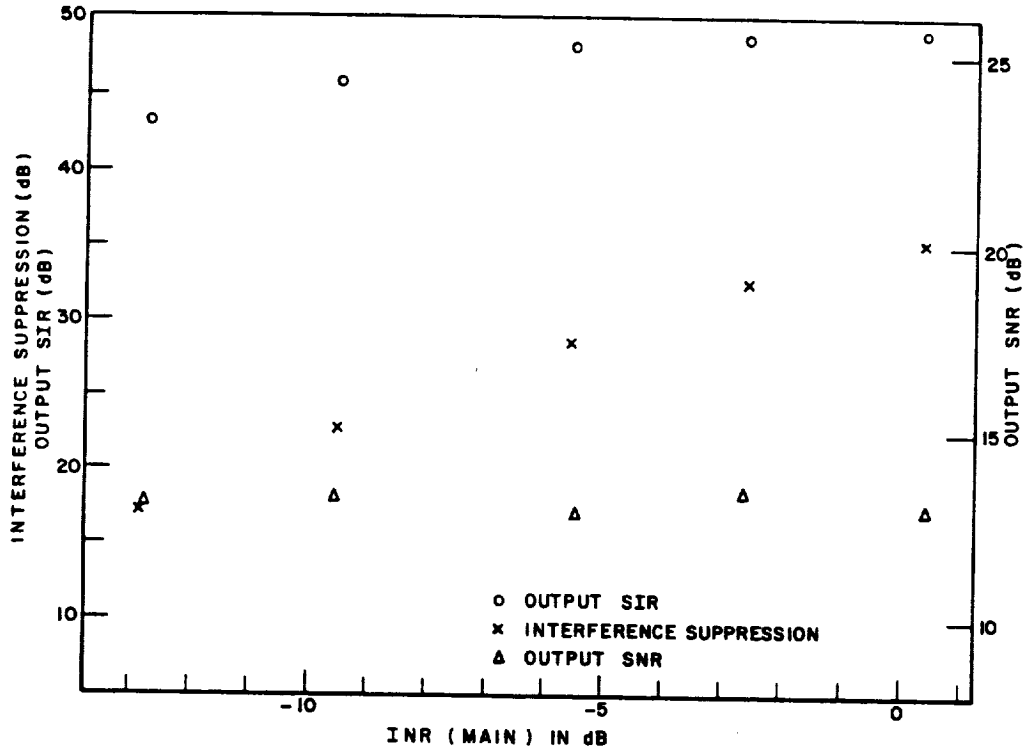

Figure 3.5: Performance versus INR(main). One interfering signal, INR(aux - 1) = 8.8 dB, SNR(main) = 13.6 dB, $\theta_1 = 4°$.

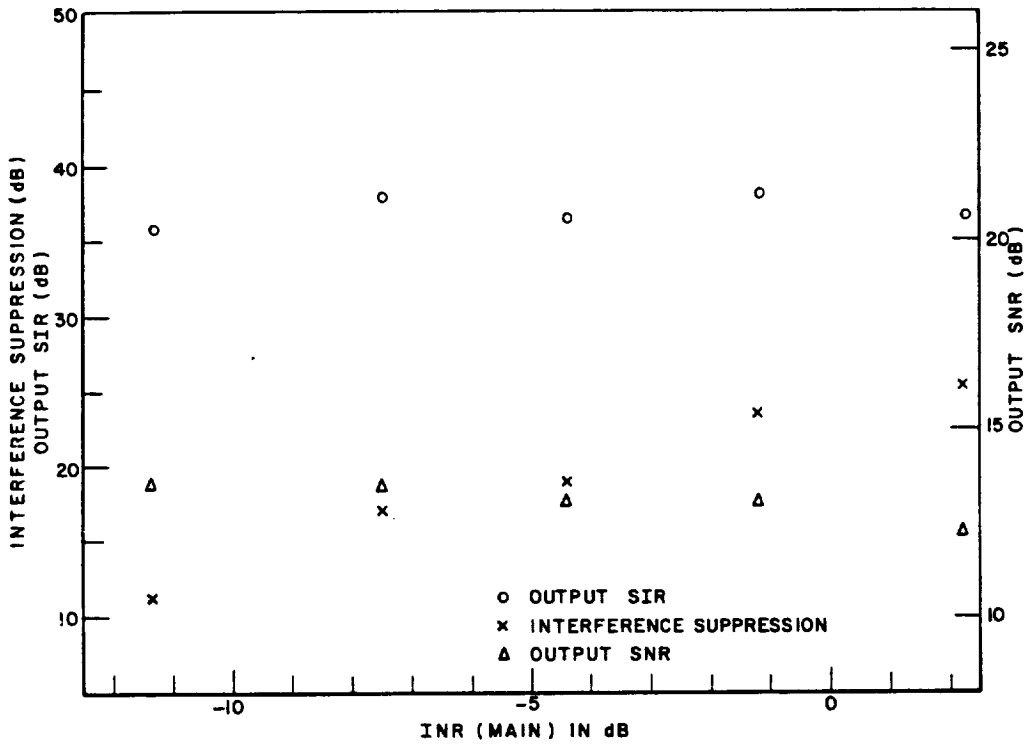

Figure 3.6: Performance versus INR(main). Two interfering signals, INR_1(aux-1) = INR_2(aux-2) = 8.8 dB, SNR(main) = 13.6 dB, $\theta_1 = 4°$, $\theta_2 = -4°$.

antenna where SNR=13.6 dB)which are pointed in the direction of the interfering signal. The phase shifter settings correspond to an interfering signal angle of arrival of 4 degrees off broadside. An interelement spacing of one-half wavelength is assumed in deriving the phase shifter settings. The figure shows that for INR(main)>-10 dB, the interfering signal is suppressed by more than 20 dB. Furthermore the interference suppression increases as INR(main) increases. However, the output SIR is fairly constant. This indicates that the interference is suppressed to the system limit each time. The output SNR is also quite constant. The reason for this is that the interference level in the auxiliary channel is higher than that in the main channel. Thus, the noise power added by the auxiliary channel is small [2,3].

Figure 3.6 shows the case where two interfering signals are incident on the array. Both the level of interfering signal I_1 in the main channel and the level of I_2 in the main channel are varied such that INR_1(main)=INR_2(main). (The noise power is equal in all channels.) Performance is plotted versus the total INR in the main channel. Also INR_2(aux-2)=INR_1(aux-1). Thus the auxiliary elements are of the same gain, with auxiliary element 1(AUX-1) pointed in the direction of I_1, and the AUX-2 antennas pointed towards interfering signal I_2. The phase shifters are set for an I_1 angle of arrival of 4° off broadside and an I_2 angle of arrival of $-4°$ off broadside. Again a one-half wavelength interelement spacing is assumed. Interfering signal I_1 is also present in AUX-2, and I_2 in AUX-1. As INR_1(main) and INR_2(main) are varied, INR_1(aux-2) and INR_2(aux-1) also change such that INR_1(aux-2) = INR_1(main)-3 dB and INR_2(aux-1) = INR_2(main)-

3 dB. The 3 dB difference is a constraint imposed by the design of the array simulator. Referring to the figure, the interference suppression again increases as the interference level in the main channel is increases, while the output SIR is maintained relatively constant (varying between 36 dB and 38 dB). Thus, irrespective of the interference level in the main channel, the output SIR is maintained quite high. Interfering signals 14 dB below thermal noise level are still being suppressed by 13 dB. The output SNR shows some degradation. The reason for this degradation is that for two interfering signals both auxiliary elements are active. Thus the weighted auxiliaries are contributing more noise to the array output than in the one interfering signal only case, resulting in some SNR degradation.

Figure 3.7 shows the system output for two interfering signal experiments. Figure 3.7(a) is the main channel, with both interfering signals incident. INR_1 (main) = INR_2 (main) = -5.0 dB and SNR(main)=13.6 dB. Figure 3.7(b) shows the array output after adaptation. Interference is suppressed to where it cannot be discerned from the thermal noise. Figures 3.7(c) and 3.7(d) show the same cases but with the array simulator noise removed to better view the signals and the performance obtained. Measured interference suppression is 25 dB, corresponding to the right most datapoint of Figure 3.6.

Figures 3.8 and 3.9 show the performance of the adaptive array as a function of INR_1(aux-1). Varying INR_1(aux-1) is analogous to changing the gain of the aux-1 antennas in the direction of interfering signal I_1. In Figure 3.8, INR_1(main) is fixed at -5.0 dB, and the SNR(main) is 13.6 dB. Thus the SIR in the main channel is 18.6 dB. The I_1 phase shifters

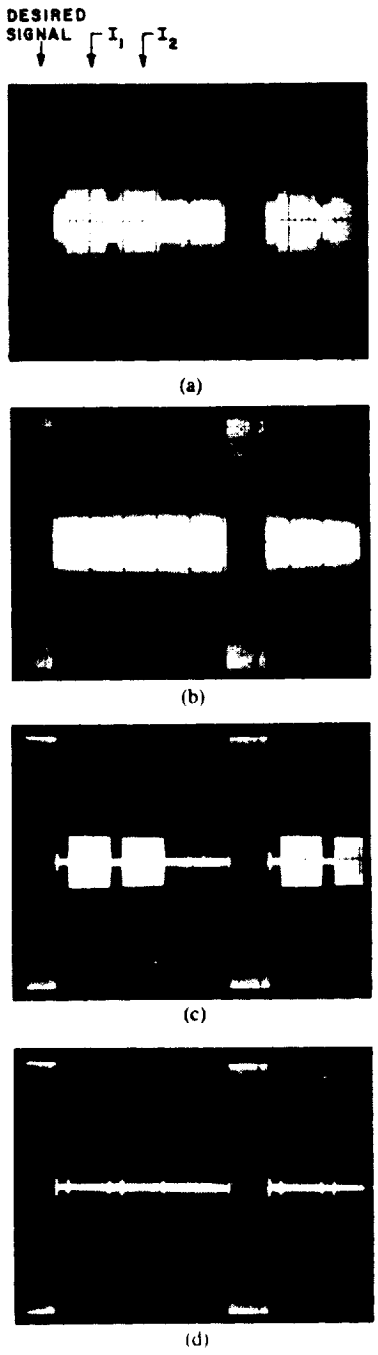

Figure 3.7: Experimental system outputs. (a) Main channel–desired signal plus two interfering signals incident. SNR = 13.6 dB, $SIR_1 = SIR_2 = 18.6$ dB. (b) Array output after adaptation, 25-dB interference suppression. (c) Main channel with array simulator noise removed. (d) Array output with noise removed.

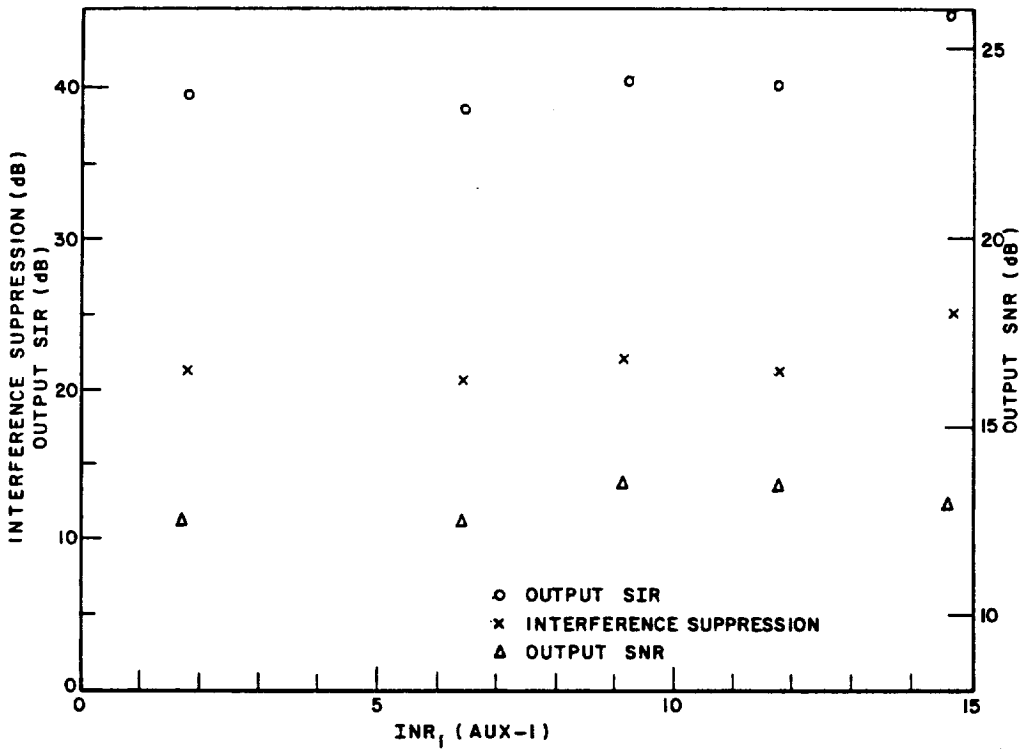

Figure 3.8: Performance versus INR_1(aux-1). One interfering signal, INR_1(main) = -5.0 dB, SNR(main) = 13.6 dB, $\theta_1 = 4°$.

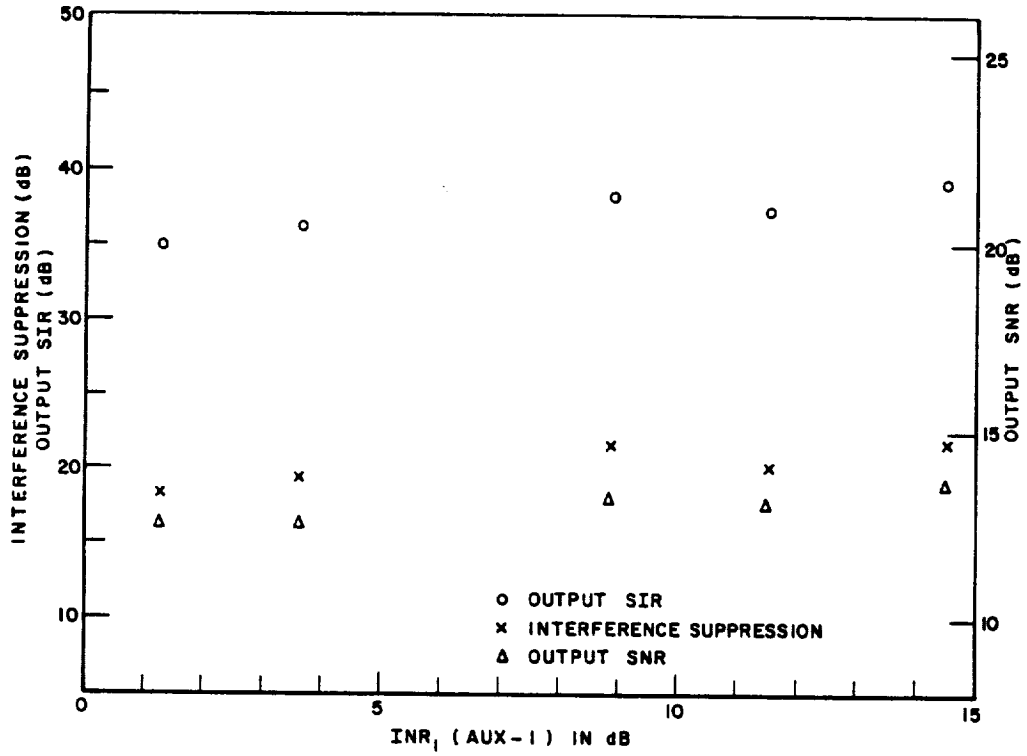

Figure 3.9: Performance versus INR_1(aux-1). Two interfering signals, INR_1(aux-1) = INR_2(aux-2), INR_1(main) = INR_2(main) = -6.5 dB, SNR(main) = 13.6 dB, $\theta_1 = 4°$, $\theta_2 = -4°$.

are fixed at values which correspond to an I_1 angle of arrival of 4° from broadside. Note that the interference suppression and output SIR do not show much variation with INR(aux-1). Even for low gain auxiliary elements (INR_1(aux-1) = 1.5 dB), the interference is being suppressed by 21 dB, yielding an SIR at the output of 40 dB. Thus, it appears that the performance in terms of interference suppression is essentially independent of the auxiliary antenna gain, as long as the gain is large enough to keep the weights from becoming too large for the system to accommodate. This behavior is due to the fact that the noise components of the signals in the two feedback loop branches have been completely decorrelated in the experimental system. The gain of the auxiliary antennas will affect the interference suppression if these noise components are only partially decorrelated [2,3]. Therefore, if complete noise decorrelation is achieved, accurate knowledge of the interfering signal angles of arrival is not required and broad beam auxiliary antennas may be used to suppress weak interference. The output SNR curve in Figure 3.8 shows a very slight dependence on INR_1(aux-1). The output SNR is smaller for low INR_1(aux-1). Since the interfering signal level in the main channel is fixed, as INR_1(aux-1) is decreased the weight magnitude necessary to cancel the interfering signal increases. This results in an increase in the noise power at the output and a decrease in output SNR.

Figure 3.9 shows the two interfering signal case. Both INR_1(aux-1) and INR_2(aux-2) are varied such that they are approximately equal. Thus the aux-1 antennas and the aux-2 antennas are of the same directivity but pointed in different directions. The aux-1 antennas are pointed towards

interfering signal I_1 and the aux-2 antennas towards I_2. The INR_1 and INR_2 in the main channel are fixed at -6.5 dB, and the SNR(main) is 13.6 dB. The performance measures plotted involve the total interference power $(I_1 + I_2)$ at the output. In this case, the results do indicate a slight dependence on INR_1 (aux-1) (and INR_2(aux-2)). As INR_1 (aux-1) is varied from 1.2 dB to 14.5 dB, the interference suppression increases from 18 dB to 21 dB. Because the desired signal is unsuppressed, the output SIR data follows the suppression curve and increases from 35 to 39 dB. Although performance is still good, it is slightly degraded from that of the one interfering signal case. This degradation is most likely because both degrees of freedom are used to cancel the interference. Thus any correlation errors will result in performance degradation. The output SNR behavior of Figure 3.9 shows a slight increase with auxiliary element gain as expected and as was observed and explained in relation to Figure 3.8.

In the results presented above, pulse modulated sinusoids were used as the desired signal and the interfering signals to enable the automatic calculation of steady state adaptive array performance. The system performance was also evaluated with broadcast television signals, again showing excellent results. In these tests [18], performance was observed through the improvement in television picture quality as the array adapted. Thus, it was shown experimentally that with modified feedback loops, an adaptive array can be used to suppress the weak interfering signals encountered in broadcast television systems. Next, the performance of this system with TVRO satellite signals was tested. To do so a ground station was built to receive signals from various geosynchronous satellite. The details of the

ground station are given in the following chapter.

Chapter 4

Ground Station and Experiments with TVRO Satellite Signals

The experimental system described above uses five antenna elements: one for the main channel and two for each auxiliary channel. To test the performance of the experimental system with actual satellite signals, these antennas should be designed to receive signals from satellites in geostationary orbit. The center frequency of these signals is approximately 4 GHz. Normally, parabolic reflector antennas are used to receive these signals. Thus, one would need five parabolic reflectors in the front end of the experimental system, which is not very practical. Alternatively, as suggested in Chapter II, one can use multiple feeds with a single parabolic reflector. The ground station built for the experimental system uses a 30 foot parabolic reflector with seven feeds. A brief description of the parabolic reflector and the feed arrangement is given below.

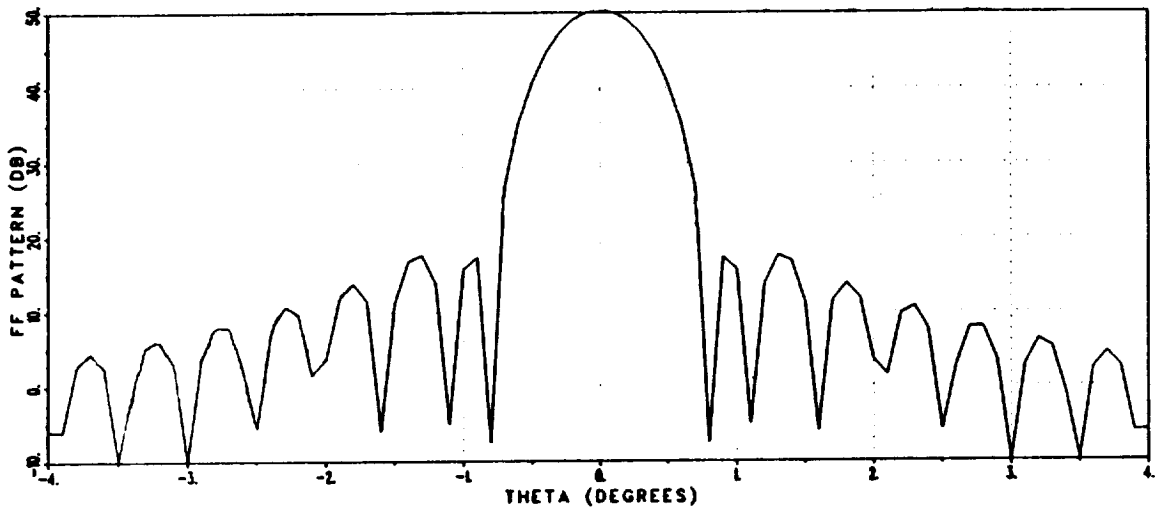

Figure 4.1: The radiation pattern of a focus fed 30 ft. parabolic reflector antenna.

4.1 The Parabolic Reflector

The reflector antenna used with the experimental system is a 30 foot center fed parabolic reflector. The focal length of the reflector is 12.5 feet. The reflector was constructed for another research project and was available for use for this research project. Servo controlled mounts position the parabolic reflector in azimuth and elevation. These mounts are designed to have a resolution of 0.1° or better even in 35 mph wind [19]. In practice, during calm winds the parabolic reflector was able to obtain 0.05° resolution even with gear backlash.

Figure 4.1 shows the radiation pattern of the reflector at 3.95 GHz. The pattern was calculated using The Ohio State University ElectroScience Laboratory's NEC reflector code [20]. In the pattern calculation the feed

taper is modeled as $E(r) = (1 - 2r^2)/3$, where r is the normalized radial distance from the center of the reflector. The aperture blockage and the scattering due to the four struts are not included in the pattern calculation. Note that the reflector has a very narrow main beam and very low sidelobes. The first sidelobe of the reflector is 0.8° away from the boresight and is 23 dB below the main beam peak. The far-off sidelobes (more than 2.5° away from the boresight) are at least 40 dB below the main beam peak. Thus, if this antenna is used to receive signals from geostationary satellites, it will in essence receive only the desired signal with virtually no interfering signal from other geostationary satellites. To establish a desired signal-to-interference ratio (SIR) in the main channel, controlled sidelobes are added to the main channel. To do so, the main channel is formed by summing the signals received by three feeds in the focal plane of the reflector. One of these feeds (prime feed) is located at the focal point of the reflector while the other two feeds designated as 'Offset Feed # 1' and 'Offset Feed # 2', respectively are displaced from the focal point such that their associated beams are pointed in the general direction of two interfering satellites. In addition, four more feeds were included in the focal plane of this reflector. The signals received by these four feeds form the input to the auxiliary channels of the experimental system. The feed platform is described below.

4.2 The Feed Platform

Figure 4.2 shows the feed distribution used in the ground station. Note that there are seven feeds. The signal feeds and the correlator feeds for the

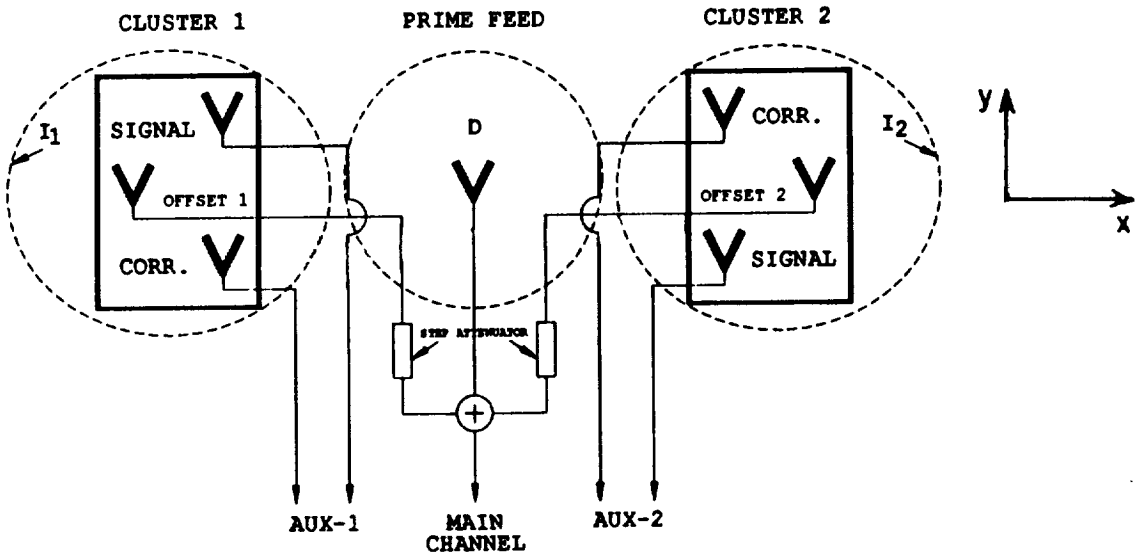

Figure 4.2: The signal and feed distribution.

two auxiliary channels are located symmetrically along a line perpendicular to the geostationary arc, which coincides with the x axis in the figure. This ensures that the phases of the signals received by the signal feeds are nearly equal in phases to the signals received by the correlator feeds. However, because of the separation between the various feeds, the noise received by them will only be partially correlated. Note that the signals received by Offset Feed #1 and Offset Feed #2 are combined with the signal received by the prime feed to form the input to the main channel. In Figure 4.2, the summer which combines these signals is explicitly shown. Step attenuators are used in each Offset branch to allow the user to control the amount of interference in the main channel. The seven feeds are divided in three groups: Cluster 1, prime feed and Cluster 2.

The signal scenario of interest is also shown in the figure. It consists of a desired signal D and two interfering signals I_1 and I_2 from two interfering satellites. Because of the narrow beamwidth of the reflector, each of the seven feeds effectively receives signal from a single geostationary satellite. For example, the prime feed will receive signal from the desired satellite and the feeds in cluster 1 will receive from interfering satellite I_1. However, since the location of interfering satellites are not exactly known and during experiments, one may want to change the interference level in the auxiliary channels and the main channel, the feeds in the two cluster are installed on two different moveable platforms. These moveable platforms displace the feeds along the x axis in the focal plane of the reflector.

In the ground station, the seven feeds are distributed on a feed platform. The feed platform was designed using the ESL CAD (computer aided de-

sign)system. The layout of the feed platform produced by the CAD system is shown in Figure 4.3. The feeds used in the ground station are circular waveguides with a flange and chokes and are commonly known as scalar feeds. These feeds are similar to a corrugated horn with 90° flare angle. Before installing the feeds on the feed platform, their outer ring was cut off and their throat height was adjusted to obtain the desired illumination of the reflector surface. In the experimental system, the feed platform is positioned within a stainless steel pipe bent into a circle. Thus, the entire feed platform can rotate. This adjustment helps one to align the feed platform with the geostationary arc. Furthermore, each feed can be installed either as vertically polarized or horizontally polarized (with respect to the geostationary arc). This permits the user to match the feed polarization to the polarization of the signal to be received.

A picture of the ring and feed platform is shown in Figure 4.4. Other views of the feed platform are shown in Figures 4.5 and 4.6. Figure 4.7 shows a picture of the parabolic reflector with the feed platform in place.

The signals received from the seven feeds should be processed before these signals can be used with the adaptive processor whose intermediate frequency is 69 MHz. The hardware used to process the satellite signals received by the various feeds is discussed below.

4.3 The Receive System

Figure 4.8 shows a block diagram of the receive system which amplifies and down-converts the signals received by the various feeds. The first stage on

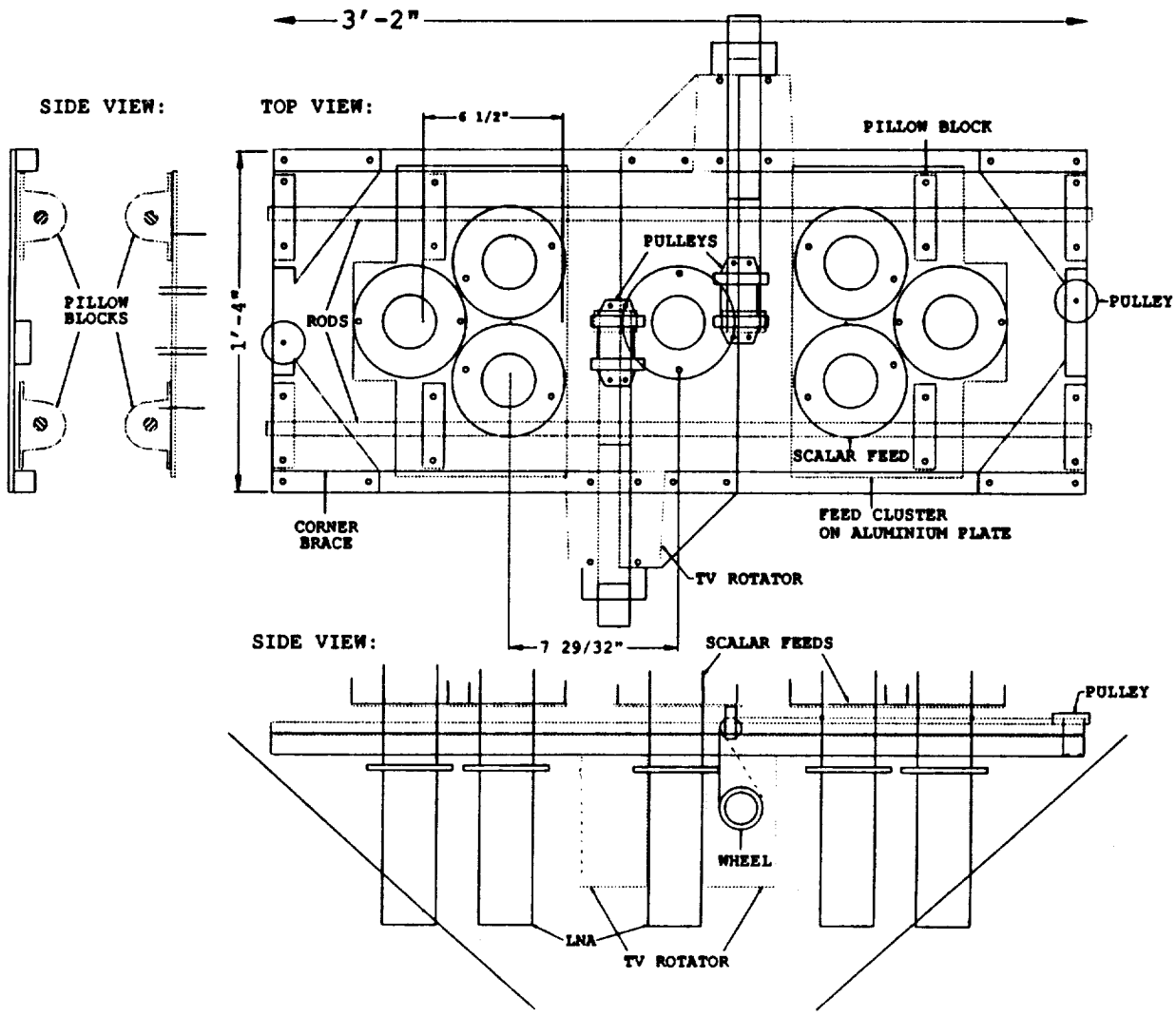

Figure 4.3: The feed platform layout.

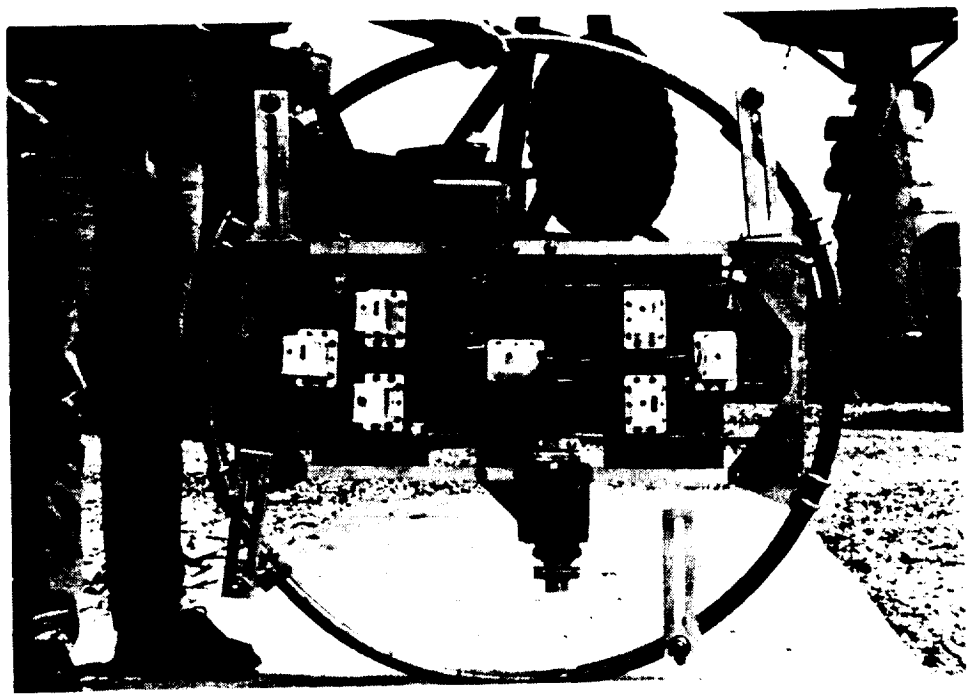

Figure 4.4: A picture of the feed platform and the ring, a bottom view.

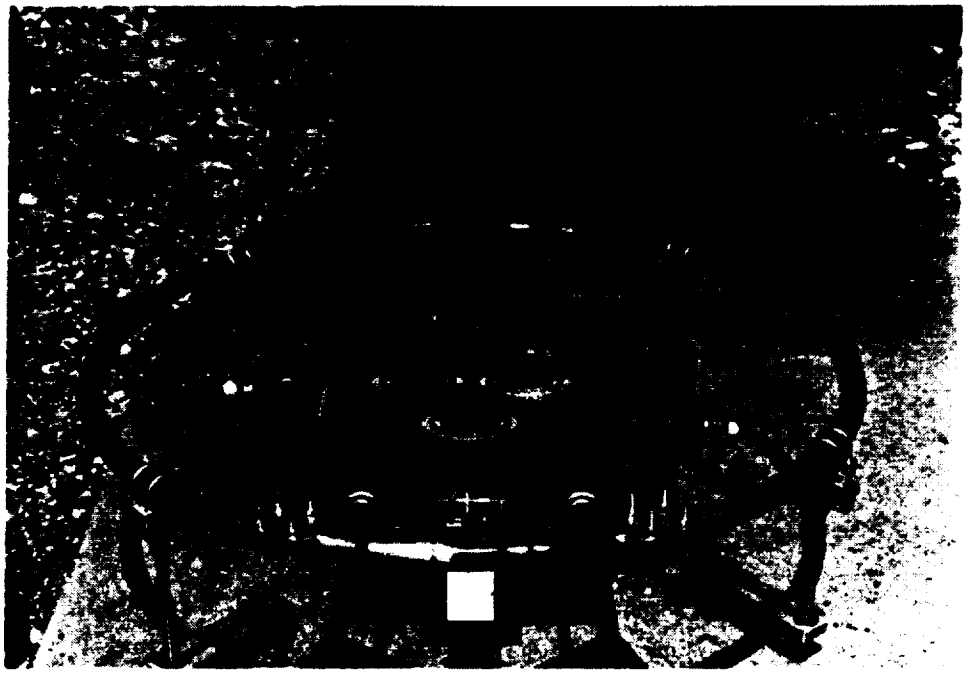

Figure 4.5: A picture of the feed platform and the ring, a top view.

Figure 4.6: A picture of the feed platform and the ring, a side view.

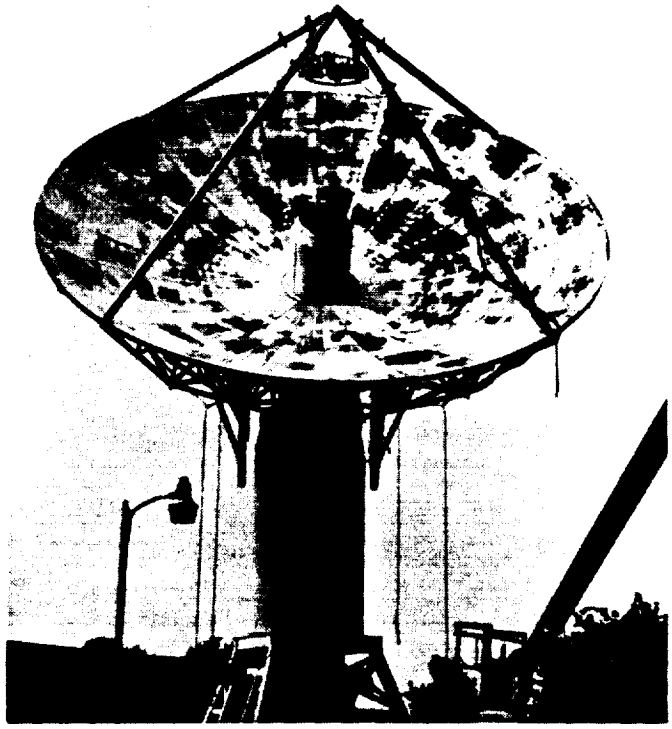

Figure 4.7: A picture of the parabolic reflector and the feed platform.

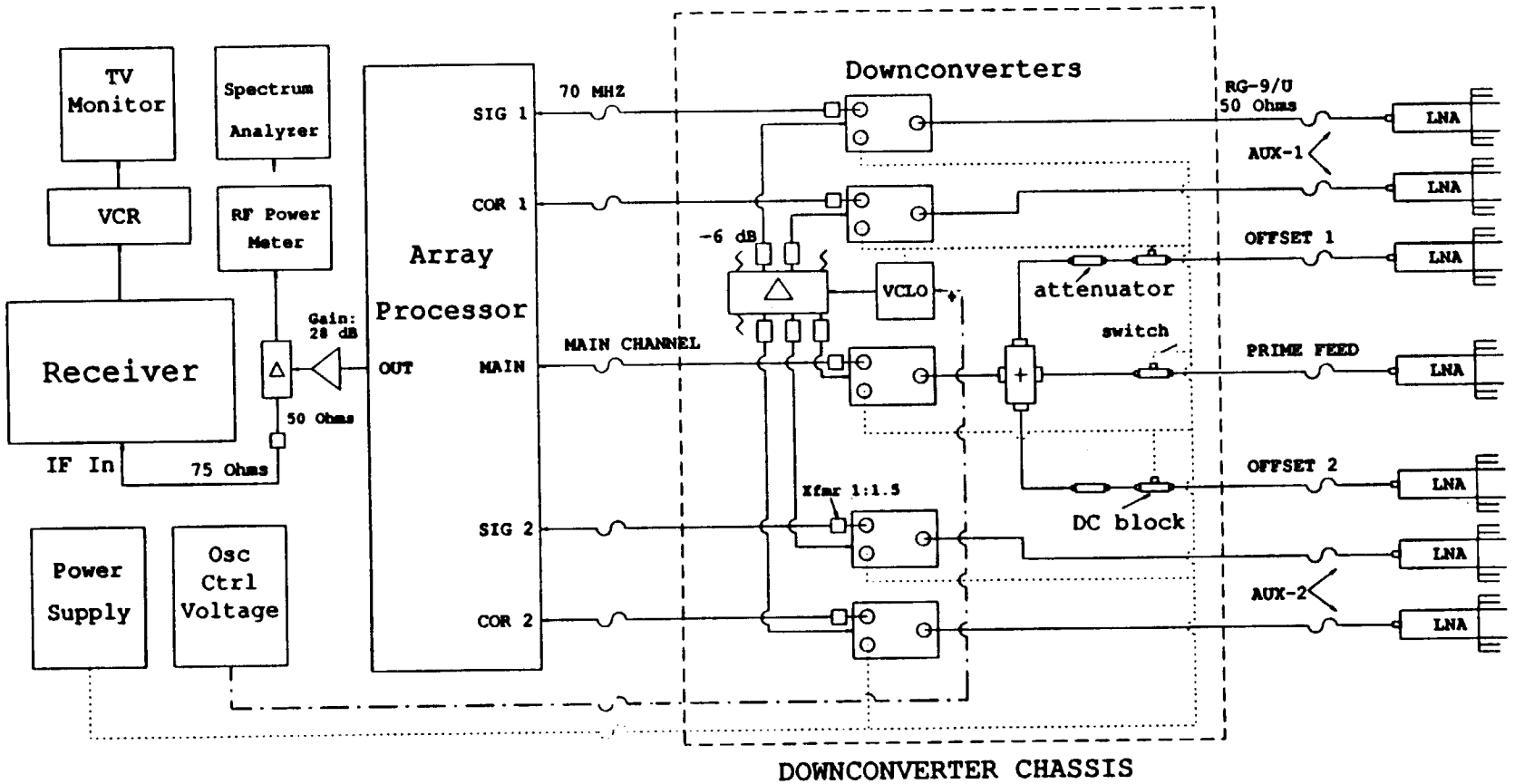

Figure 4.8: The receive system block diagram.

the diagram contains the feeds which, as described previously, convert the downlinked electromagnetic waves into electrical signals. Following each feed, the received signals are transferred directly to a low-noise amplifier (LNA). The LNA is used to preamplify the incoming signal and to establish the system signal-to-noise ratio due to its substantial gain. The amplified signal is carried by a 39 foot long RG-9/U coaxial cable to a chamber, called the tub, just below the parabolic reflector. The loss in this RG-9/U cable at 4 GHz is 7 dB. However, since the signal-to-noise ratio is determined by the LNA, the power loss of this cable does not appreciably affect the overall receive system signal-to-noise ratio.

Inside the tub is the downconverter chassis. The tub provides a barrier to harsh weather elements. Signals received by the feeds enter the tub through watertight bulkhead connectors and pass into downconverters. Note that there are five downconverters on the downconverter chassis. Each downconverter is comprised of a balanced mixer, a filter, and an amplifier. The mixer converts a signal within the 3.7-4.2 GHz band down to the 70 MHz intermediate frequency (IF). A known frequency is inject into the mixer from a local oscillator (LO). The resulting signal then passes through a bandpass filter with a center frequency of 70 MHz and a 3 dB bandwidth of 35 MHz. The signal is then amplified to counteract mixer and filter losses. The output impedance of the downconverter is 75 ohms. However, the coaxial cable which was previously available had a 50 ohm impedance. A transformer is used to match the two impedances.

The frequency of the LO is voltage controlled (VCLO). In order for each of the downconverters to have the same phase reference, a common VCLO

is used. To do so the downconverters were modified. As can be seen on the system block diagram, an eight port power divider is used in this design. All unused outputs are terminated.

From the downconverter chassis, all the received signals are carried from the tub by RG-58/U coaxial cable into the main building. The array processor is located inside this building. The satellite signals are fed into the array processor. The output of the array processor is transferred through a power divider to a commercially available satellite TV receiver. The other output of the power divider drives the RF power meter. The satellite receiver has an input impedance of 75 ohms, while the array processor has a 50 ohm impedance. Therefore, a transformer is used to match the impedance of the receiver with the impedance of the array processor. Through FM demodulation the satellite receiver produces a composite video signal. This signal can be recorded by a video cassette recorder (VCR), viewed on a television (TV) monitor, or analyzed by a spectrum analyzer.

Note that the amplified signals received by three feeds are summed to form the main channel. Attenuators in series with the Offset Feeds are used to control the amplitude of the interference in the main channel in known fixed steps. A set of four relays, configured as shown in Figure 4.9, provide four combinations of attenuation. For easy adjustment of this attenuation, the relays are controlled from inside the main building.

The LNAs require DC power to operate. The DC supply voltage for these electrical components is carried along the same RG-9/U coaxial cable which was described previously to carry the received satellite signals. Since one cable carries both the radio frequency (RF) signal and the DC supply

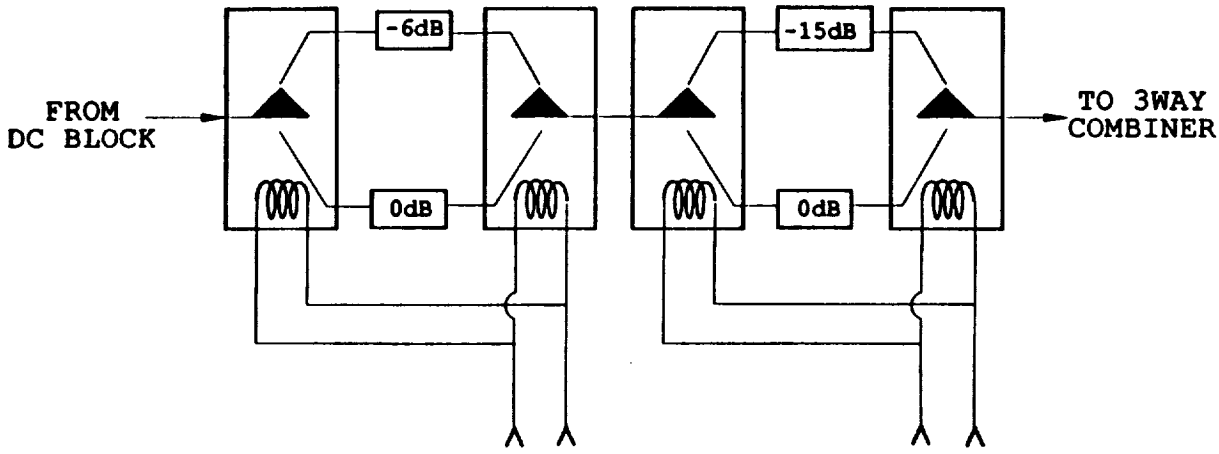

Figure 4.9: The configuration of the four relays.

power, only one cable per LNA is required. As described previously, attenuators are included in the Offset Feeds of the main channel of the receive system. Because this attenuator attempts to attenuate both the DC power supply voltage as well as the RF signal a DC block is placed between the LNA and the attenuator. Using a DC block, the DC power supply voltage is blocked from traveling into the attenuator. For proper operation, the down converter in the main channel was modified so that it would no longer output a DC voltage at its RF input port. A 16 volt direct current power supply provides the power for the downconverters, LNAs, and VCLO. In practice the maximum current drawn from this power supply is 1.6 amperes.

The signals in the main channel are controlled by three switches in series with the three main signal power supply branches. These switches are located inside the main building. Since a switch turns off the DC power to a LNA, it effectively removes its corresponding signal from the main channel. Through the control of three such switches, the operator can easily receive only a desired signal, only an interfering signal, both a desired an an interfering signal, or other combinations of these three signals in the main signal branch. These switches provide a quick method of system demonstration. A detailed description of the various components used in the received system is given in Steadman's thesis [8]. Using the receive system, the performance of the experimental adaptive array processor with actual satellite signals was studied. In the study, Telstar 301 at 96° West Longitude was used as the desired satellite; while Galaxy 3 at 93.5° West Longitude and Westar at 99° West Longitude were used as the source of interference #1

(I_1) and interference #2 (I_2), respectively. Channel 9 (center frequency of 3.88 GHz) signals were used since all three satellites have concurrent TV programs on this channel. The results of the study are summarized below.

4.4 System Performance Using Actual Satellite Signals

In the results presented here, the performance of the experimental system is characterized qualitatively in terms of the quality of the steady state video picture. The reason for this is that in the case of actual satellite signals, the power in various signals (desired and interfering signals) has to be measured in the presence of noise. Since in the presence of equal or larger amount of noise the power of a signal can not be measured accurately, the measured interference suppression can be misleadingly small. For the same reason, initially, the INR in the main and auxiliary channels is selected to be more than 0 dB. The INR in the main channel is typically between 0 and 10 dB.

In the first series of experiments, no desired signal is included in the main channel. The reason for this is that to determine that the array is operating correctly, one has to visually ascertain when the interference is indeed suppressed. In the presence of a desired signal, an interfering signal contaminates the picture quality. As the array adapts, this contamination should no longer be observable. Judging when the interference is no longer objectionable is a subjective process, and thus is not precise or definite. On the other hand, in the absence of the desired signal, one can clearly see when the interference is suppressed. In this case, if the adaptive weights are

Main Channel		Corr. Branch #1		Mag.(Weight #)		Final
I+N	N	I+N	N	#1	#2	Picture
-44.2	-45.5	-38.5	-44.5	0.359	0.023	Noise
-50.2	-51.5	-38.5	-44.5	0.275	0.007	Noise
-59.2	-60.5	-38.5	-44.5	0.070	0.025	Noise

Table 4.1: Interfering source I_1, both auxiliary loops are activated, no desired signal present, INR(Main Channel) $\sim$ 2.3 dB, (powers are in dBm).

Main Channel		Corr. Branch #1		Mag.(Weight #)		Final
I+N	N	I+N	N	#1	#2	Picture
-43.2	-52.2	-36.4	-43.4	0.326	0.008	Noise
-50.2	-51.5	-38.5	-44.5	0.275	0.007	Noise
-39.8	-50.4	-44.2	-48.7	0.842	0.172	Noise

Table 4.2: Interfering source I_1, both auxiliary loops are activated, no desired signal present, the attenuation of Offset feed #1 is 6.0 dB, (powers are in dBm).

correct, only noise should be seen on the television monitor. A spectrum analyzer should also show only noise.

4.4.1 Experiments with a Single Interfering Signal

Tables 4.1 and 4.2 show the results of the experiments when only interference #1 (I_1) is present in the main channel. Thus, for this adaptive array experiment the LNAs for the Offset Feed #2 and the prime feed are turned off. Each of these tables corresponds to a different signal scenario, and the tables indicate the state of the array after adaptation. The tables list respectively from left to right: the interference power (I) plus noise

power (N) and the noise power in the main channel from Offset Feed #1 after attenuation, the interference plus noise power and the noise power in correlator branch #1, the magnitude of the steady state weight values for feedback loop #1 and #2, and finally the quality of the video picture after adaptation. We take the INR of the auxiliaries to be that of the correlator branch since the weight control algorithm directly samples the signals and noise present in this branch. In Table 4.1 the INR in the main channel is constant, $\sim$ 2.3 dB, while the interference power received by Offset Feed #1 is attenuated by 0, 6, and 15 dB. In Table 4.2 the attenuation of the signal received by Offset Feed #1 is held constant while the INR in the main channel varies. Note that for all values of INR in the main channel and auxiliary channel #1, the final picture after adaptation contains only noise. Thus the interference has been suppressed. Also in Table 4.1, as the interference level in the main channel is reduced by an increase in the received signal attenuation, the weight value for auxiliary channel #1 decreases, which is expected. Note that the weight of feedback loop #2 is very small in magnitude. Moreover, it was observed that if the weight was set to zero there was no visible difference in the interference suppression. The reason for such a low magnitude of weight for auxiliary channel #2 can be attributed to the fact that the level of I_1 in auxiliary channel #2 is very small. The antennas associated with auxiliary channel #2 are pointed in the general direction of I_2, and not I_1. It should also be noted that both auxiliaries also receive the desired signal from the geostationary satellite Telstar 301 through their sidelobes. However, with there being an extremely weak desired signal in the main channel (received through the

Main Channel		Corr. Branch #2		Mag.(Weight #)		Final
I+N	N	I+N	N	#1	#2	Picture
-44.5	-53.4	-33.2	-41.8	0.007	0.451	Noise
-47.3	-50.3	-33.3	-38.2	0.049	0.392	Noise
-46.8	-51.0	-34.7	-39.2	0.017	0.345	Noise
-49.3	-51.0	-41.5	-42.5	0.020	0.206	Noise
-51.0	-53.4	-36.4	-41.8	0.008	0.208	Noise

Table 4.3: Interfering source I_2 both auxiliary loops are activated, no desired signal present, the attenuation of Offset Feed #2 is 10 dB, (powers are in dBm).

sidelobes of Offset Feed #1) the correlation of the desired signal components is much lower in magnitude than the correlation of the interfering signal components. Therefore, the array suppression is not affected. Note that the interference power measured in auxiliary channel #1 is actually the sum of three signals ($I = I_1 + I_2 + D$), however the powers of I_2 and D (the desired signal) are both very small in comparison to power of I_1; therefore, $I \sim I_1$. Thus, one may approximate the INR of auxiliary channel #1 (INR_1) as the INR in auxiliary channel #1 due to $I_1(I_1NR_1)$. Likewise since the beam associated with auxiliary channel #2 is pointed in the general direction if 1_2, the INR of auxiliary channel #2 is approximately equal to the INR of auxiliary channel #2 due to $I_2(INR_2 \sim I_2NR_2)$. In all of the above experiments, except for the test on row three of Table 4.2 auxiliary channel #2 received signals from satellite source #2.

Table 4.3 shows the results obtained for an interfering signal from satellite source #2. Here, the LNAs for Offset Feed #1 and the prime feed

are turned off while the LNA for Offset Feed #2 is operational. The signals received by Offset Feed #2 are attenuated by 10 dB. The INR in the main channel and also in auxiliary channel #2 is adjusted by the linear displacement of the feed cluster #2 in the focal plane. Again note that the magnitude of the weight value of the inactive auxiliary channel, which in this case is auxiliary channel #1, is very small. The same reasoning holds as before in that in this case auxiliary channel #2 receives a small amount of interference from satellite source #1 through its sidelobes. As in prior experiments, only noise was visible after the interference was suppressed for all obtainable values of INR in the main channel.

4.4.2 Experiments with Two Interfering Signals

Next, the array performance is tested in the presence of two interfering signals. These experiments are again performed with no desired signal present from the prime feed of the main channel. Tables 4.4 and 4.5 shows the results for two interfering signals, from the two Offset Feeds. Each of these tables corresponds to a different signal scenario, and the tables indicate the state of the array after adaptation. The tables list respectively from left to right: the interference plus noise power in the main channel from Offset Feed #1 after attenuation and the interference plus noise power in the main channel from Offset Feed #2 after attenuation and the noise power in the main channel after the attenuation of each Offset Feed, the interference plus noise power and the noise power in correlator branch #1, the interference plus noise power and the noise power in correlator branch #2, and finally the quality of the video picture after adaptation. In Table

Main Channel			Corr. Branch 1		Corr. Branch 2		Final
$(I+N)_1$	$(I+N)_2$	N	I+N	N	I+N	N	Picture
-39.1	-47.0	-47.5	-43.4	-44.8	-34.7	-42.5	Noise
-48.1	-47.0	-50.4	-43.4	-44.8	-34.7	-42.5	Noise
-54.1	-47.0	-50.8	-43.4	-44.8	-34.7	-42.5	Noise
-39.1	-49.3	-47.5	-43.4	-44.8	-41.5	-42.5	Noise
-48.1	-49.3	-50.4	-43.4	-44.8	-41.5	-42.5	Noise
-54.1	-49.3	-50.8	-43.4	-44.8	-41.5	-42.5	Noise

Table 4.4: Interfering sources I_1 and I_2 both auxiliary loops are activated, no desired signal present, the INR(Main channel) is constant for Offset Feed #1, the attenuation is 10 dB for Offset Feed #2 for two sets of experiments (powers in dBm).

Main Channel			Corr. Branch 1		Corr. Branch 2		Final
$(I+N)_1$	$(I+N)_2$	N	I+N	N	I+N	N	Picture
-47.5	-47.3	-50.0	-44.3	-43.0	-33.3	-37.2	Noise
-52.2	-44.5	-55.2	-36.4	-43.4	-33.2	-41.8	Noise
-48.1	-47.0	-50.4	-43.4	-44.8	-34.7	-42.5	Noise
-53.4	-51.0	-54.5	-38.2	-43.4	-36.4	-41.8	Noise

Table 4.5: Interfering sources I_1 and I_2, both auxiliary loops are activated, no desired signal present, the attenuation is 15 dB for Offset Feed #1, the attenuation is 10 dB for Offset Feed #2 (powers in dBm).

4.4 the INR in the main channel due to Offset Feed #1 was constant while the corresponding attenuator is varied in fixed steps of 6, 15, and 21 dB. However the INR and interference power in the main channel due to Offset Feed #2 is constant. In these experiments the attenuator in the Offset Feed #2 is always set at 10 dB. Therefore, in Table 4.4 the INR in the main channel varies with the attenuation of Offset Feed #1 while the INR of the auxiliaries is constant. For the two sets of experiments shown the INR in the main channel due to Offset Feed #1 is approximately 3.2 dB while due to Offset Feed #2 was approximately 1.8 dB and 0.5 dB respectively. In Table 4.5 the attenuation of the Offset Feed #1 is set a 15 dB and Offset Feed #2 is set at 10 dB while the INR in the main channel varies. In the main channel the INR due to the interfering signal $I_1(I_1NR)$ and INR due to interfering signal $I_2(I_2NR)$ vary independently. In these experiments with two interfering signals it was observed that both weight value adapted and were of significant magnitude. Both interfering signals were suppressed in these tests regardless of the INR used in the main channel and the auxiliaries.

The first series of experiments were carried out with no desired signal in the main channel. In the absence of the desired signal in the main channel, the suppression of the interfering signal could be observed on the television monitor or spectrum analyzer while the array adapted. To complete the testing of the experimental system, its performance was evaluated in the presence of the desired signal. In this case, the presence of interfering signals will contaminate the picture quality. As the array adapts, this contamination should no longer be observable. However, as pointed out

before, judging when the interference is no longer objectionable is a subjective process, and thus is not precise. To get around this problem, at the beginning of each experiment the interfering signals were observed on the television monitor and spectrum analyzer. This was accomplished by switching off the LNA for the prime feed in the main channel. Then the weights of the auxiliary channels were found adaptively in the presence of the desired signal (prime feed LNA is turned on). After the weights reached their steady state value, only the desired video could be observed on the television monitor. At this point to check the level of the interfering signals, the desired signal was removed from the main channel (prime feed LNA is turned off). If the interfering signals were suppressed by the adaptive array, one should see only noise on the television monitor and spectrum analyzer. The experiments in the presence of a desired signal in the main channel are described below.

4.4.3 Experiments in the Presence of the Desired Signal

As pointed out before, the auxiliary channels also receive some desired signals for Telstar 301. In the presence of a strong desired signal in the main channel, one, therefore, needs an appropriate steering vector to avoid the cancellation of the desired signal. The method used to determine the steering vector for these experiments is described first.

The i^{th} component of the steering vector is given by [6]

$$u_{si} \approx \frac{1}{N}\sum_{k=1}^{N} y_{di}(k) z_d^*(k) \tag{4.1}$$

where N is the number of samples used for the correlation estimate, and $y_{di}(k)$ and $z_d(k)$ are, respectively, the complex samples of the signals received in the i^{th} auxiliary channel and the main channel due to the desired signal only. In the experimental system, u_{si} is determined insitu by using the samples collected by the system computer. To do so the LNAs of the two Offset feeds of the main channel are turned off and the auxiliary channel weights are set to zero. Thus, the main channel is effectively receiving the desired signal only which is also the array output. The array output is then correlated with the two correlator branches to obtain the steering vector. Since the desired signal in the auxiliary channels is quite weak and is buried under noise (SNR $\approx$ -25 dB), one needs to use a lot of samples to obtain a good estimate of the steering vector. In the experiments described here, 32000 samples were used to obtain the steering vector.

In the experimental system, the desired signal power is observed to vary as much as 3 dB. This variation is largely due to changes in the television programming. Therefore, in the experiments presented here, the steering vector amplitude was updated every time the weights were updated. To do so the desired signal power in the main channel was estimated from the autocorrelation of the array output samples. The steering vector amplitude was then adjusted according to the desired signal power. When the interference is not nulled, this procedure will cause some error in the estimate of the desired signal power. The estimate, however, will improve as the adaptive array starts nulling the interfering signals.

Tables 4.6 and 4.7 show the performance of the experimental system in the presence of a desired signal and two interfering signals. Each entry

Main Channel			Corr. Branch 1		Corr. Branch 2		Final
-41.3	-48.3	-39.0	-35.3	-40.3	-32.9	-35.4	Noise
-50.3	-48.3	-39.4	-35.3	-40.3	-32.9	-35.4	Noise
-56.3	-48.3	-39.5	-35.3	-40.3	-32.9	-35.4	Noise

Table 4.6: Interfering sources I_1 and I_2, both auxiliary loops are activated, a desired signal present, the attenuation of Offset Feed #1 is 6, 15, 21 dB; the attenuation is 10 dB for Offset Feed #2 (powers in dBm).

Main Channel			Corr. Branch 1		Corr. Branch 2		Final
-45.0	-48.3	-41.4	-38.2	-42.8	-33.0	-34.7	Noise
-50.3	-48.3	-39.4	-35.3	-40.3	-32.9	-35.4	Noise
-46.6	-49.6	-39.4	-38.8	-40.8	-37.2	-37.6	Noise

Table 4.7: Interfering sources I_1 and I_2, both auxiliary loops are activate, a desired signal present, the attenuation is 15 dB for Offset Feed #1, the attenuation is 10 dB for Offset Feed #2 (powers in dBm).

in these tables corresponds to different interference scenario. The desired signal in the main channel is fixed at -22.6 dBm. The tables list, the interference plus noise power in the main channel from Offset Feed #1 after attenuation, the interference plus noise power in the main channel from Offset Feed #2 after attenuation, the total noise power in the main channel (received from all three feeds), the interference plus noise and the noise power in the correlator branch #1, the interference plus noise and the noise power in the correlator branch #2 and the quality of the television picture after the weights have reached the steady state and the desired signal is removed from the main channel (prime feed LNA is turned off). Note that the final picture contains noise only. Thus, both interfering signals are nulled. If the prime feed LNA was left on, one could see the desired signal on the television monitor.

In Table 4.6, the interference power in the main channel due to I_1 is varied by changing the attenuator setting while all other signal levels are kept fixed. Thus, this table represents the scenario where the sidelobe level of the main antenna is varied in the direction of the interfering signal I_1. In Table 4.7, the level of two interfering signals is varied by moving the two feed clusters. Thus, this table represents the scenario where the angle of arrival of the two interfering signals is varied. In all the cases, the interfering signals are suppressed quite effectively. An interesting observation to be made from the entries in Tables 4.6 and 4.7 is that interference to noise ratio for the two interfering signals in the main channel $\left(\frac{(I+N)_i}{N}, i = 1, 2\right)$ is below 0 dB. Thus, the experimental system is successfully nulling weak interfering signals.

To further demonstrate the ability of the experimental system to null weak interfering signals, experiments were conducted when controlled amount of noise was injected in various channels of the adaptive system. In this case the adaptive weights were obtained in the presence of the controlled noise while the system performance was evaluated in the absence of the controlled noise. The controlled noise was injected by combining the down-converted signals received by the various feeds with the noise generated by the four noise sources of the array simulator. The set up used to do is shown in Figure 4.10. Note that the noise injected in various channels is uncorrelated. Further, the noise in the signals branches of the two auxiliary channels is uncorrelated to the noise in their correlator branches.

Table 4.8 shows an experiment with one interfering signal. Thus the power for the prime feed LNA and Offset Feed #2 LNA is turned off. This table lists respectively from left to right: the interference plus ambient noise power in the main channel from Offset Feed #1 after attenuation and the noise power in the main channel which includes the injected noise power, the interference plus ambient noise power and the total noise power in correlator branch #1, the interference plus ambient noise power and the total noise power in correlator branch #2, the steady state weight for feedback loop #1, and finally the quality of the video picture after adaptation. In the experiments the ambient noise power is -57.7 dBm for the main channel, -44.1 dBm for auxiliary channel #1, and -38.6 dBm for auxiliary channel #2. The injected noise power has a 6 MHz bandwidth. The injected noise was removed prior to judging the video picture quality after adaptation. Otherwise the injected noise may mask a weak interfering signal to a point

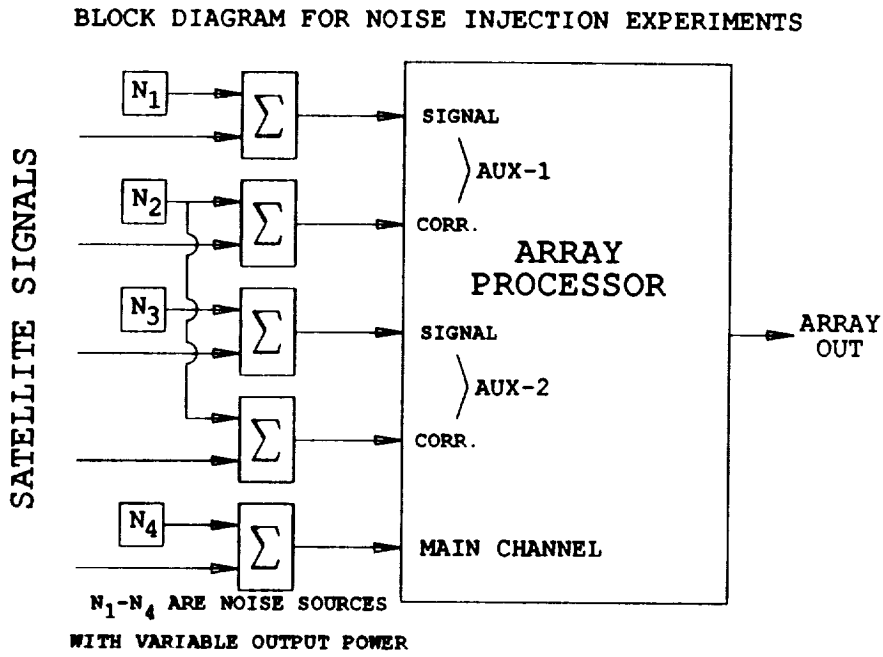

Figure 4.10: Block diagram for noise injection experiment.

Main Channel		INR(Corr. Branch #)				Weight #1	Final Picture
		#1		#2			
$(I+No)_1$	N	I+No	N	I+No	N		
-47.1	-31.0	-39.5	-30.8	-39.0	-30.3	0.162-0.160j	Noise
-47.1	-37.0	-39.5	-30.8	-39.0	-30.3	0.186-0.189j	Noise
-47.1	-42.9	-39.5	-30.8	-39.0	-30.3	0.177-0.241j	Noise
-47.1	-57.7	-39.5	-30.8	-39.0	-30.3	0.173-0.206j	Noise
-47.1	-31.0	-39.5	-36.2	-39.0	-34.7	0.163-0.216j	Noise
-47.1	-37.0	-39.5	-36.2	-39.0	-34.7	0.165-0.210j	Noise
-47.1	-42.9	-39.5	-36.2	-39.0	-34.7	0.171-0204j	Noise
-47.1	-57.7	-39.5	-36.2	-39.0	-34.7	0.174-0.204j	Noise
-47.1	-31.0	-39.5	-40.5	-39.0	-39.0	0.157-0.201j	Noise
-47.1	-37.0	-39.5	-40.5	-39.0	-37.3	0.176-0205j	Noise
-47.1	-42.9	-39.5	-40.5	-39.0	-37.3	0.179-0.225j	Noise
-47.1	-57.7	-39.5	-40.5	-39.0	-37.3	0.168-0214j	Noise

Table 4.8: Noise injection experiment, both auxiliary loops are activated, no desired signal present.

where it is not visible. As can be noted in Table 4.8, by using modified feedback loops we are able to suppress the interference below the noise level even when the INR in the auxiliaries is less than 0 dB.

This concludes the testing of the experimental system with geosynchronous satellite signals. It has been shown that the system can effectively null two interfering signals while preserving the desired video signal. The interfering signals may be below the noise level in the main channel. The experimental system is a sidelobe canceller with two auxiliary channels. The modified feedback loops are used to control the weights of auxiliary channel. The modified feedback loops helps in suppressing the weak interfering signals. In the next two chapters, the sample matrix inversion (SMI) algorithm to control the weights of an adaptive array is described and the modification required to achieve the desired suppression of weak interfering signal is discussed. The implementation of the modified SMI algorithm on the experimental system and its performance using bench generated signals as well as using geosynchronous satellite signals is also presented.

Chapter 5

Modified SMI Adaptive Antenna Array

In the above discussion, the feedback loops used to update the weights of an adaptive array were modified to obtain the required suppression of weak interfering signals. The weights of an adaptive array can also be updated using sample matrix inversion (SMI) algorithm [9,10]. The SMI algorithm is an open loop algorithm in the sense that the array output is not used to update the array weights. Instead the weights are updated using a covariance matrix obtained from the samples of the signal received by various antenna elements. In the case of SMI adaptive antennas, the main as well as auxiliary channels are sampled and weighted. Thus, an SMI adaptive antenna is a fully adaptive system. One can, however, normalize the weights such that the weight of the main channel is always unity.

In situations, where the number of samples used to estimate the covariance matrix is large, the SMI weights are the same as the steady state of a fully adaptive array with feedback loops. Thus, the performance of the two adaptive arrays will be the same and, a conventional SMI adaptive array

will face the same problem in our application, i.e., one may not obtain the required suppression of weak interfering signals. To overcome this difficulty, a modification to the SMI algorithm was found [11,12]. It was shown that the modified SMI algorithm can provide the required interference suppression.

In the modified SMI algorithm, the estimated covariance matrix is redefined to reduce the effect of thermal noise on the weights of the adaptive array. This is accomplished by subtracting a fraction (F) of the smallest eigenvalue of the original covariance matrix from its diagonal terms. In situations where the number of degrees of freedom of adaptive arrays is larger than the number of interfering signals, the smallest eigenvalue of the sample covariance matrix is equal to the noise power in the individual antenna elements. Thus, subtracting a fraction of the smallest eigenvalue from the diagonal terms of the covariance matrix is equivalent to reducing the thermal noise in individual antenna elements which in turn increases the input interference-to-noise ratio (INR). The adaptive array, therefore, will respond to the interfering signals and will suppress them. The larger the input INR, the larger the interference suppression [11]. Thus, by adjusting the fraction of the smallest eigenvalue which is subtracted from the diagonal terms, on can obtain the required interference suppression.

A detailed theoretical analysis of the modified SMI adaptive arrays was carried out under this grant. In the analysis [13,14], the effect of the number of samples used to estimate the covariance matrix on the performance of the modified SMI was studied. To this end, a statistical theory based on the sample covariance matrix was developed in order to characterize the

weights and output power of the modified SMI array with the number of samples as a parameter. Much of the theory is applicable to any signal scenario including wideband signals. The statistical theory was verified using Monte Carlo computer simulations. It was found that the number of samples required to obtain the maximum interference suppression as predicted by theory increases with an increase in the value of the fraction (F). The bias as well as the variance in the power of various signals at the array output increases with an increase in the value of F. Thus, one should use a lot more samples in estimating the covariance matrix.

The jitter in the adaptive array weights also increased with an increase in the value of F. It was found that by excluding the noise eigenvectors of the covariance matrix from the weight calculations, one can reduce the jitter in the adaptive array weights. A few sample results of our study are given below. In the sample results, an adaptive array with four auxiliary elements is considered. The main antenna is highly directive and is pointed in the direction of the desired signal. The auxiliary antennas are less directive and are pointed in the general direction of the interfering signals. The desired signal is incident from broadside direction to the array. The SNR of the desired signal is 14.6 dB in the main antenna while it is -10 dB in the auxiliary antennas. The performance of the array is studied when an interfering signal which arrives 30° from broadside is incident on the array. The INR is -5 dB in the main antenna while it is -3 dB in the auxiliaries. The antenna configuration is shown in Figure 5.1. Figures 5.2 – 5.4 show the SINR and INR at the array output for $F = 0$, 0.8 and 0.9, respectively as a function of the number of samples (K) used to estimate the covariance

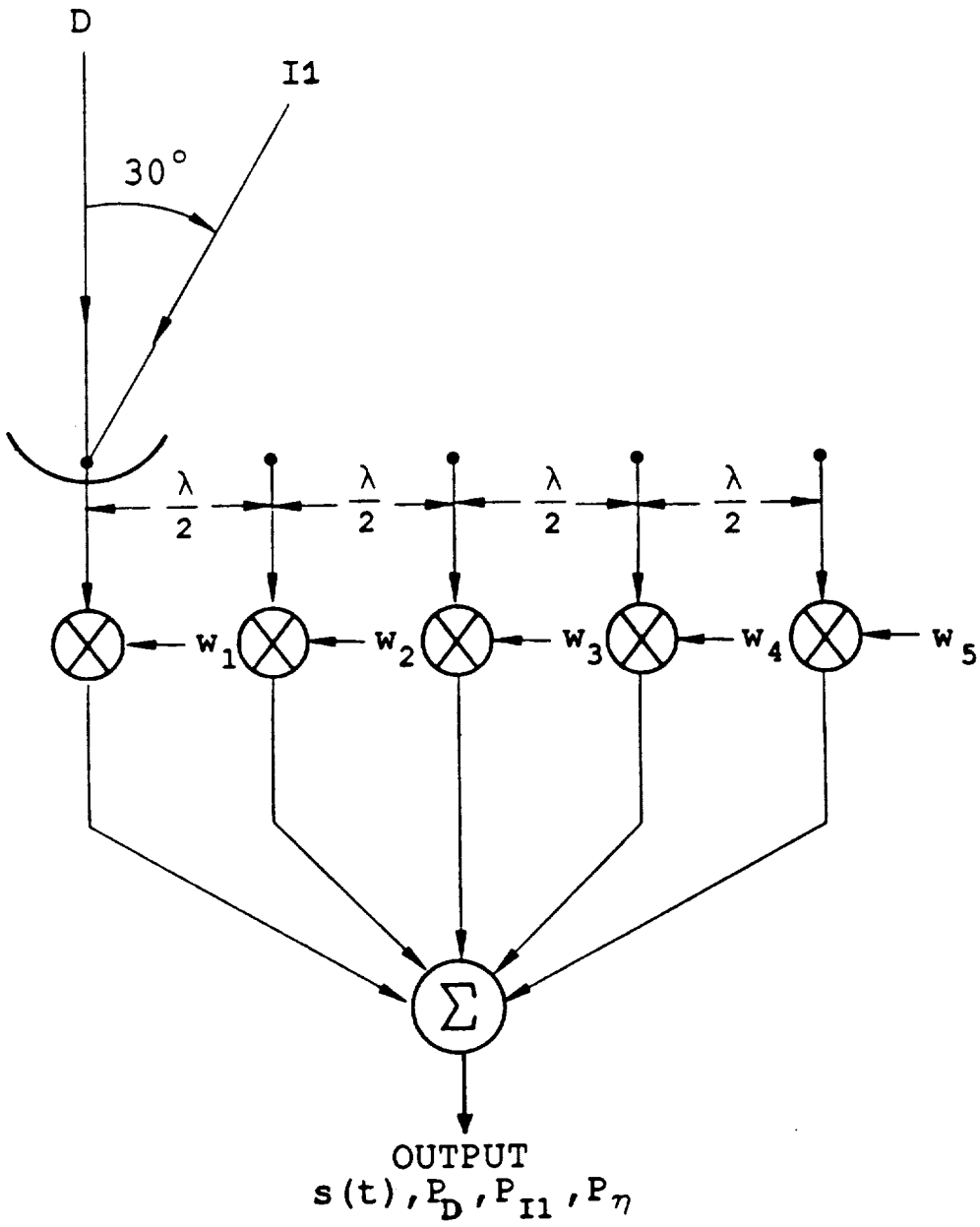

Figure 5.1: Adaptive antenna array with 4 auxiliary elements receiving a desired signal from broad side and a weak interference signal from 30° off broadside.

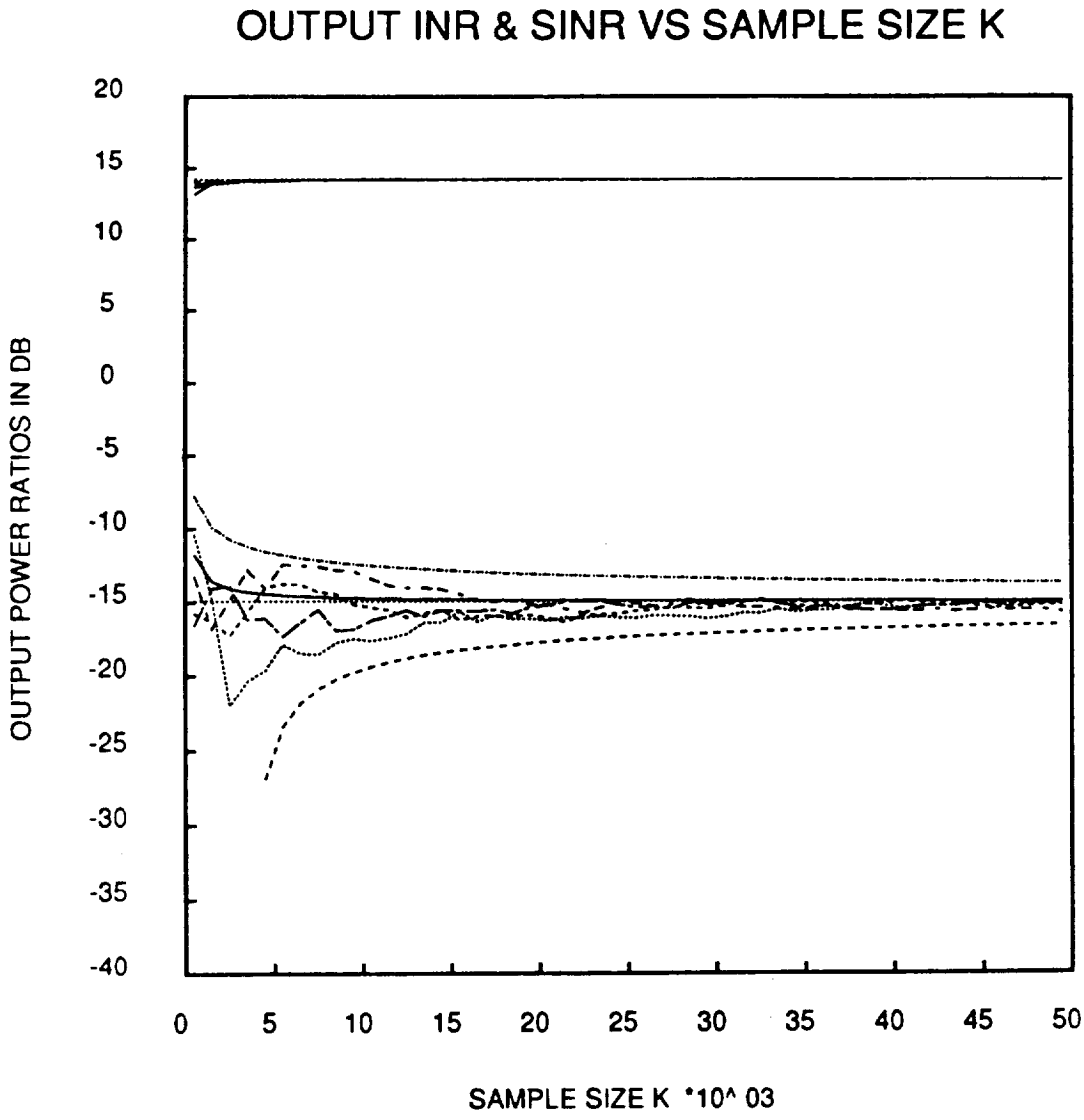

Figure 5.2: Plot of output INR and SINR versus number of snapshots K for $F = 0$.

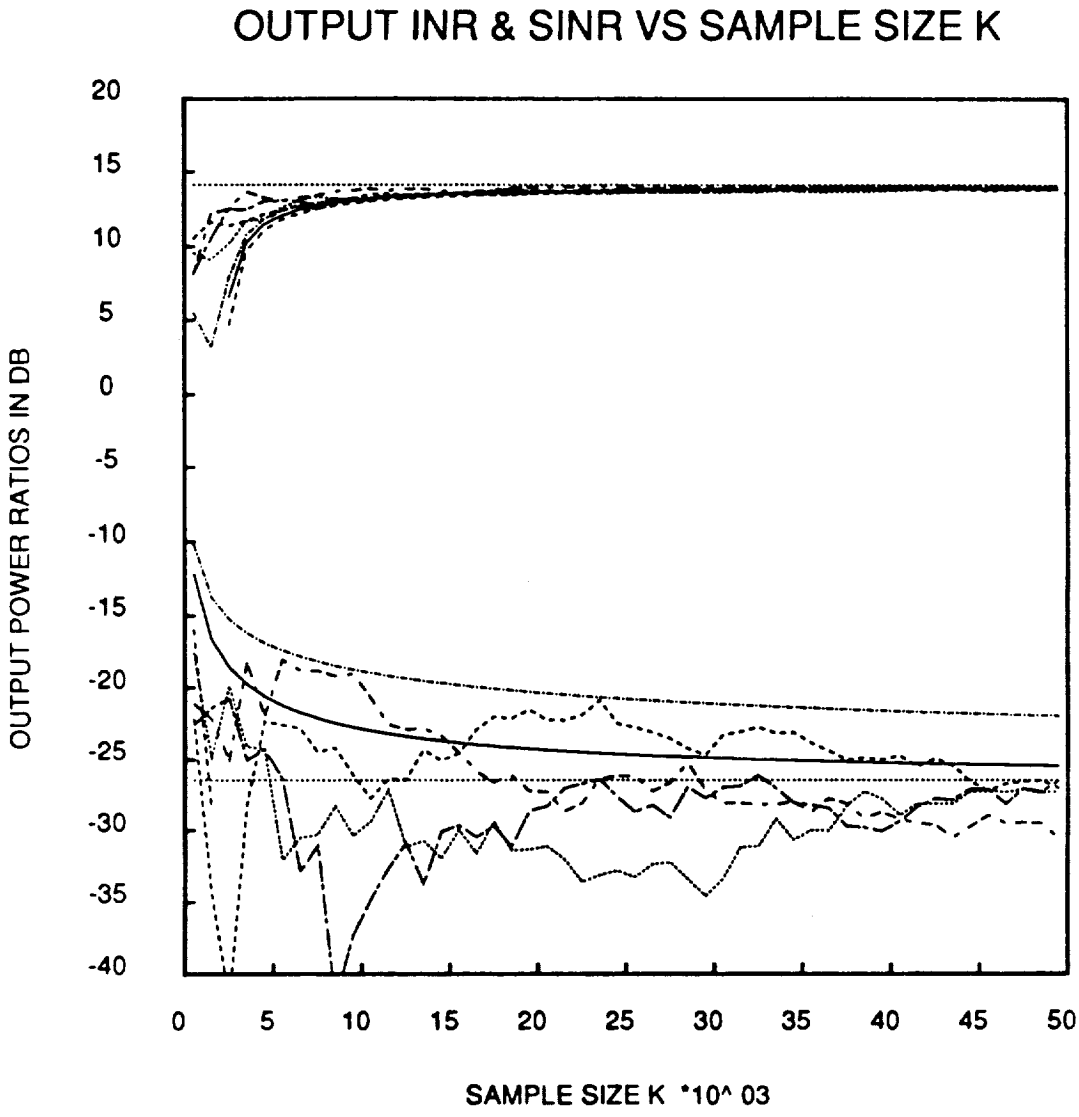

Figure 5.3: Plot of output INR and SINR versus number of snapshots K for $F = 0.8$.

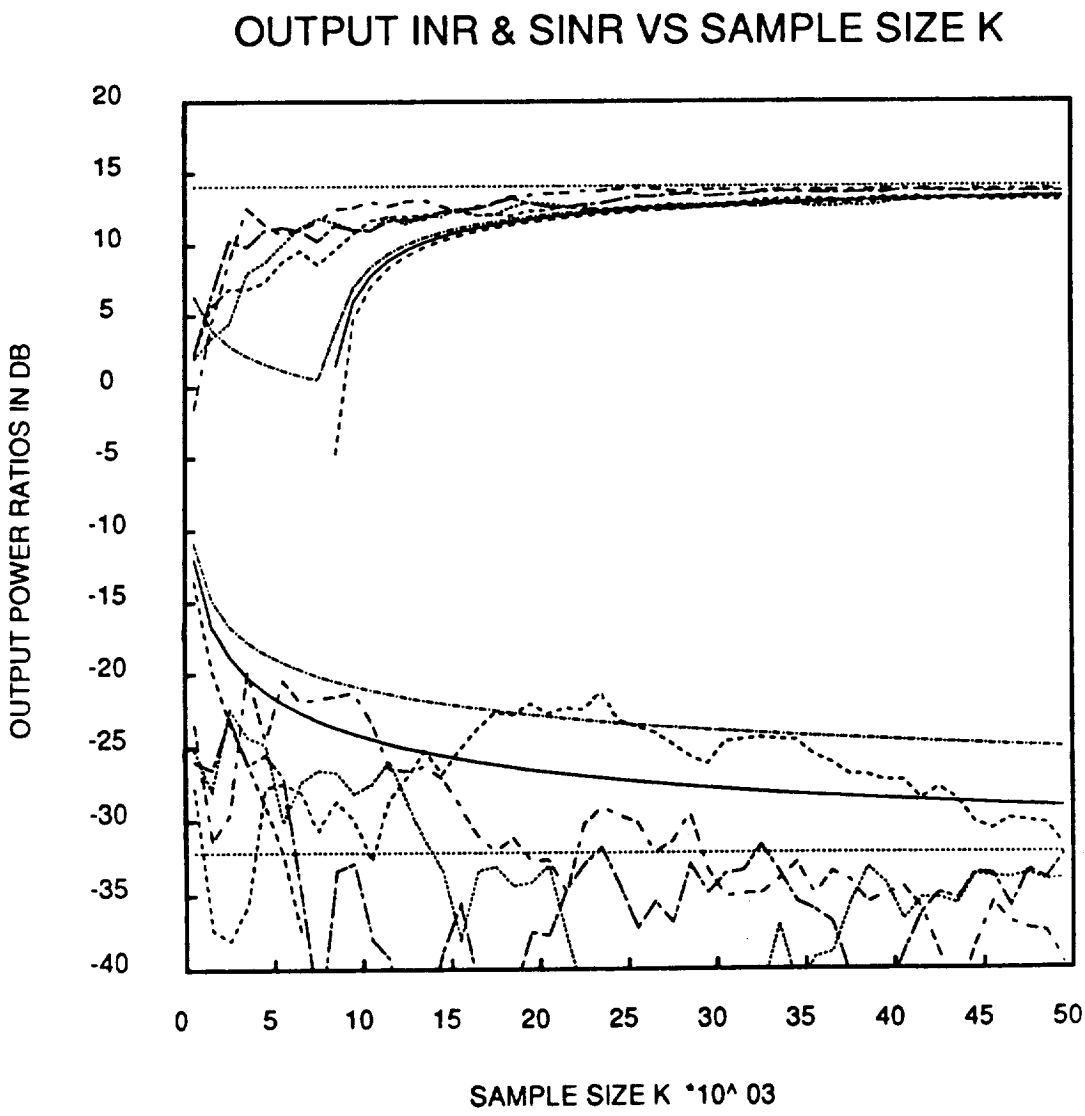

Figure 5.4: Plot of output INR and SINR versus number of snapshots K for $F = 0.9$.

matrix. In each figure, a series of plots are given. A typical figure consists of

1. A straight horizontal line giving the value of the performance measure assuming the true covariance matrix is known.

2. The expected value of the performance measure which is a smooth curve that lies among the various simulation runs and asymptotically approaches the true covariance results.

3. Two smooth curves showing the 95% confidence interval ($\pm$ 2 standard deviation) of the performance measure.

4. A number of jagged lines representing the results of monte carlo simulations

In the Monte Carlo simulations, the same set of noise seeds were used for each plot for the purpose of comparisons. Note that the output INR decreases with an increase in the value of F. The decrease in the INR, however, is accompanied by an increase in the number of snap shots required to estimate the covariance matrix. For example, comparing the plots in Figures 5.2 and 5.3, one can see that setting $F = 0.8$ increases interference suppression by about 12 dB as compared to standard SMI ($F = 0$). However, it takes approximately 30,000 snapshots (samples) to obtain the additional interference suppression. For an application in which the signal environment changes sufficiently fast, increasing K may not be practical. In the application considered here, however, it may very well be practical.

Rather than look at the power ratios let us back up and look at the powers themselves. Figures 5.5 – 5.7 show the desired signal power (P_D) for $F = 0$, $F = 0.8$, and $F = 0.9$, respectively. Similarly, Figures 5.8 – 5.10 and Figures 5.11– 5.13 show the interference powers and noise powers, respectively. The statistical bias and 95% confidence intervals resulting from the statistical analysis overlay the four trial runs and the infinite snapshot curve. Note that in all cases the statistical curves and the trial runs seem to agree rather well. The plots show that the bias and variance of the output powers tend to increase with the fraction F.

The outstanding feature of this group of plots is the comparatively large bias and variance of the interference signal power. Specifically, for $F = 0.9$, after 50,000 snapshots the difference between the upper bound of the confidence interval and the infinite snapshot interference level is about 7.5 dB whereas it is only 1.25 dB and 0.03 dB for noise and desired signal powers, respectively. The explanation is intuitive from an array pattern viewpoint. Since the modified SMI algorithm is designed to minimize interference power it will "try" to form a pattern null in the interference signal direction. As a result, the gain of the pattern in the interference direction and therefore the interference power will be extremely sensitive to inaccuracy in the covariance estimate. In fact, as F is increased the null should steepen and the interference power bias and variance should increase. On the other hand, the slope of the pattern in the desired signal direction should be small since the pattern maximum occurs near this direction, hence, the small variance in the desired signal power.

For large values of F, the variation in the noise power at the array

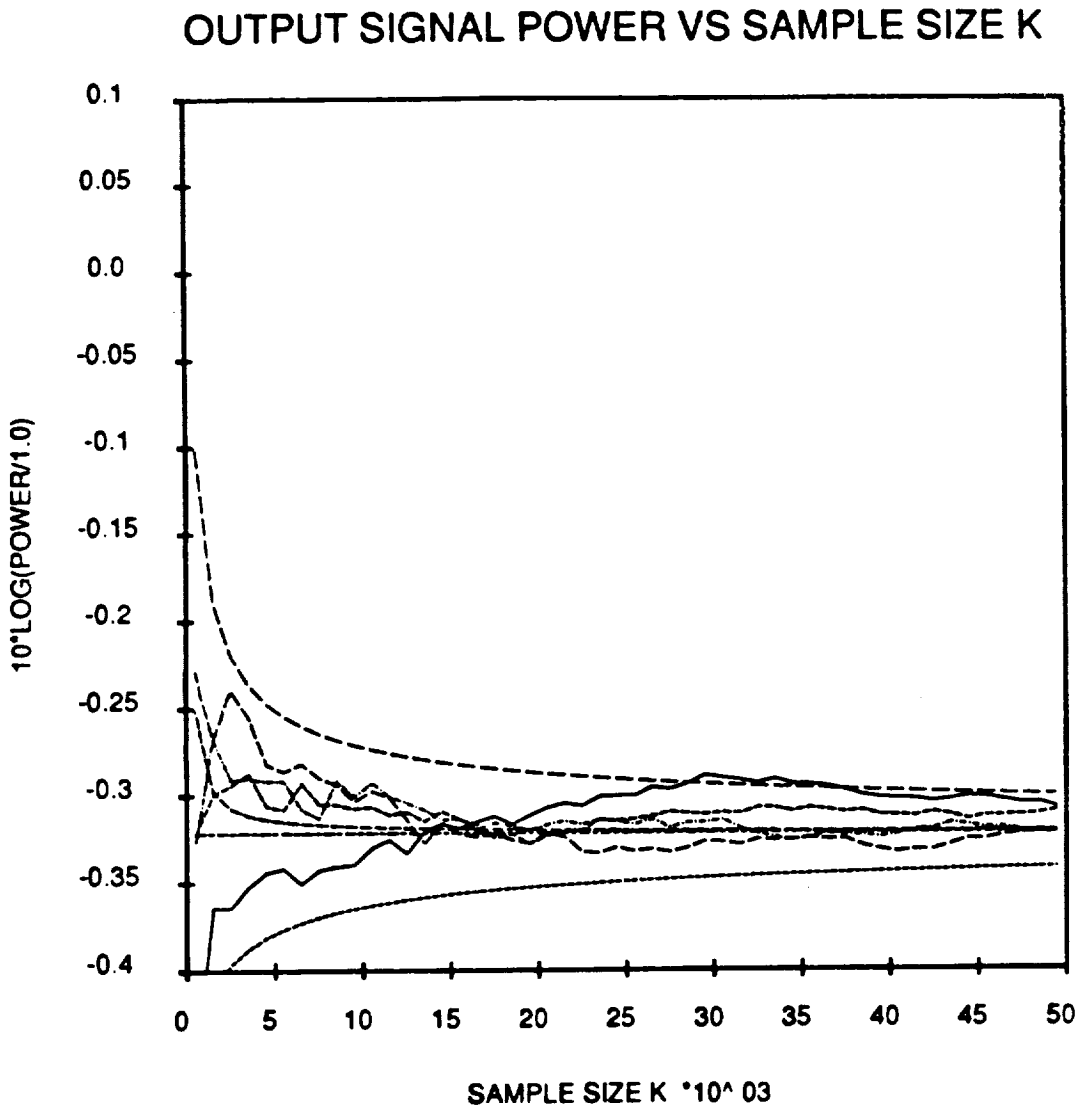

Figure 5.5: Plot of output desired signal power P_D versus number of snapshots K for $F = 0.0$.

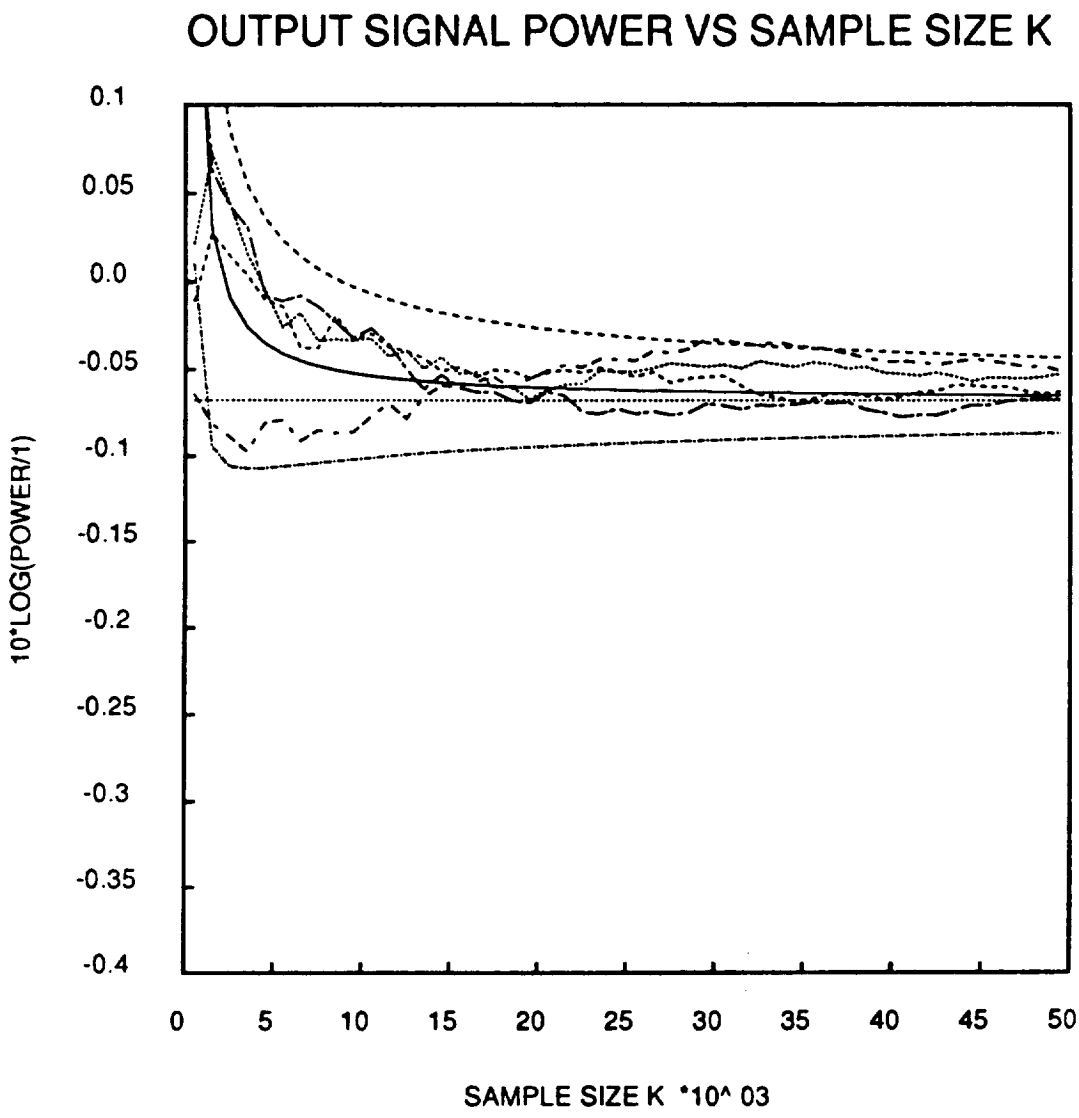

Figure 5.6: Plot of output desired signal power P_D versus number of snapshots K for $F = 0.8$.

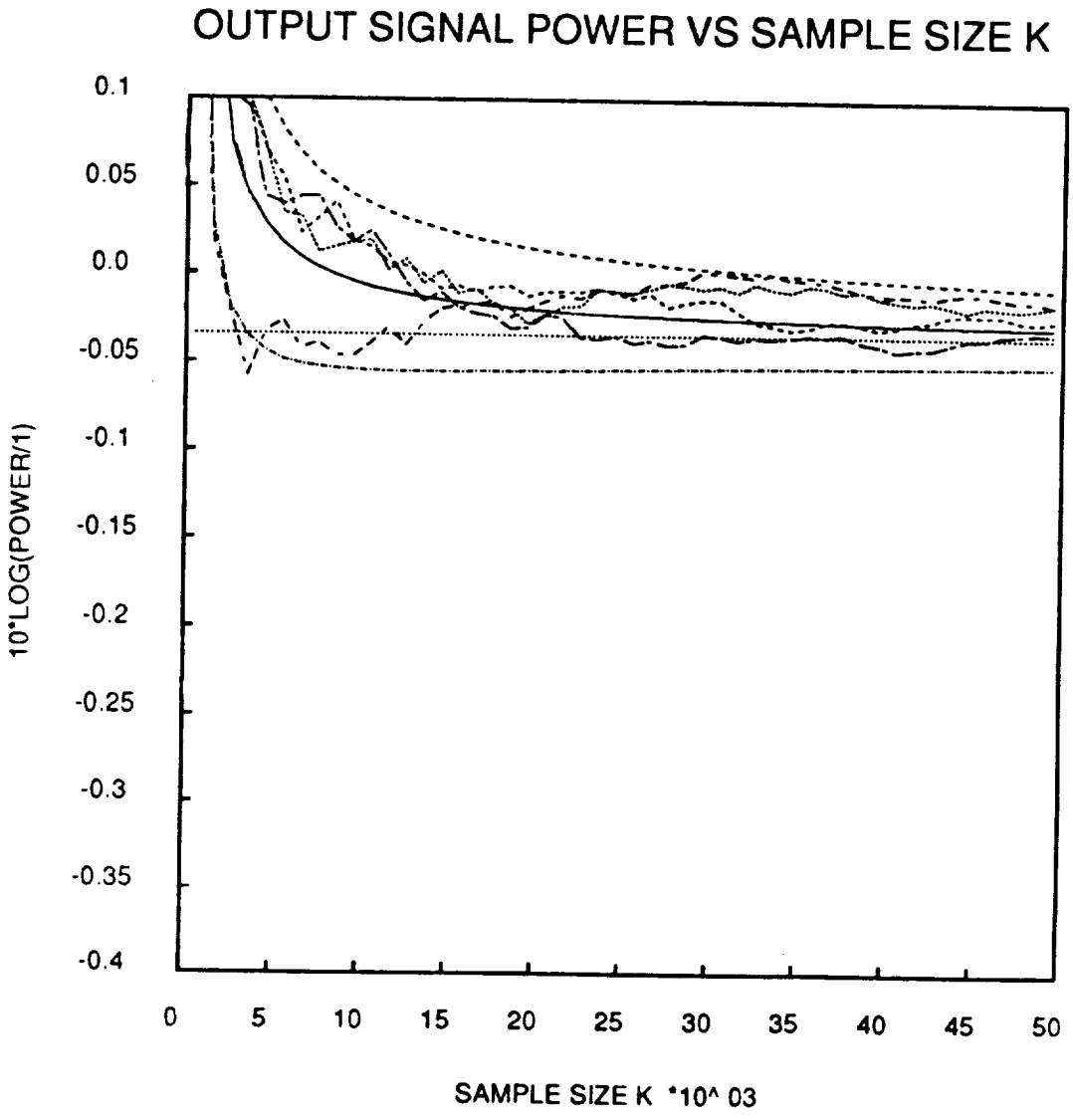

Figure 5.7: Plot of output desired signal power P_D versus number of snapshots K for $F = 0.9$.

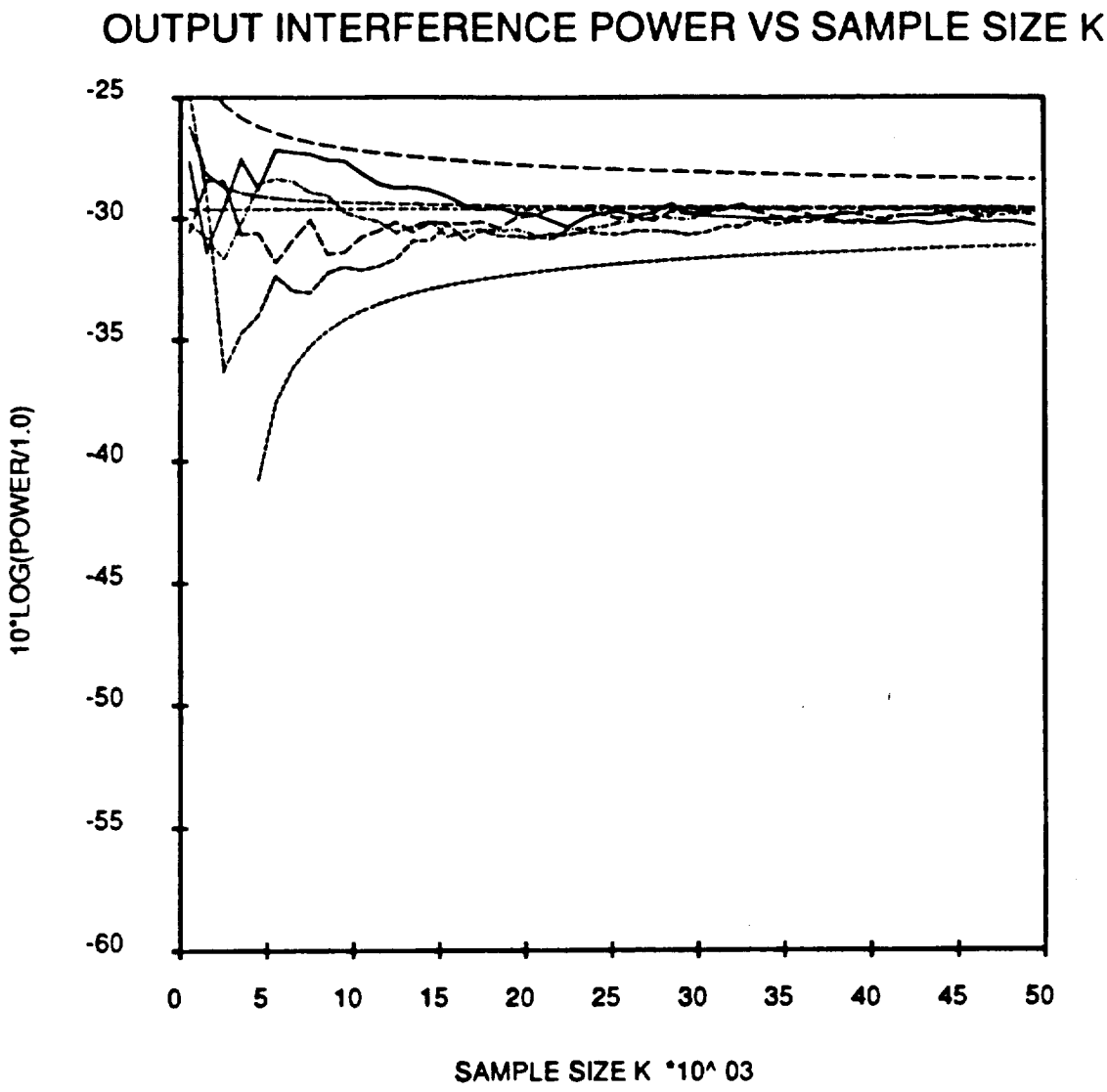

Figure 5.8: Plot of output interference signal power P_I versus number of snapshots K for $F = 0.0$.

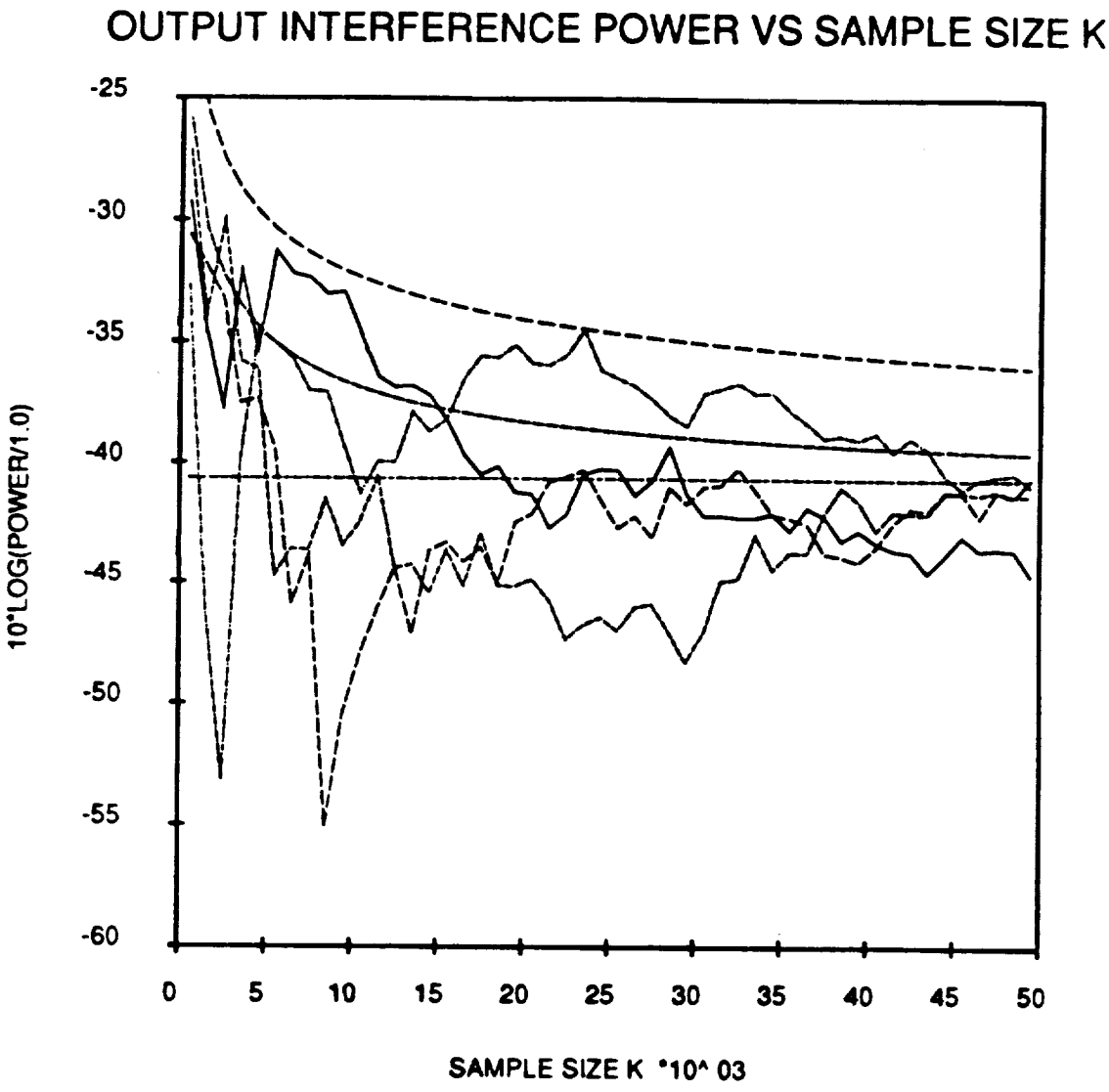

Figure 5.9: Plot of output interference signal power P_I versus number of snapshots K for $F = 0.8$.

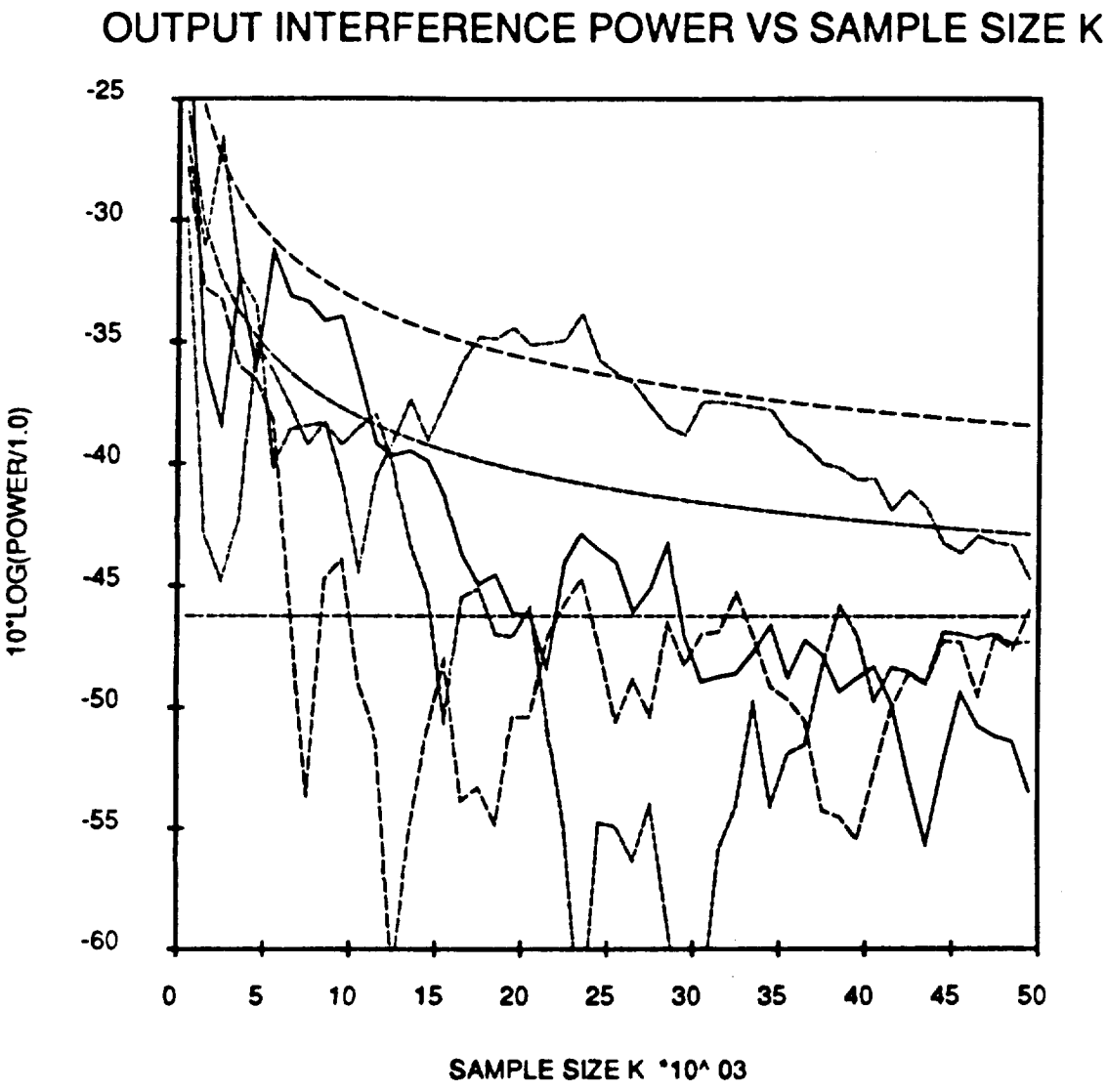

Figure 5.10: Plot of output interference signal power P_I versus number of snapshots K for $F = 0.9$.

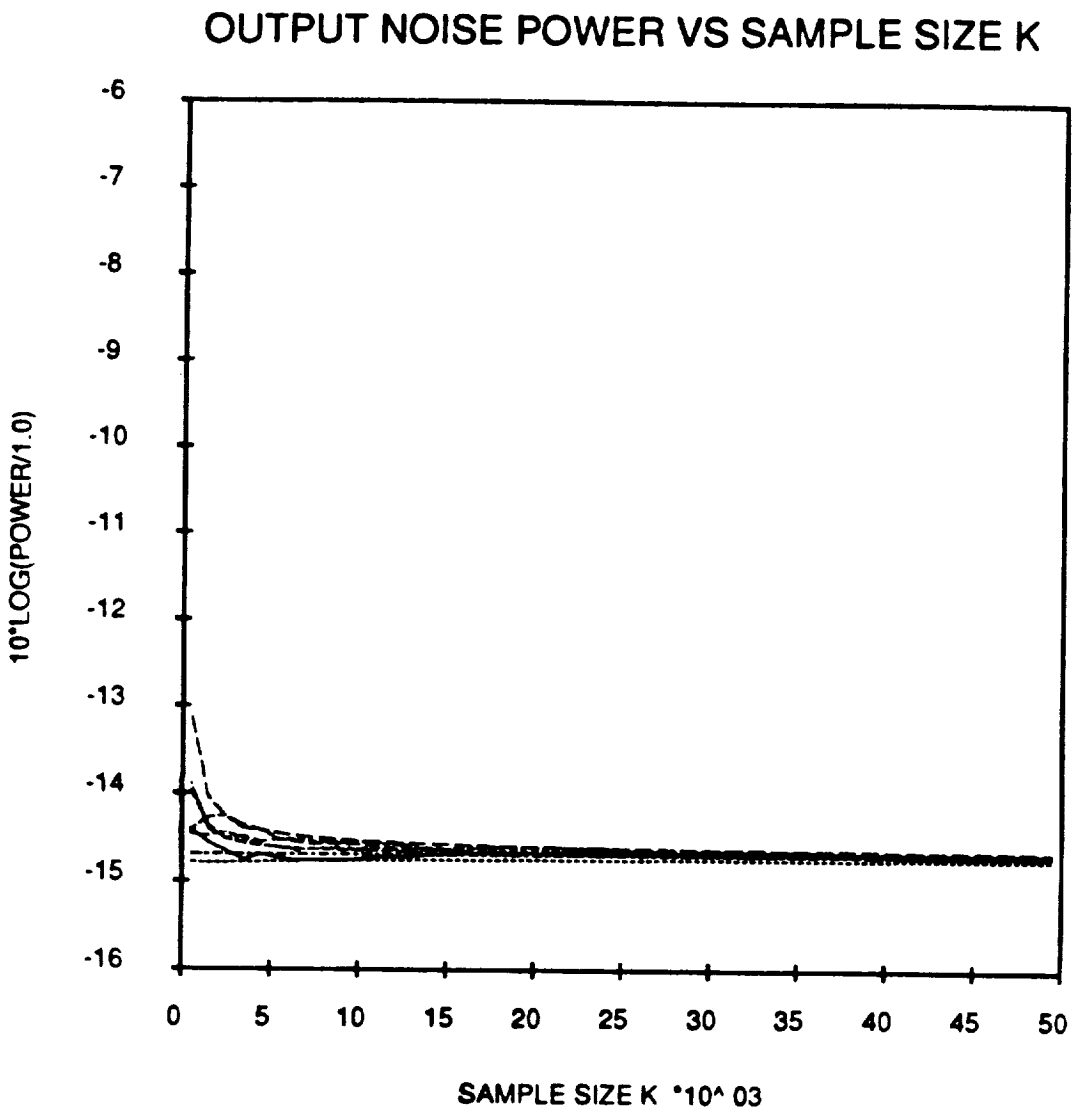

Figure 5.11: Plot of output noise power P_η versus number of snapshots K for $F = 0.0$.

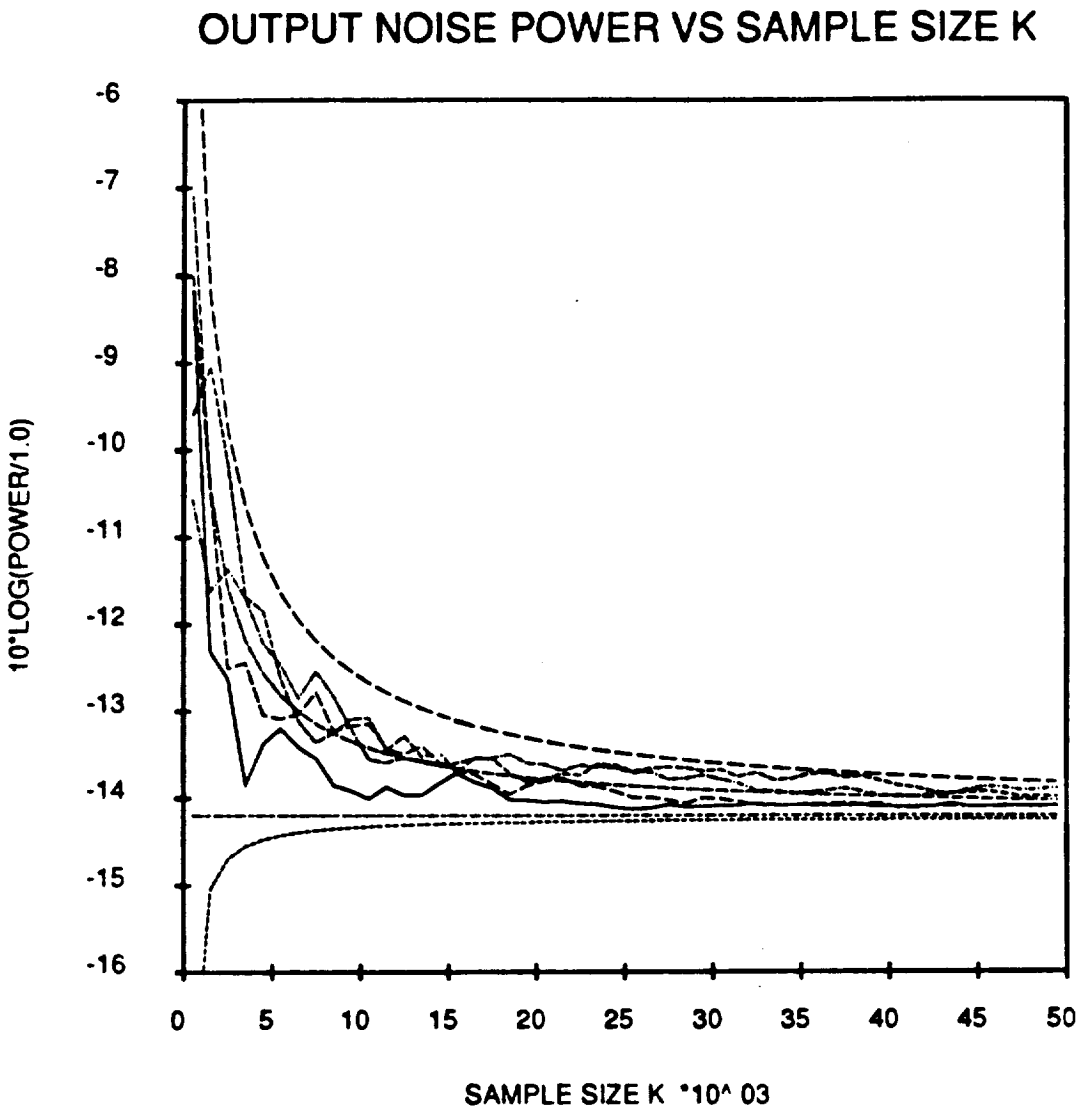

Figure 5.12: Plot of output noise power P_η versus number of snapshots K for $F = 0.8$.

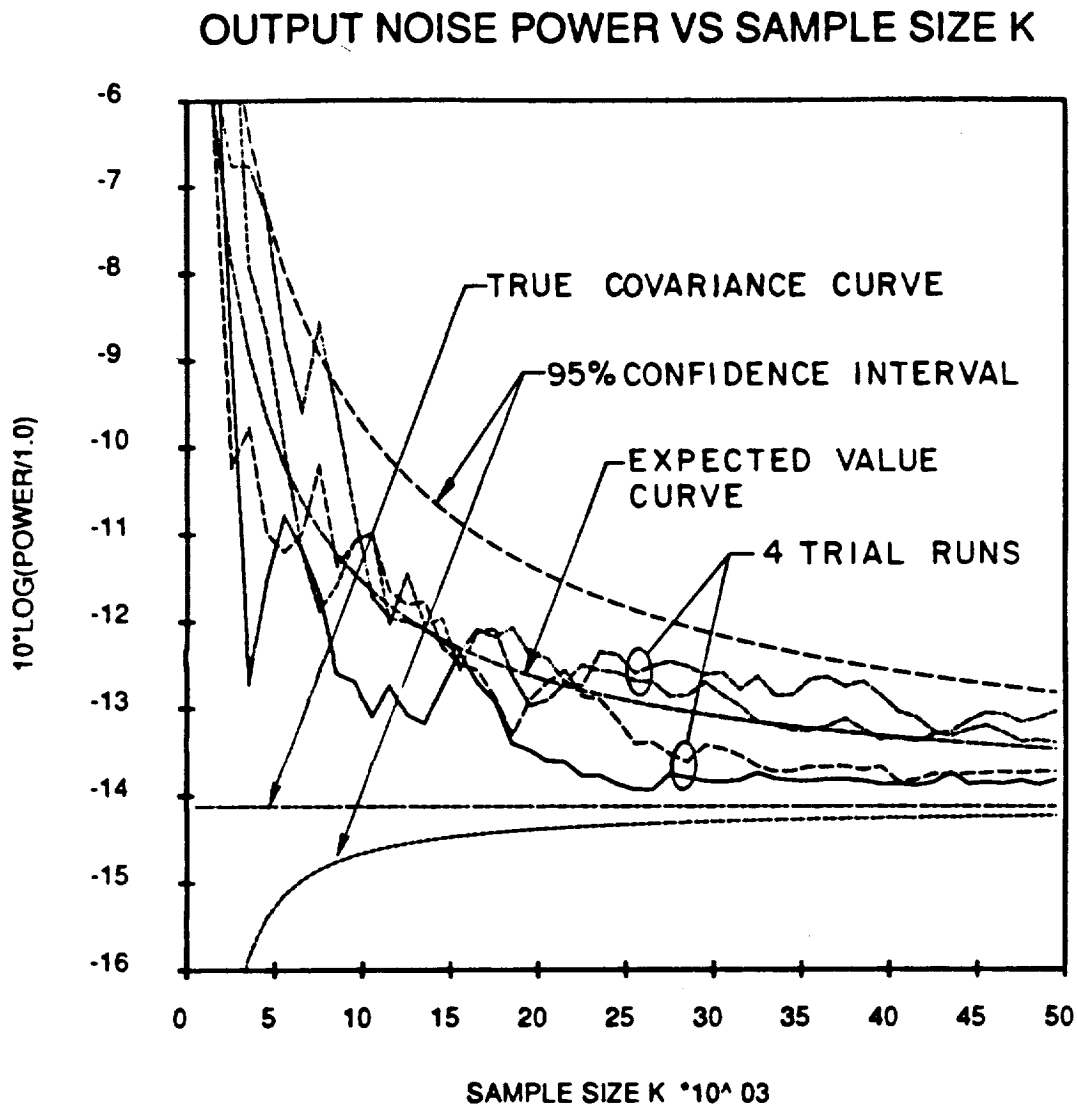

Figure 5.13: Plot of output noise power P_η versus number of snapshots K for $F = 0.9$.

output is quite significant. The variation in the noise power indicates that their is some jitter in the array weights even for large values of K. The same can be seen in the plots of Figures 5.14 and 5.15, where the real and imaginary parts of the main channel weight and the first auxiliary channel weight, respectively are plotted. F is set equal to 0.8 in these figures. One can decrease the weight jitter by excluding the noise eigenvector of the covariance matrix in the weight calculations [21]. If one does that, the weight values of the two channels (main and first auxiliary) will be as shown in Figures 5.16 and 5.17. Again F = 0.8 in these figures. Note that the jitter in the weights is no longer present.

Figures 5.18 – 5.20 show the level of the various signals at the array output when only the signal eigenvectors are used to compute the array weights. F is set equal to 0.8 in these plots. Comparing the plots in these figures with those in Figures 5.6, 5.9 and 5.12, respectively, one can see that the variation in the noise power at the array output is reduced significantly. The variation in the desired signal power and interfering signal power at the array output is more or less unchanged, which is expected. Thus, excluding the noise eigenvector from weight calculations will help in stabilizing the array weights. The number of samples required to obtain the true covariance matrix, however, will remain unchanged. Therefore, if one wants to increase the interference suppression by increasing the value of the fraction F, one should use more samples to estimate the covariance matrix.

The modified SMI algorithm was also implemented on the experimental system discussed in the previous chapters. To implement the SMI algo-

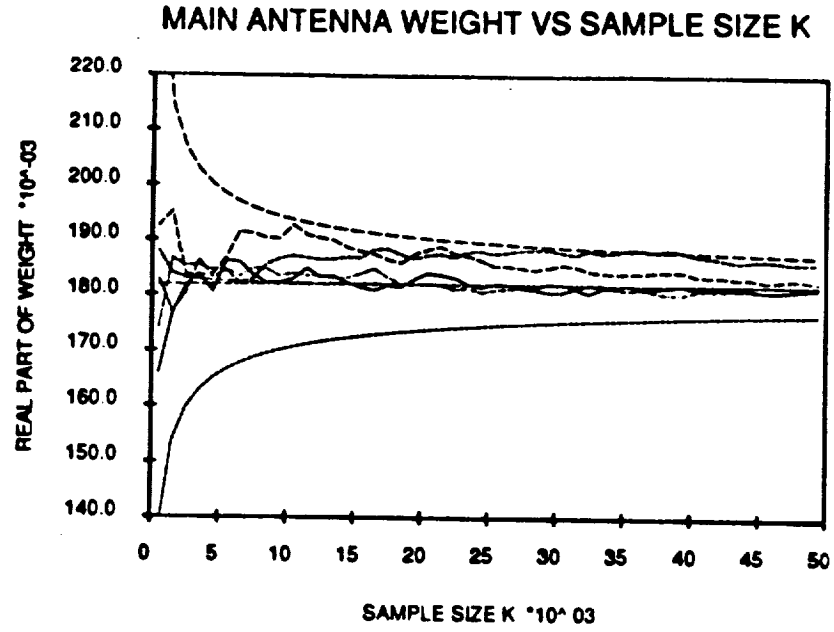

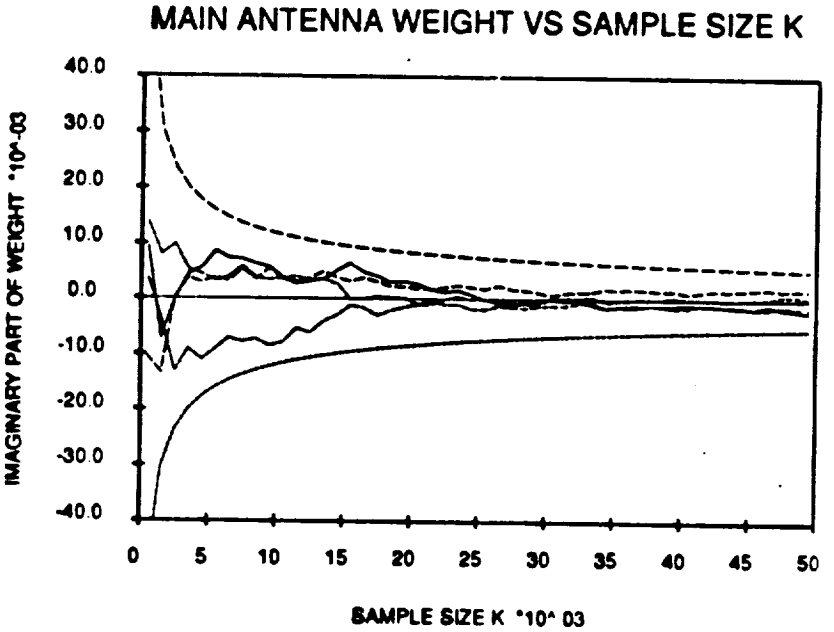

Figure 5.14: Real and imaginary parts of main element weight W_1 versus number of snapshots K for $F = 0.8$.

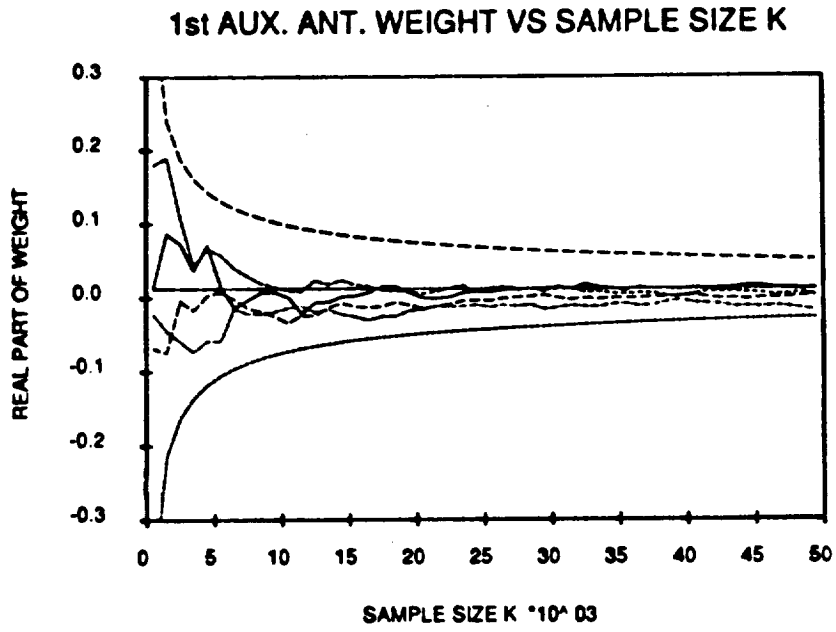

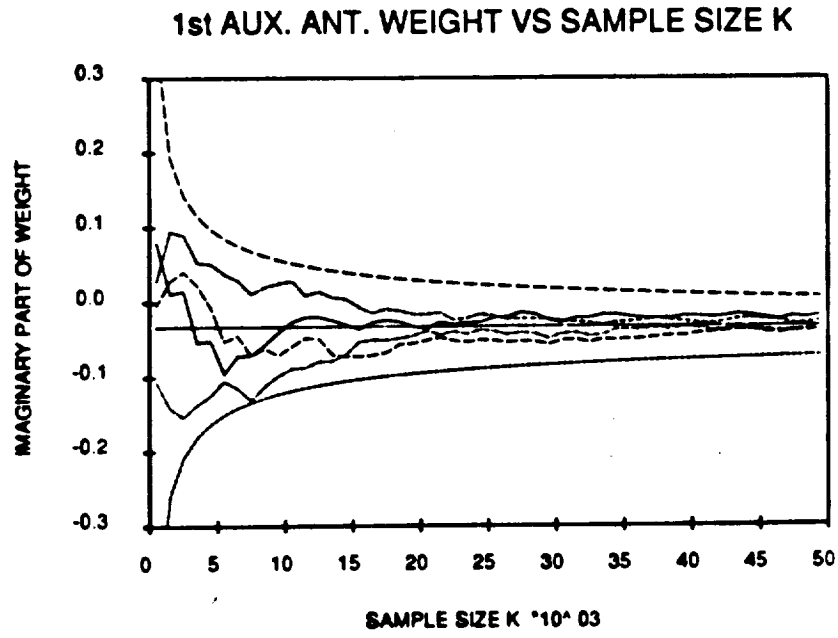

Figure 5.15: Real and imaginary parts of first auxiliary element weight (W_2) versus number of snapshots K for $F = 0.8$.

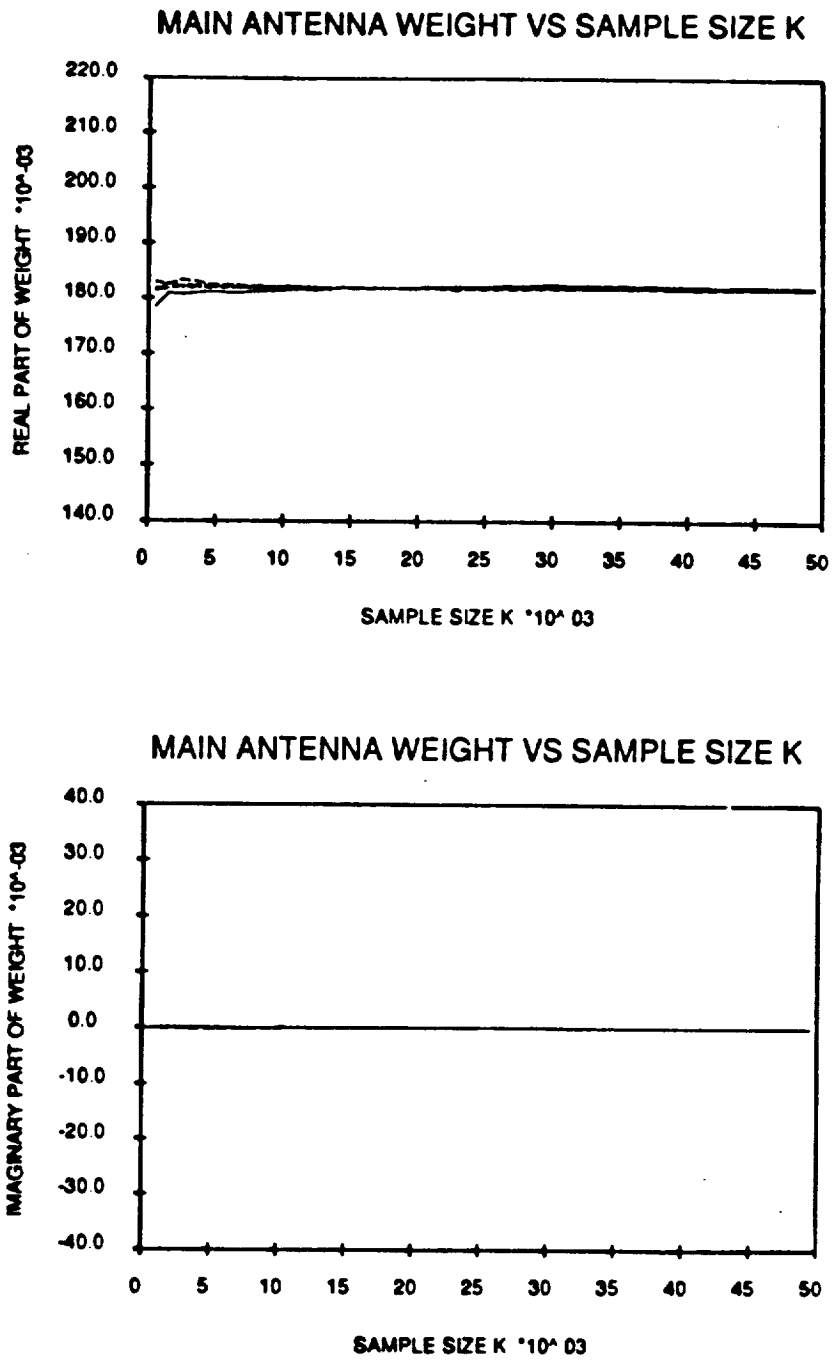

Figure 5.16: Real and imaginary parts of main element weight (W_1) versus number of snapshots K for $F = 0.8$. Only signal eigenvectors are used in the weight expression.

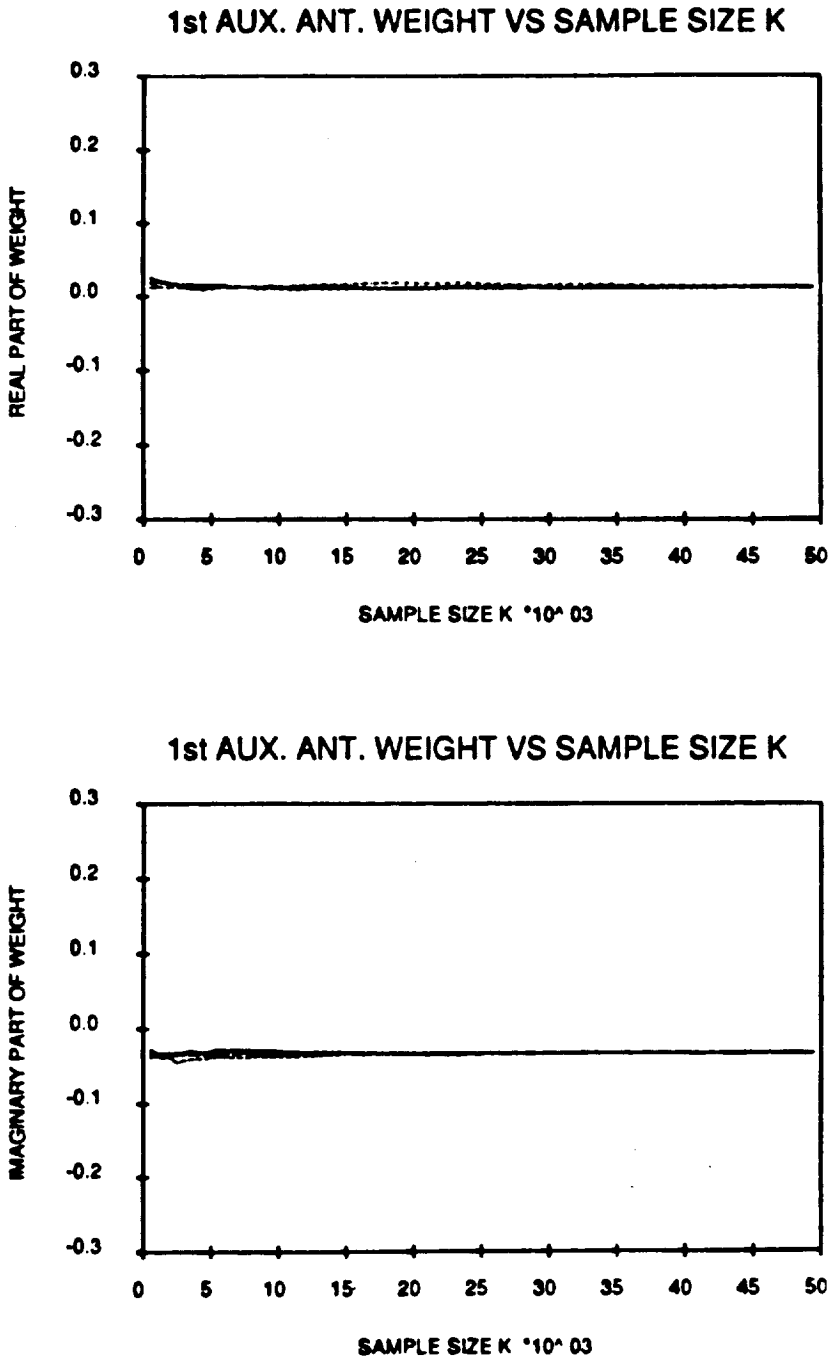

Figure 5.17: Real and imaginary parts of first auxiliary element weight (W_2) versus number of snapshots K for $F = 0.8$. Only signal eigenvectors are used in the weight expression.

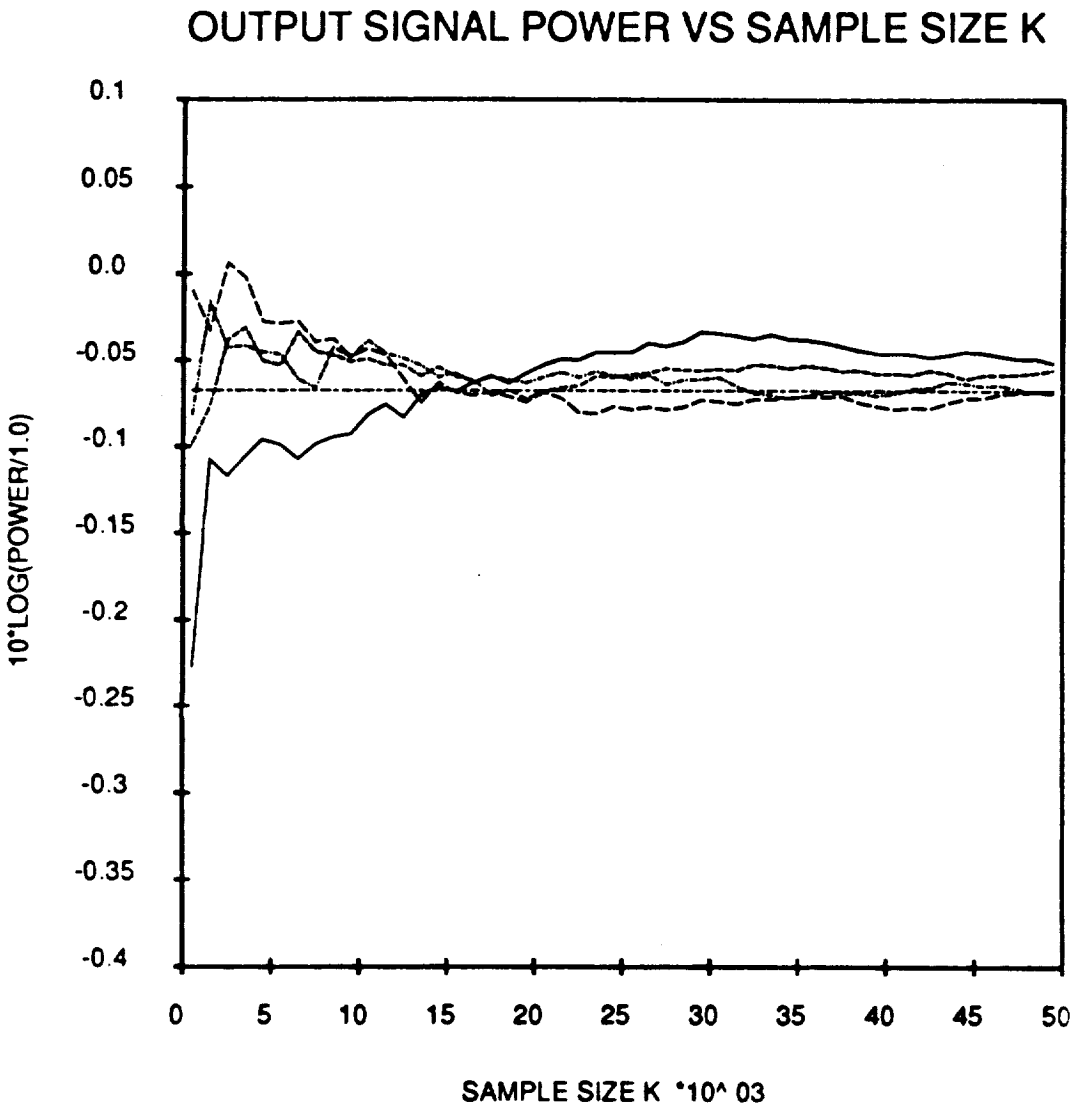

Figure 5.18: Plot of output desired signal power P_D versus number of snapshots K for $F = 0.8$. Weights were found using only the signal eigenvectors.

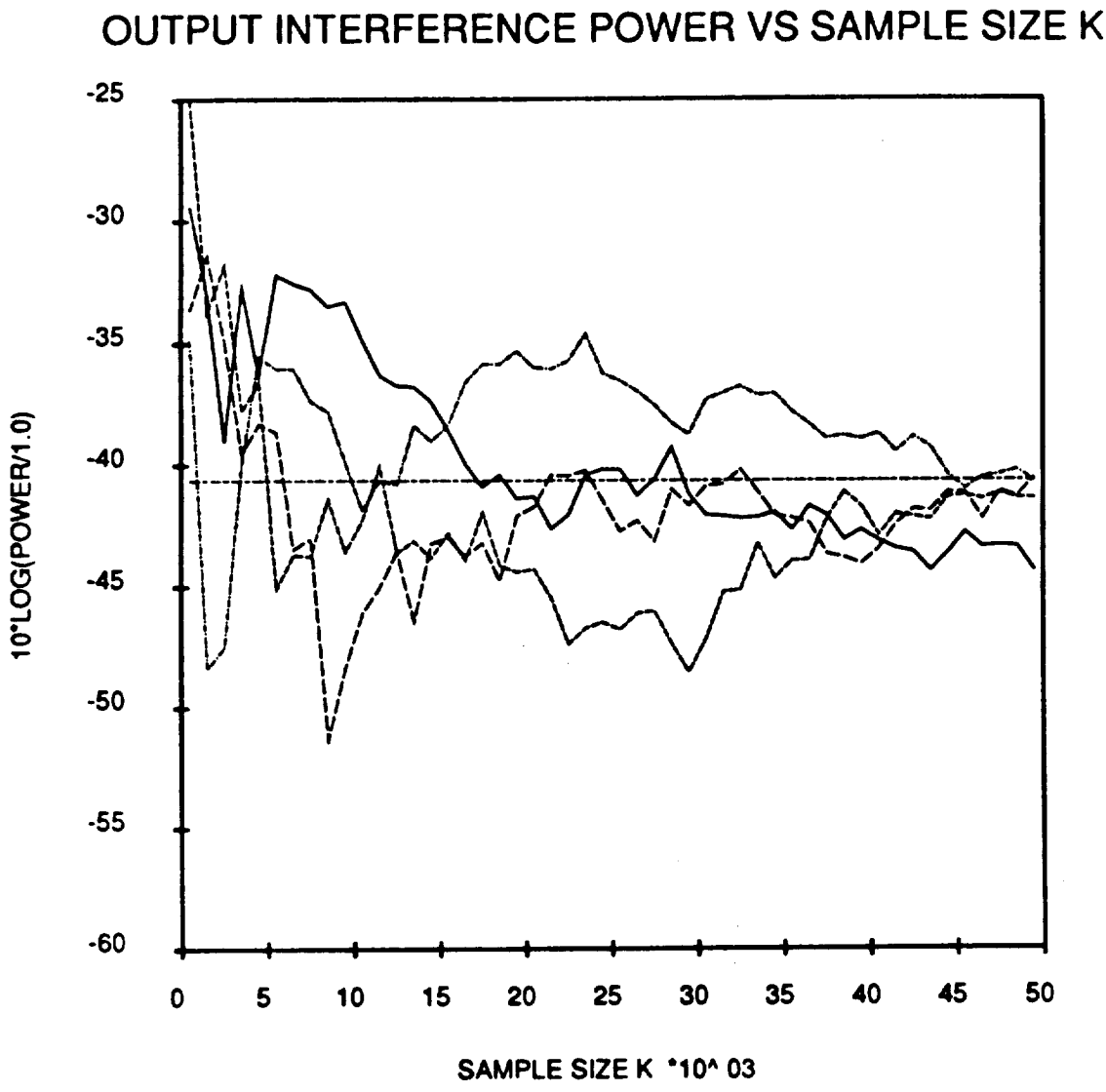

Figure 5.19: Plot of output interference signal power P_I versus number of snapshots K for $F = 0.8$. Weights were found using only the signal eigenvectors.

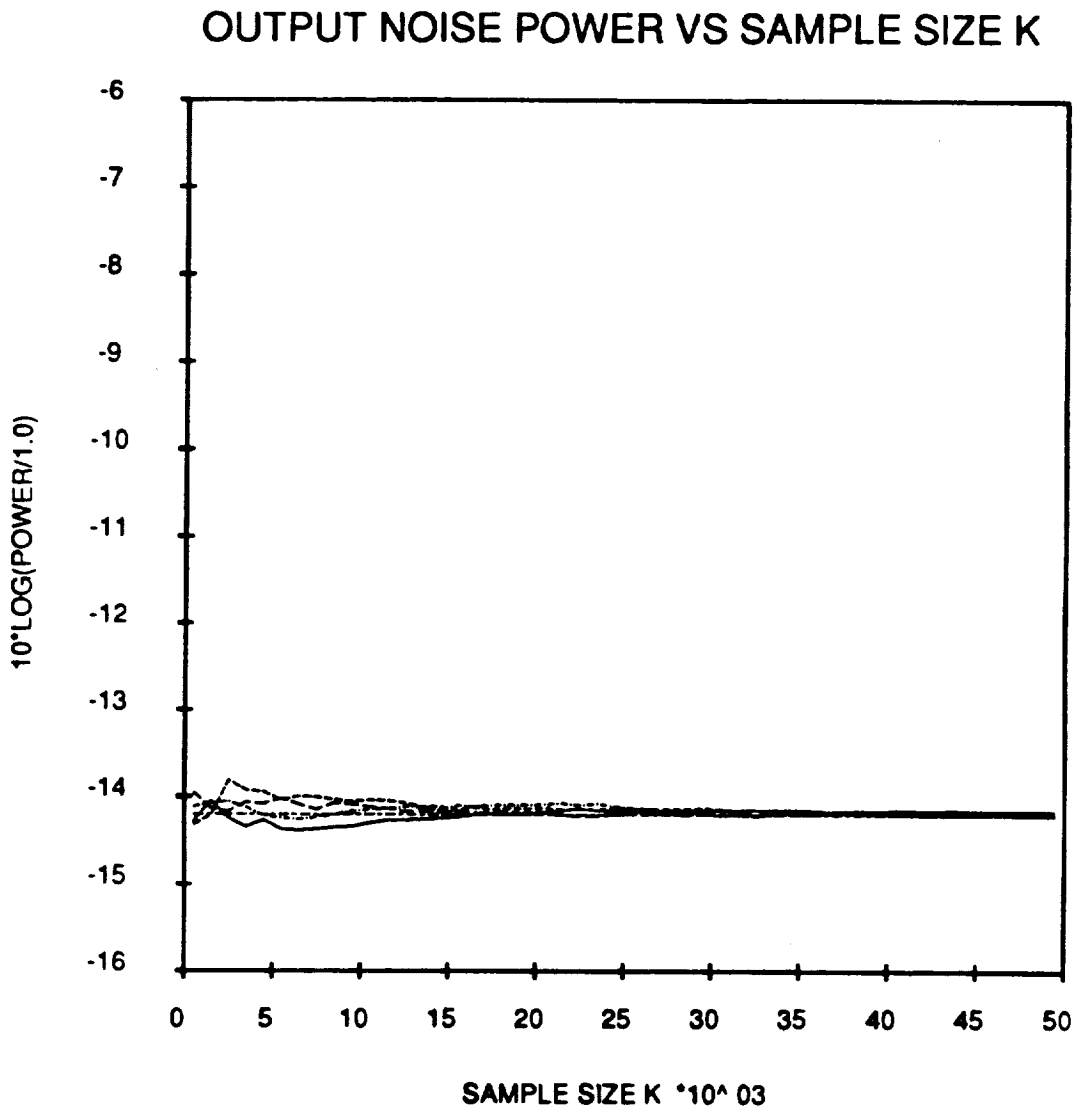

Figure 5.20: Plot of output noise signal power P_η versus number of snapshots K for $F = 0.8$. Weights were found using only the signal eigenvectors.

rithm, some hardware as well as software changes were made to the original experimental system. These changes are discussed in the next chapter. The performance of the experimental SMI adaptive array is also discussed there.

Chapter 6

Experimental Implementation of the Modified SMI

The modified SMI algorithm has been implemented on the experimental system discussed in the previous chapters. Since the experimental system is a sidelobe canceller and uses modified feedback loops to control the auxiliary channel weights, some hardware as well as software alterations were necessary in implementing the modified SMI algorithm. These changes are summarized below. For more details, one is referred to [15].

6.1 Sampling and Weighting the Main Channel

An SMI adaptive antenna requires that the main channel as well as the auxiliary channels be sampled and weighted adaptively. In the experimental system, the main channel is not equipped with a vector-demodulator(VDM) and a vector modulator (VMOD). Thus, the main channel can not be sampled or weighted directly. Instead of changing the hardware, new software

was developed to achieve the above goals. To sample the main channel, the weights of the two auxiliary channels are set to zero. Note that under these conditions, the array output signal is equal to the main channel signal except for some gain/attenuation and phase shift due to real system components. Thus, one can use the output VDM to sample the main channel. These samples are then scaled in the software to offset the gain/attenuation and phase shift. The scaling of the samples is described in the next section.

The problem of weighting the main channel was taken care of by normalizing the array weights such that the main channel weight is always unity. Thus, one does not require a VMOD in the main channel.

6.2 Scaling the Signal Samples

The SMI algorithm is an open-loop algorithm in the sense that the weights are computed using the samples of the signals received by various antenna elements. The output signal is not used in the weight computation. Thus, for the optimum performance the value of the signal samples should be exactly equal to the signal levels at the respective ideal VMOD. To meet this requirement, the samples read from the A/D converters in the experimental system are scaled in the software before estimating the covariance matrix. The scaling compensates for the losses and phase shift through the non-ideal hardware components of the array processor in the experimental system. Figure 6.1 compares the block diagram of the ideal system to our experimental processor. The 9 dB attenuators in the auxiliary channels represent the inherent loss through the vector modulators when the weights

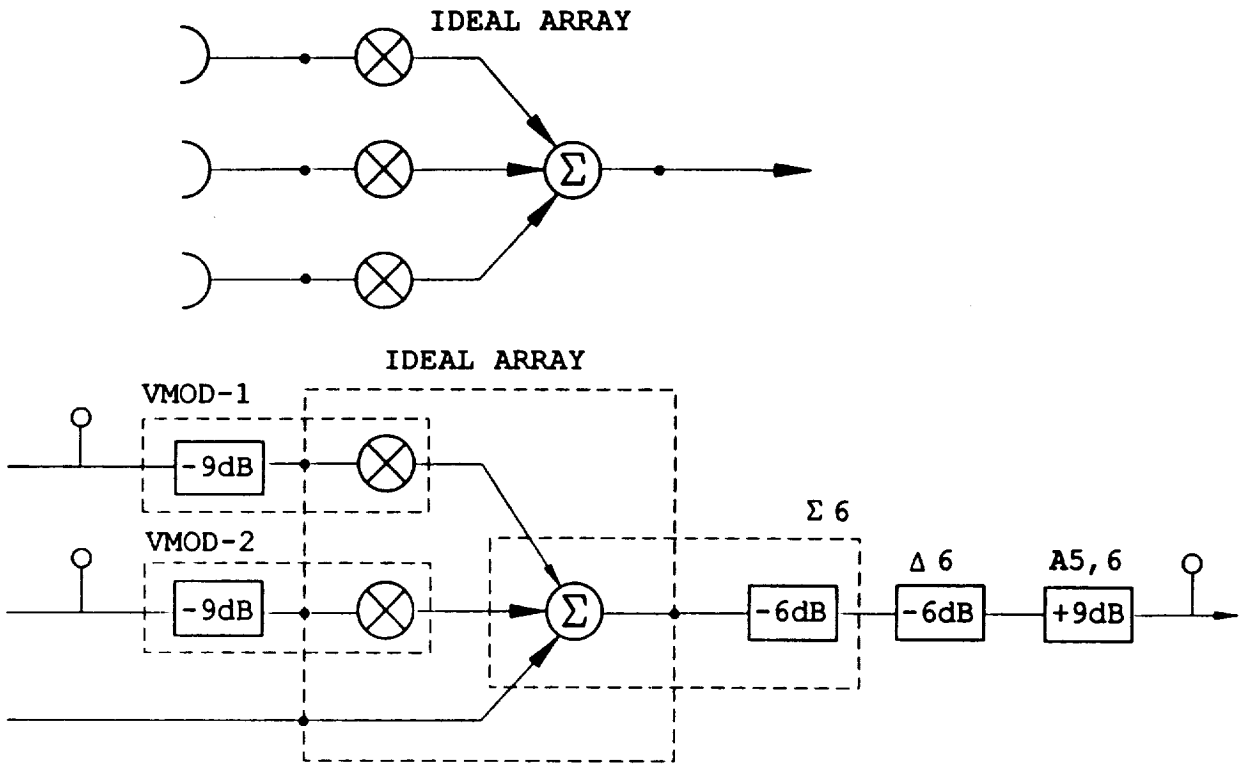

SIMPLE MODEL OF EXPERIMENTAL SYSTEM

Figure 6.1: Comparison of an ideal array with the experimental system.

are equal to unity. The first 6 dB attenuators at the output represents the loss through the summer, Σ_1 (see Figure 3.4); while the second 6 dB attenuator represents loss through the 4-way power divider $\Delta 6$ in the array processor. The 9 dB gain accounts for the fact that A5 and A6 are set at a value 9 dB higher than A1 - A4 in order to use the full dynamic rang eof the A/D convertor. Note that since the array weights are normalized, the absolute settings of A1 - A6 are not important. Thus, the auxiliary channel samples should be attenuated by 9 dB; while the main channel samples should be amplified by 3 dB before estimating the covariance matrix. This scaling of samples is done in software as soon as the samples are retrieved from the A/D convertors.

The scaling of samples described above represents a coarse amplitude adjustment in that the loss or gain values of the various components listed above is not exact. For example, the inherent loss through the VMOD is not exactly equal to 9 dB. Furthermore, phase shifts through the real devices have not yet been offset. A further scaling of the sampled signals is, therefore, done using a calibration technique. This technique is described in [15].

The fine scaled samples are then used to estimate the covariance matrix and to update the array weights using the modified SMI algorithm. The PDP 11/23 computer used in the experimental system is used to compute the new weights. In the case of bench generated signals, the computer is also used to evaluate the system performance. The computer code and the procedure used to read the sampled results, update the array weights and evaluate the system performance is described in [15], where a listing

of the computer code is also attached. Some tests performed to evaluate the system performance are described below. The tests include the bench generated signals as well as the TVRO signals received by the ground station described in the last chapter. The system performance using bench generated signals is described first.

6.3 Performance Using Bench Generated Signals

To evaluate the system performance using bench generated signals, the signals simulator and the array simulator in the experimental system were used. The signal scenario consisted of a desired signal and a weak interfering signal. Thus, interfering signal #2, I_2, was turned off. The array simulator in the experimental system simulates a five element array. The SMI algorithm requires only 3 antenna elements. One for the main channel and one each for the two auxiliary channels. Therefore, only three outputs of the array simulator were used for the SMI experiments. Two of the three outputs were the main channel and the AUX-1 signal branch (see Figure 3.3). The third output was either AUX-2 signal branch or AUX-1 correlator branch. The Aux-1 signal branch and Aux-2 signal branch (or Aux-1 correlator branch) outputs were split into two parts using two-way power dividers. One output of the two-way power divider was connected to the VMOD, while the other was connected to VDM for sampling.

Figures 6.2 – 6.4 show the output SINR and the output INR of the experimental system as a function of the number of samples (K) used in

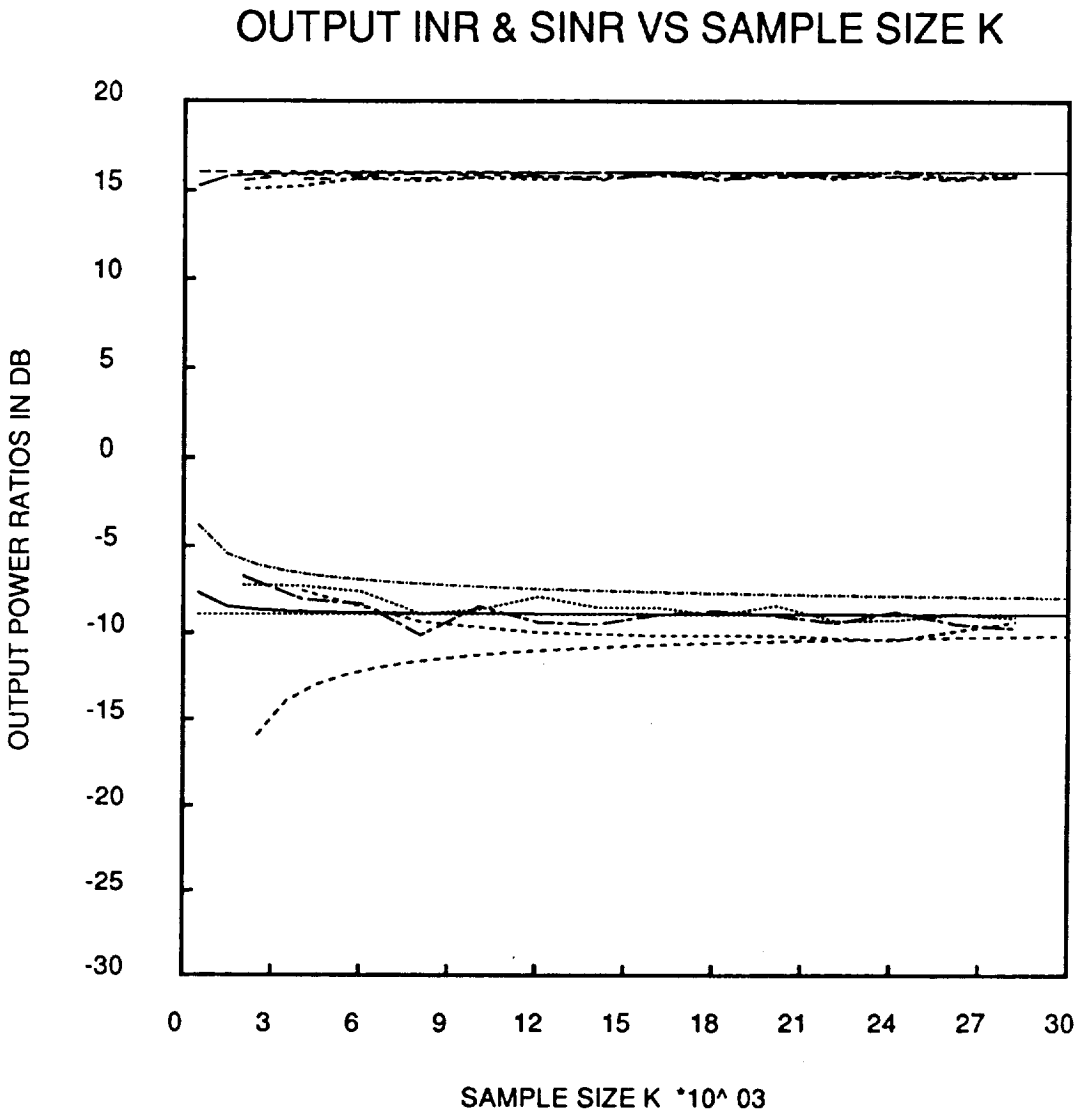

Figure 6.2: Output INR and SINR versus number of snapshots (K). The figure shows 3 experimental curves, expected value, 95% confidence interval and the infinite sample value, $F = 0$.

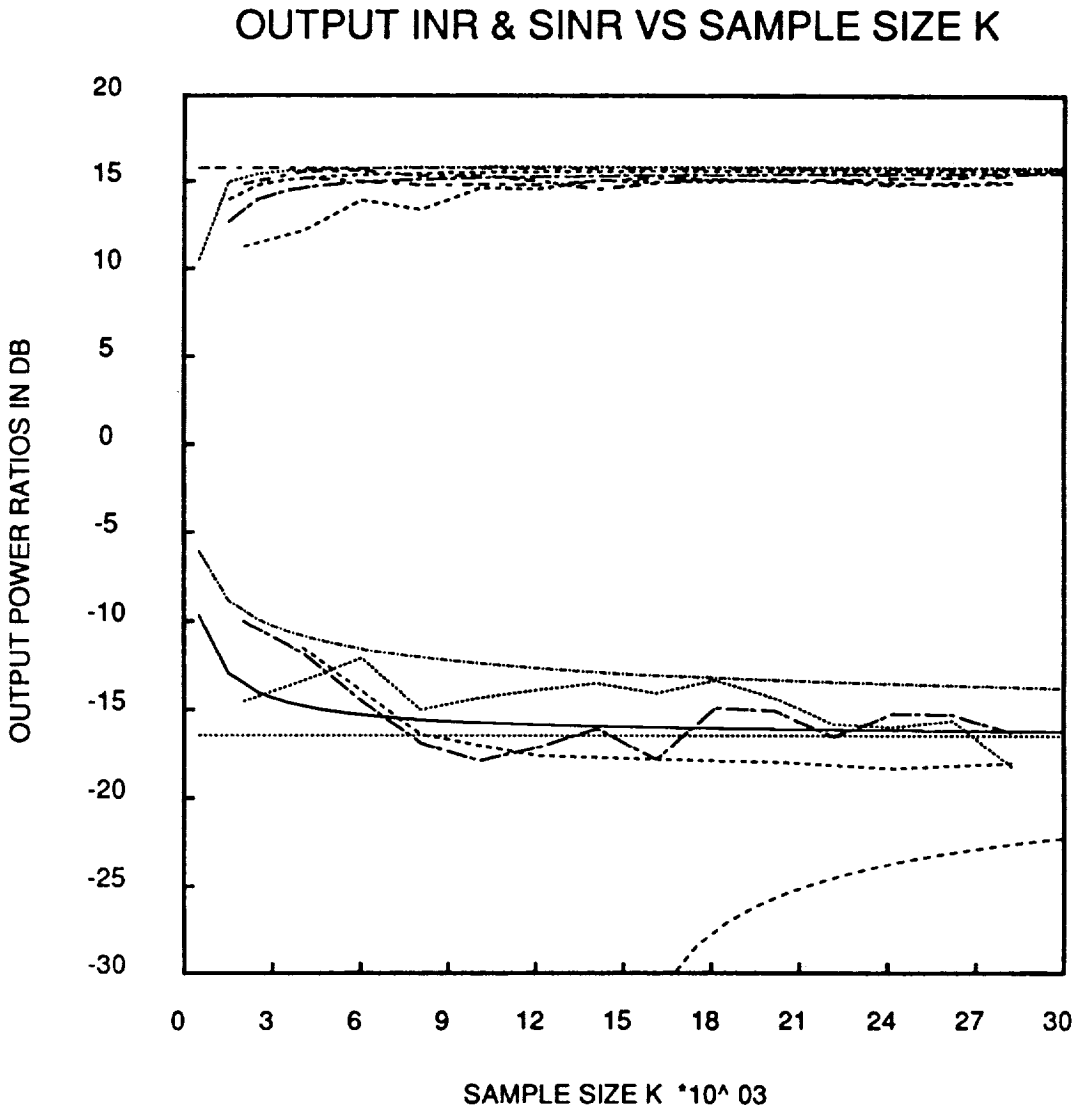

Figure 6.3: Output INR and SINR versus number of snapshots (K). The figure shows 3 experimental curves, expected value, 95% confidence interval and the infinite sample value, $F = 0.7$.

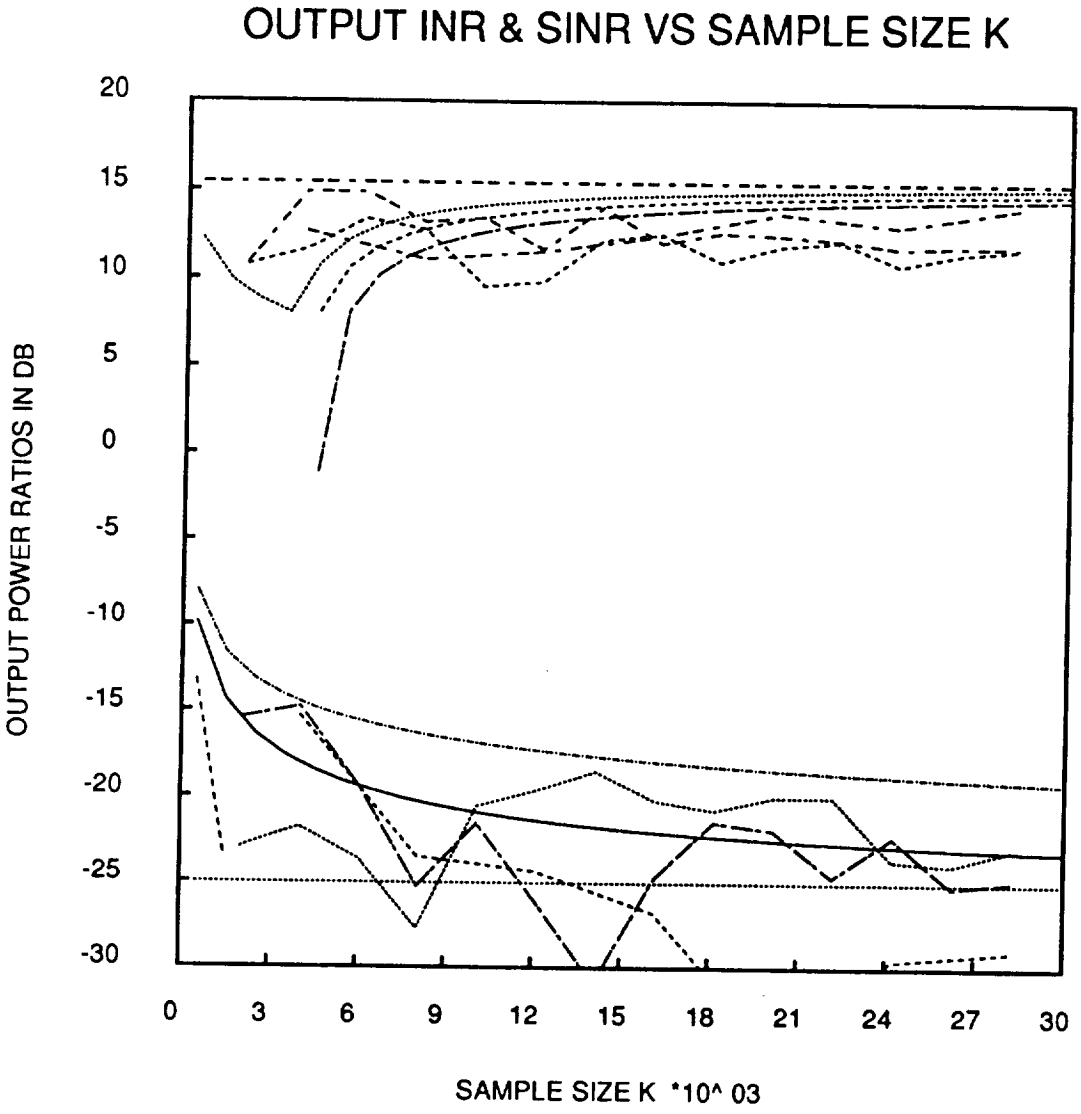

Figure 6.4: Output INR and SINR versus number of snapshots (K). The figure shows 3 experimental curves, expected value, 95% confidence interval and the infinite sample value, $F = 0.9$.

the estimation of the covariance matrix for fraction, F, equal to 0., 0.7 and 0.9, respectively. The SNR in the main channel is 17.17 dB. The desired signal level in the auxiliary channel is negligible. The INR (main) is equal to -2.08 dB; while INR in the two auxiliaries is 0.09 dB and -15 dB, respectively. The interference signal arrives at 21° from broadside for half wavelength spaced elements. The noise power is approximately the same in all channels. The statistical performance as obtained from theory [13,14] is also shown in the figure. Note that the experimental output INR curves show good agreement with the theoretical performance. The output INR decreases with an increase in the value of the fraction, F. However, one requires more samples to obtain the desired interference suppression.

For small values of F, the experimental output SINR also shows good agreement with the theoretical output SINR. However, as the fraction, F, is increased to 0.9, the experimental output SINR shows degradation up to 3.5 dB beyond that predicted by theory even after 28000 snapshots are used in the covariance matrix estimate. In order to examine this behavior more closely it is helpful to observe the signal powers themselves.

Figure 6.5 shows the output desired signal power curves for $F = 0$, $F = 0.7$, and $F = 0.9$. From the plots in the figure, one can see that the desired signal power is certainly not the cause of the experimental SINR degradation noted above since excellent agreement is observed between theoretical and experimental desired signal power curves. Note that the desired signal power has relatively small variance and changes very little as a function of F. The explanation for these observations is that the input desired signal power in the auxiliary elements is very small and thus the choice of weights

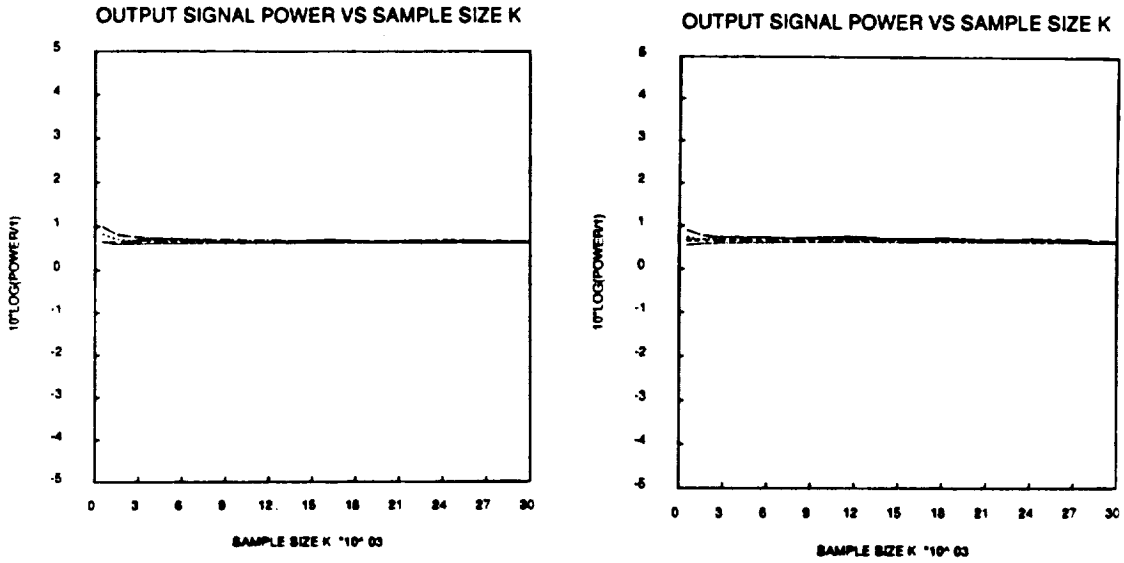

(a) $F = 0$ (b) $F = 0.7$

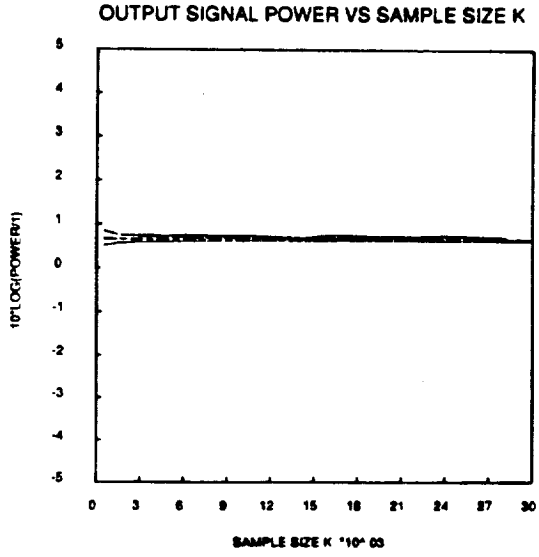

(c) $F = 0.9$.

Figure 6.5: Output desired signal power versus number of snapshots K.

does not affect the output desired signal power.

Figure 6.6 shows the output interference power for $F = 0$, $F = 0.7$, and $F = 0.9$. Again we see a reasonable agreement between the experiment and the theory for all three values of F. The ideal (infinite-K) interference suppression (horizontal line) increases as expected from -25 dB to -32 dB to -40 dB as F increased from 0 to 0.7 to 0.9. It is more practical to note that the upper bound of the confidence interval decreases by approximately 10 dB over these values of F. In other words, we see that the interference power variance increases as F increases. Note again that the experimental behavior of the interference power is not responsible for the degraded output SINR, especially since the output interference power is small compared to the noise power.

Figure 6.7 shows the output noise power curves for the three values of F. The experimental noise power performance is seen to degrade with respect to the predicted by theory as F increases. For $F = 0.9$, the experimental noise power curves are as much as 3 dB higher than the confidence interval upper bound. The high noise power, thus, accounts for the degradation in the experimental output SINR.

As pointed out in the last chapter, the large variation in the noise power is due to the large weight jitter; which, increases with an increase in the value of the fraction. One can observe the large variation in the weight values in the plots of Figures 6.8 and 6.9, where the auxiliary channel weight values are plotted. In these plots, F is set equal to 0.9. Note that though the experimental weights lie within the 95% confidence interval of the statistical weights, the variation in the weights, specially for the

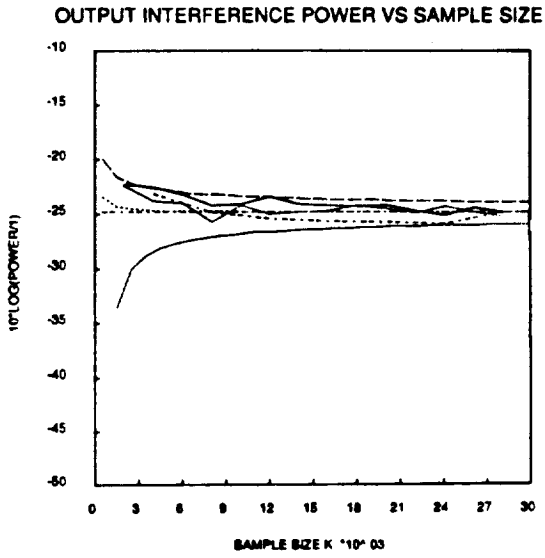

(a) $F = 0$

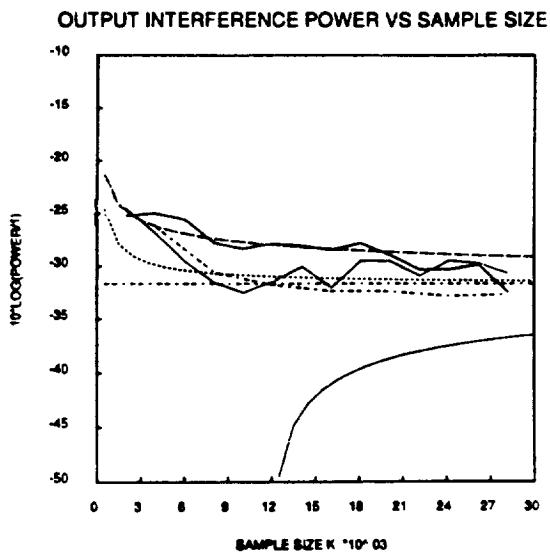

(b) $F = 0.7$

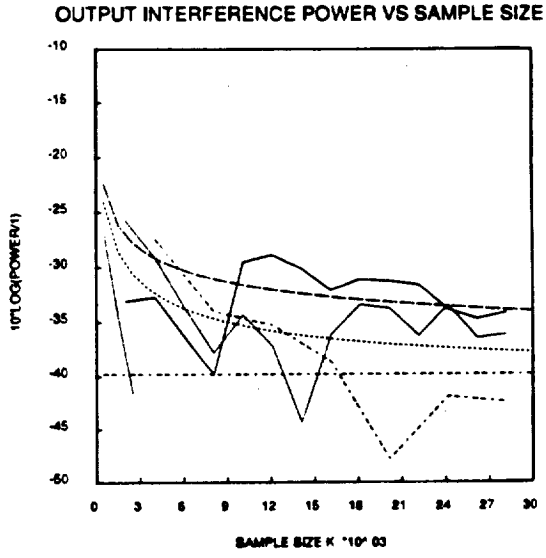

(c) $F = 0.9$

Figure 6.6: Output interference power versus number of snapshots K.

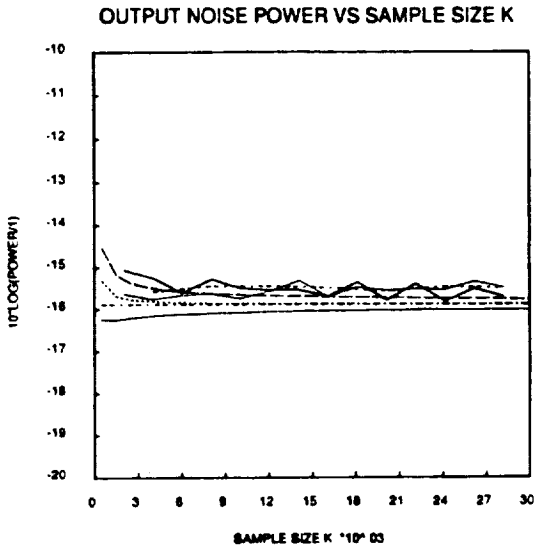

(a) $F = 0$

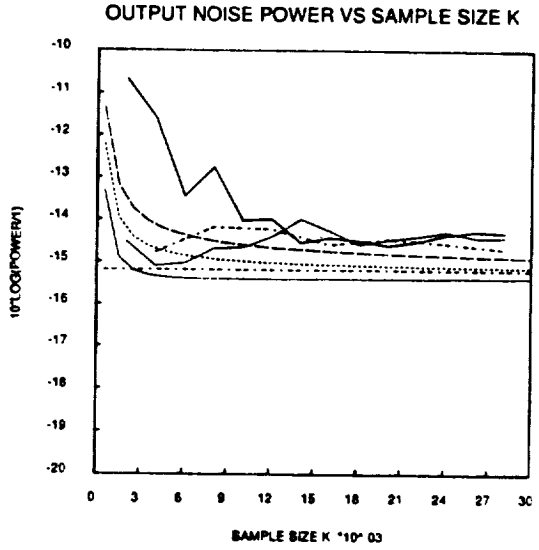

(b) $F = 0.7$

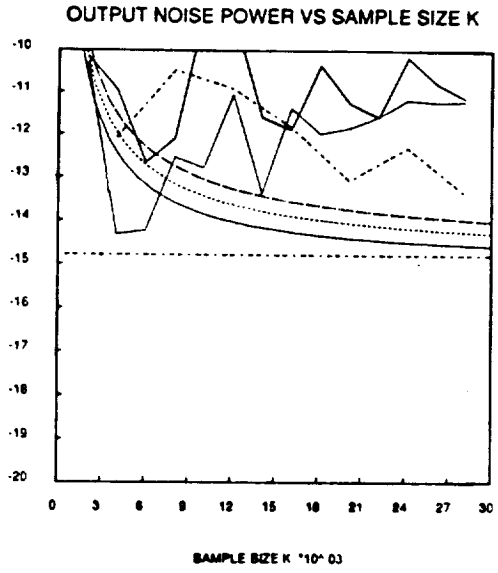

(c) $F = 0.9$

Figure 6.7: Output noise power versus number of snapshots K.

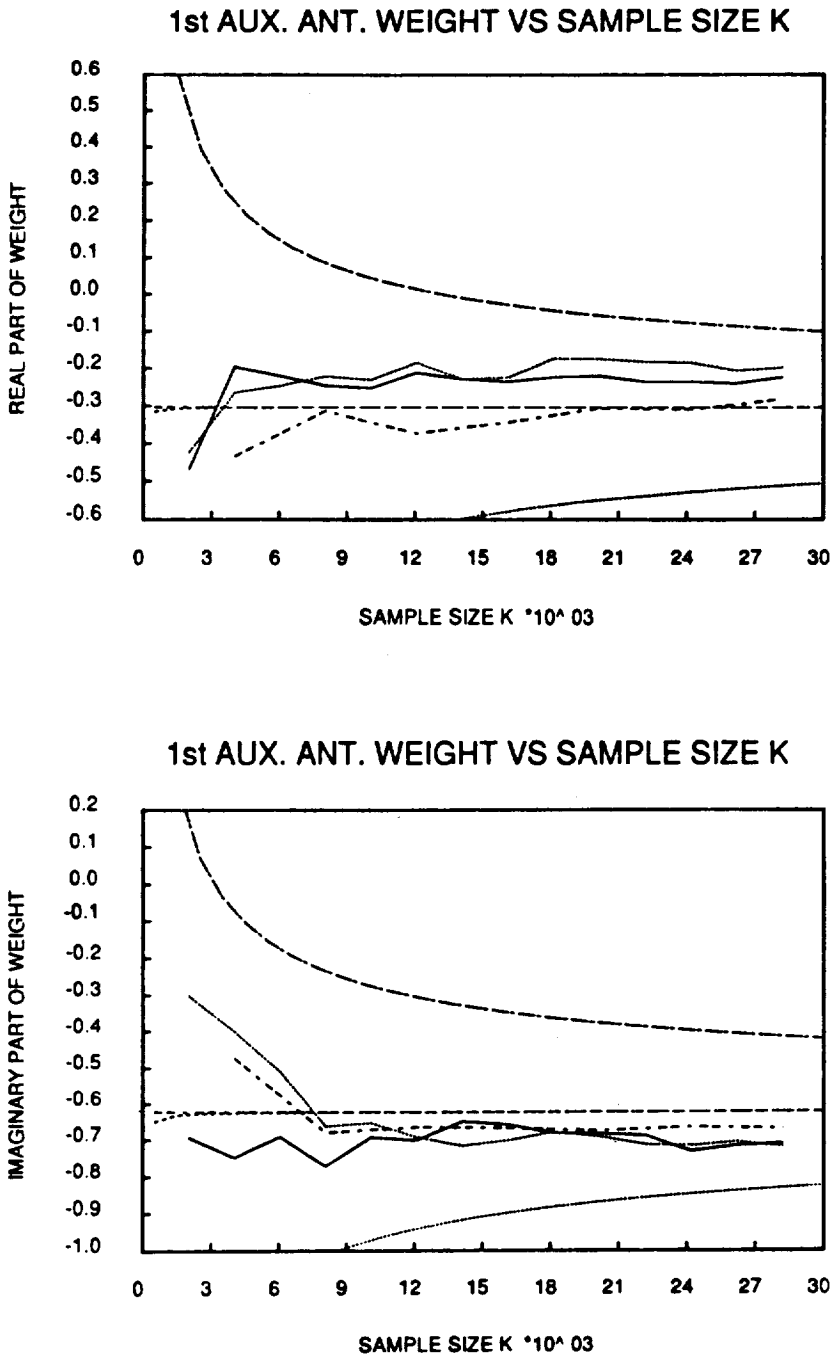

Figure 6.8: Real and imaginary parts of the auxiliary channel # 1 weight versus K. $F = 0.9$.

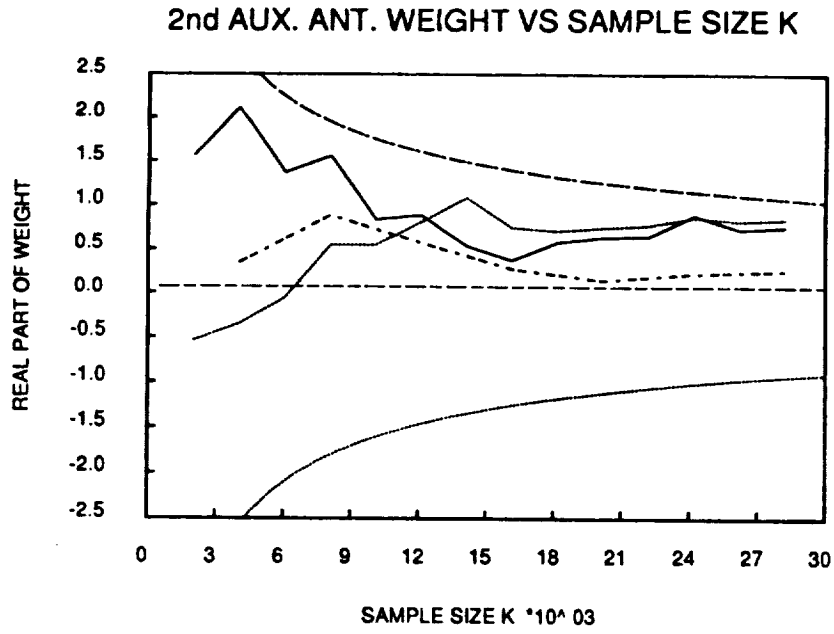

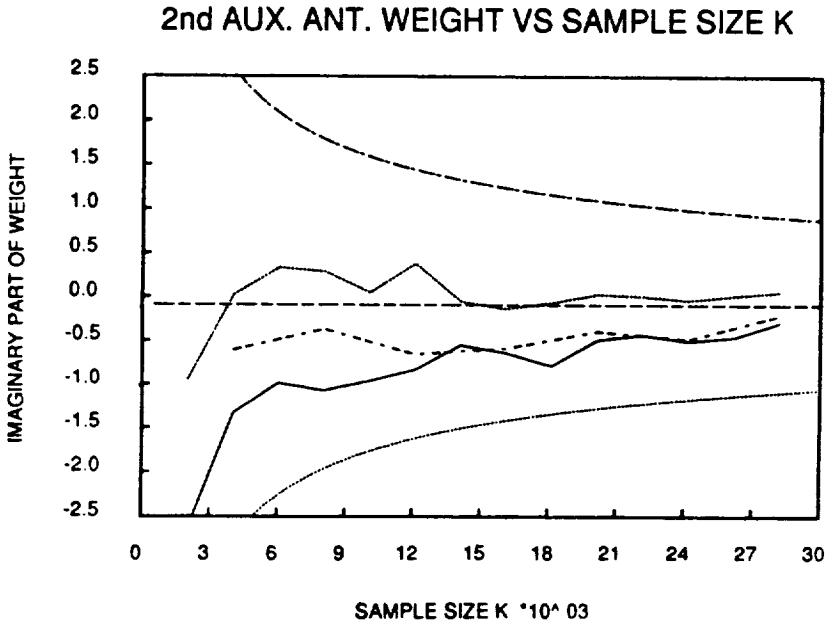

Figure 6.9: Real and imaginary parts of the auxiliary channel # 2 weight versus K. $F = 0.9$.

auxiliary channel #2 is very large. For such large weight variations, the statistical theory fails and thus the experimental results differ from the theoretical prediction [14].

One way to reduce the weight jitter, as mentioned in the last chapter, is to exclude the noise eigenvectors from weight calculations. In this case, the noise power at the array output will be close to its steady state value and the output SINR will not degrade. The same can be seen in the plots of Figure 6.10, where the output noise power of the system is plotted. F is set equal to 0.9 in these plots and the weights are computed using only signal eigenvectors. For the plots in this figure, SNR in the main channel is 17.277 dB and the INR in the main channel is -1.7467 dB. The INR in the auxiliary channel #1 and auxiliary channel # 2 is, respectively, 0.7685 dB and -19 dB. Again the desired signal in the auxiliary channel is negligible and the noise power level in all the channel is approximately equal. Note that the output noise power does not vary much with the number of samples used in the estimate of the covariance matrix. Thus, the output SINR of the experimental should be within the theoretical bounds.

Figure 6.11 shows the output SINR and the output INR of the experimental system. All the parameters are the same as in Figure 6.10. Note that the experimental output SINR shows a good agreement with the theoretical predicted values. The output SINR is approximately equal to the SNR in the main channel. Thus, the interference is suppressed without adversely affecting the SNR. The experimental output INR lies within the theoretical predicted values. The small discrepancy between the experimental values and the theoretical predicted values is due to the reason that

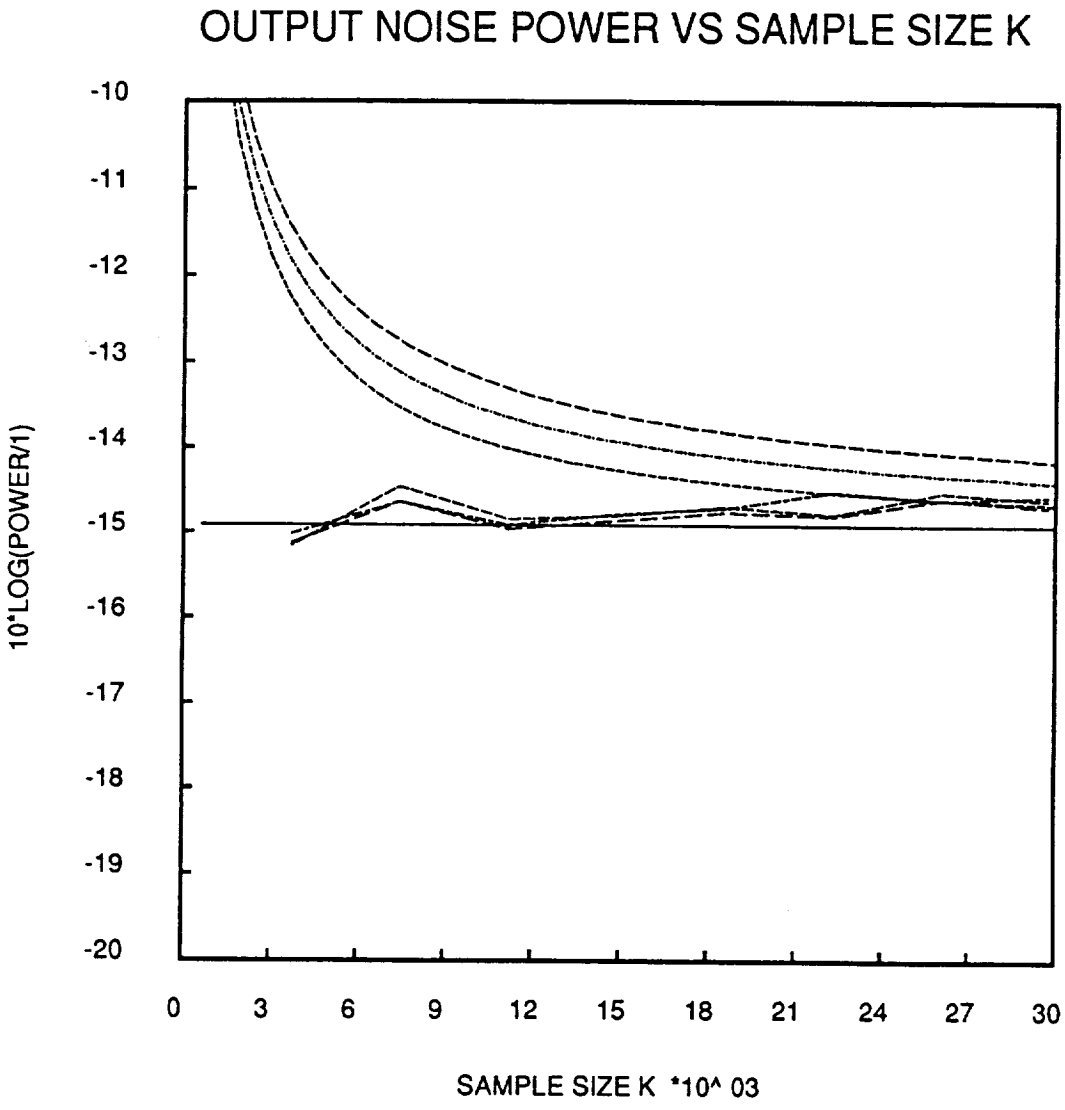

Figure 6.10: Output noise power versus the number of snapshots. $F = 0.9$ and only two eigenvectors are used in the weight computation.

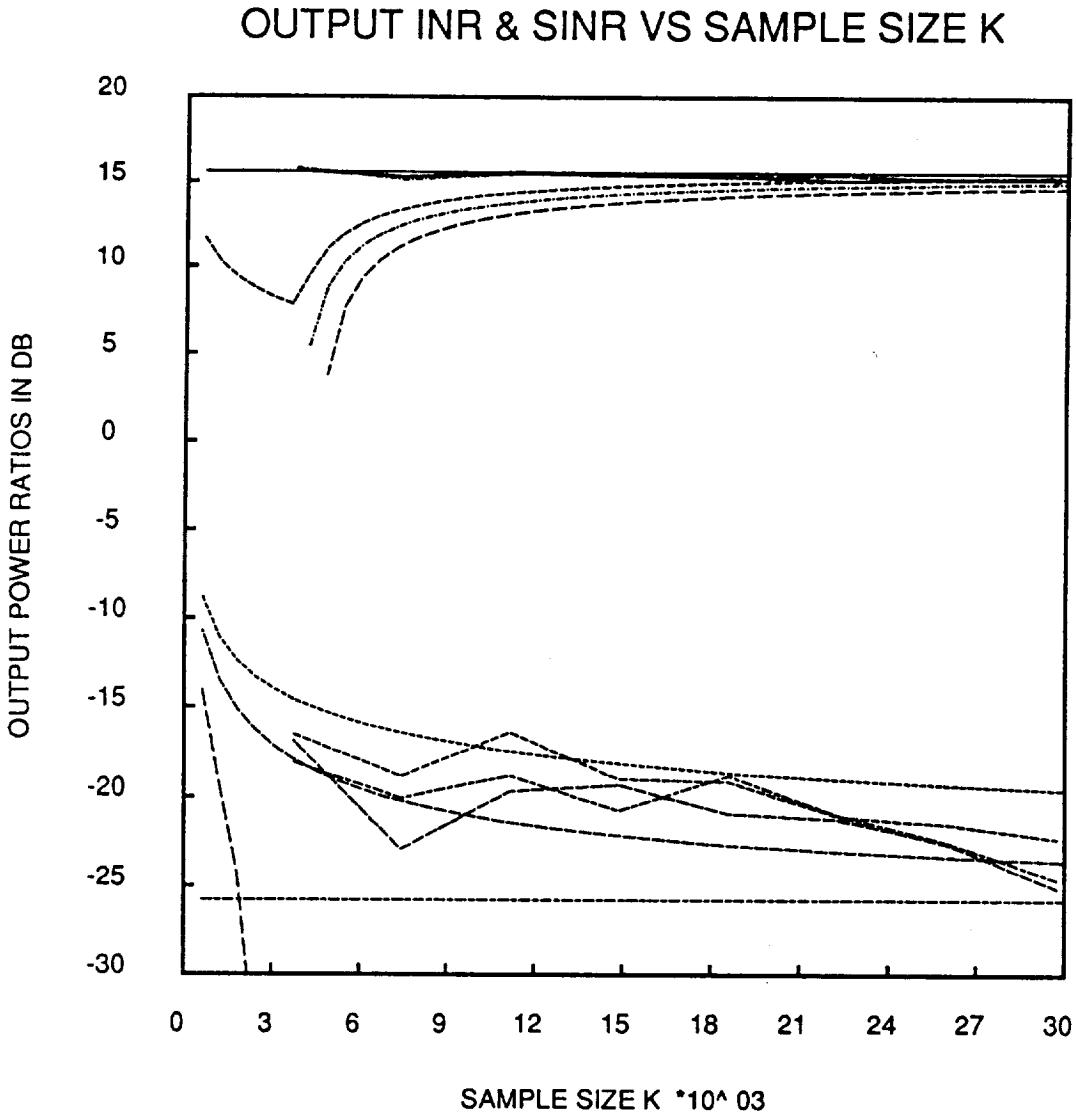

Figure 6.11: Out INR and SINR versus K. $F = 0.9$ and only two eigenvectors are used in the weight computation.

the theoretical values are obtained using the model in which all eigenvectors are used to compute the array weights. Note that if one uses 30,000 samples to estimate the covariance matrix, the output INR will be approximately -22 dB; while the output SINR will be approximately 16 dB. Thus, the interference is approximately 38 dB below the desired signal leel.

Figure 6.12 shows the performance of the experimental system versus the fraction F when the number of samples used in the estimation of the covariance matrix is fixed at 30,000. All the parameters are the same as in Figures 6.10 and 6.11. Note that the experimental results show a good agreement with the theoretically predicted values. The output INR decreases with an increase in the fraction, F; while the output SINR shows a very small degradation with an increase in the value of F. Thus, the modified SMI algorithm can be used to increase the suppression of weak interfering signals.

Figure 6.13 shows the performance of the system when the level of the interference signal in the auxiliary channel #2 is increased (aux-1 correlator signal is used as input to the auxiliary channel # 2). The SNR in the main channel is 17.160 dB. The INR in the main channel is -1.8333 dB. The INR in the auxiliary channel # 1 and auxiliary channel # 2 is, respectively, 0.888 dB and 0.705 dB. Again the desired signal in the auxiliary channel is negligible and the noise power in all the channel is approximately equal. The system performance is plotted versus F when the number of samples used to estimate the covariance matrix is fixed at 30,000. For the experimental results, only the signal eigenvectors are used to calculate the array weights. Note that the experimental results show good agreement with the

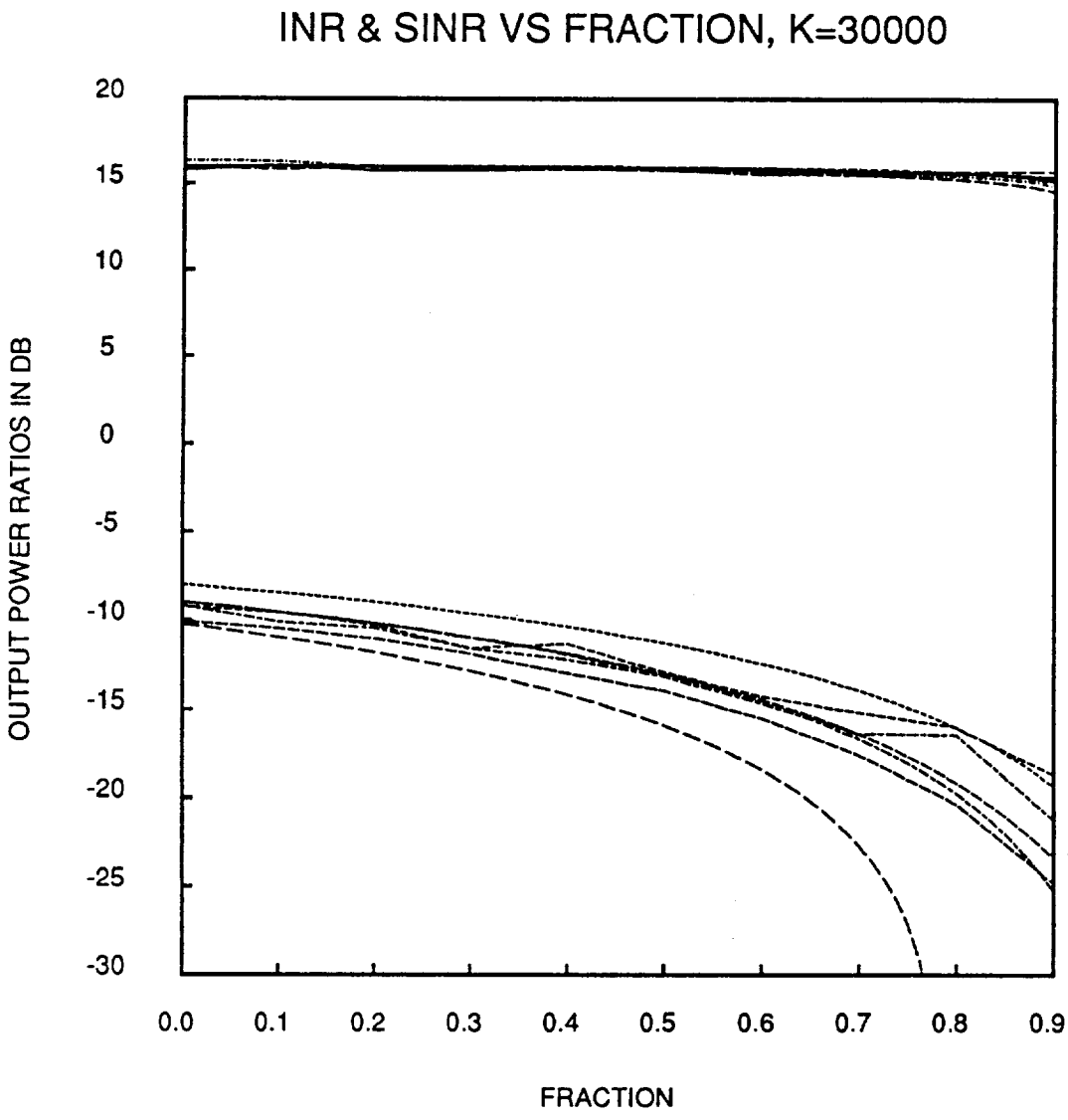

Figure 6.12: Output INR and SINR versus fraction F. K = 30,000 and only two eigenvectors are used in the weight computation.

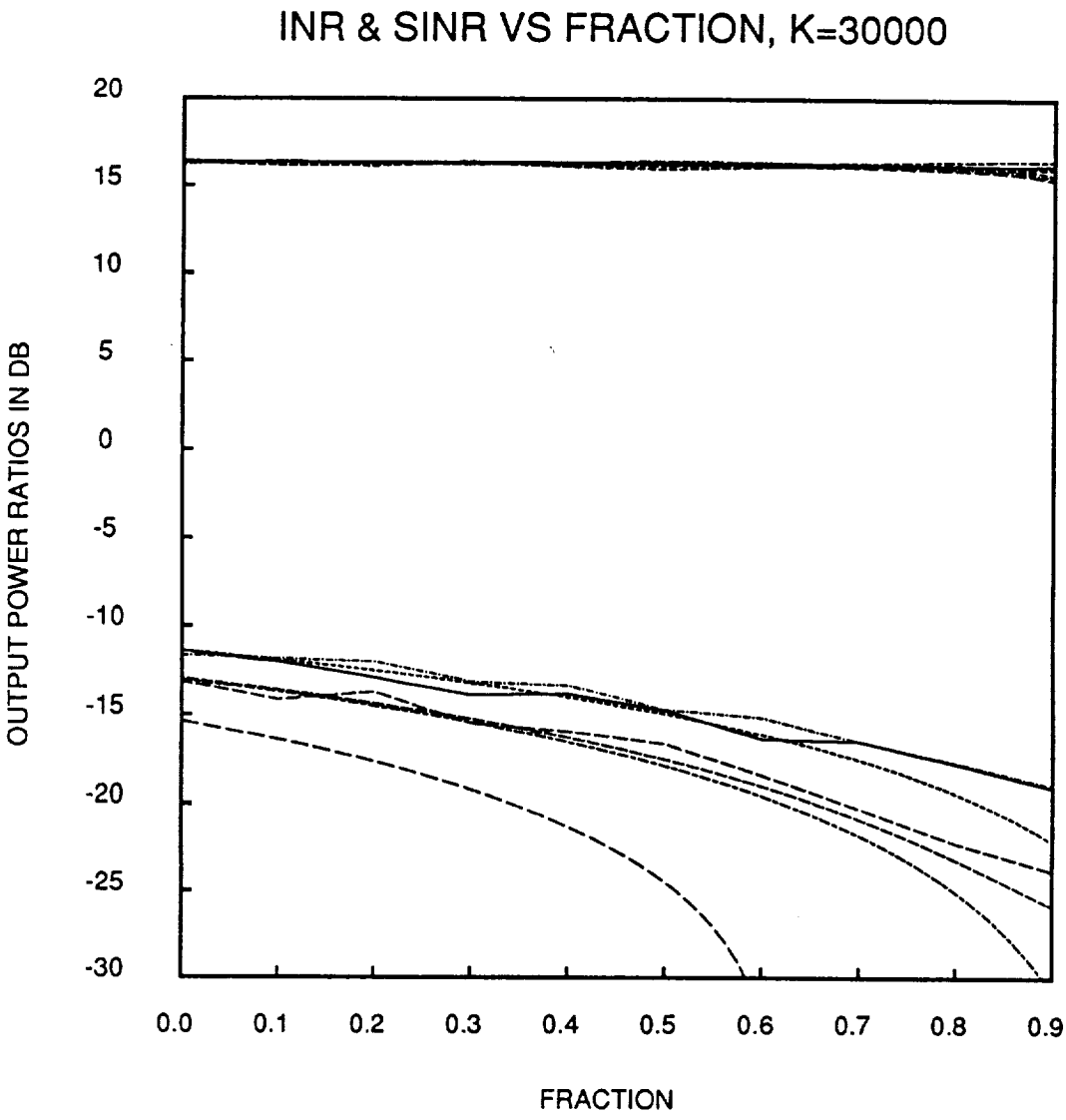

Figure 6.13: Output INR and SINR versus fraction F. The interfering signal level in the two auxiliary channels is approximately equal. K=30,000.

theoretically predicted values. The output INR decreases with an increase in the value of the fraction F; while the output SINR shows only a small degradation with an increase in F. Thus, the modified SMI algorithm can be used to increase the suppression of weak interfering signals.

In the above examples, the desired signal level in the auxiliary channels was negligible. This was done intentionally to avoid the computation of the steering vector. In this case, the steering vector is simply $[0, 0, 1]^T$. In practical systems, the desired signal in the auxiliary channels may not be negligible. In such situations, one needs to use a proper steering vector to avoid the cancellation of the desired signal. In the next experiment, the desired signal level in the auxiliary channels is increased. Now, the steering vector is obtained insitu using the procedure outlined in [15]. Figure 6.14 shows the performance of the experimental system when the desired signal level in the auxiliary channels is increased. The output SINR and the output INR of the system are plotted as a function of the fraction F. The SNR in the main channel is 17.415 dB; while the INR in the main channel is -1.62 dB. The SNR in the two auxiliary channel is -0.91 dB. The INR in the auxiliary channel #1 and the auxiliary channel #2 is, respectively, 0.807 dB and 0.905 dB. Again, the noise power in all channel is approximately equal. The number of samples used to estimate the covariance matrix is equal to 30,000. For the experimental results, only the signal eigenvectors are used to calculate the array weights. The statistical performance obtained using the theory discussed in [13,14] is also shown in the figure. Note that the experimental performance is within the theoretical bounds. The output INR of the system decreases with an increase in the value of fraction F.

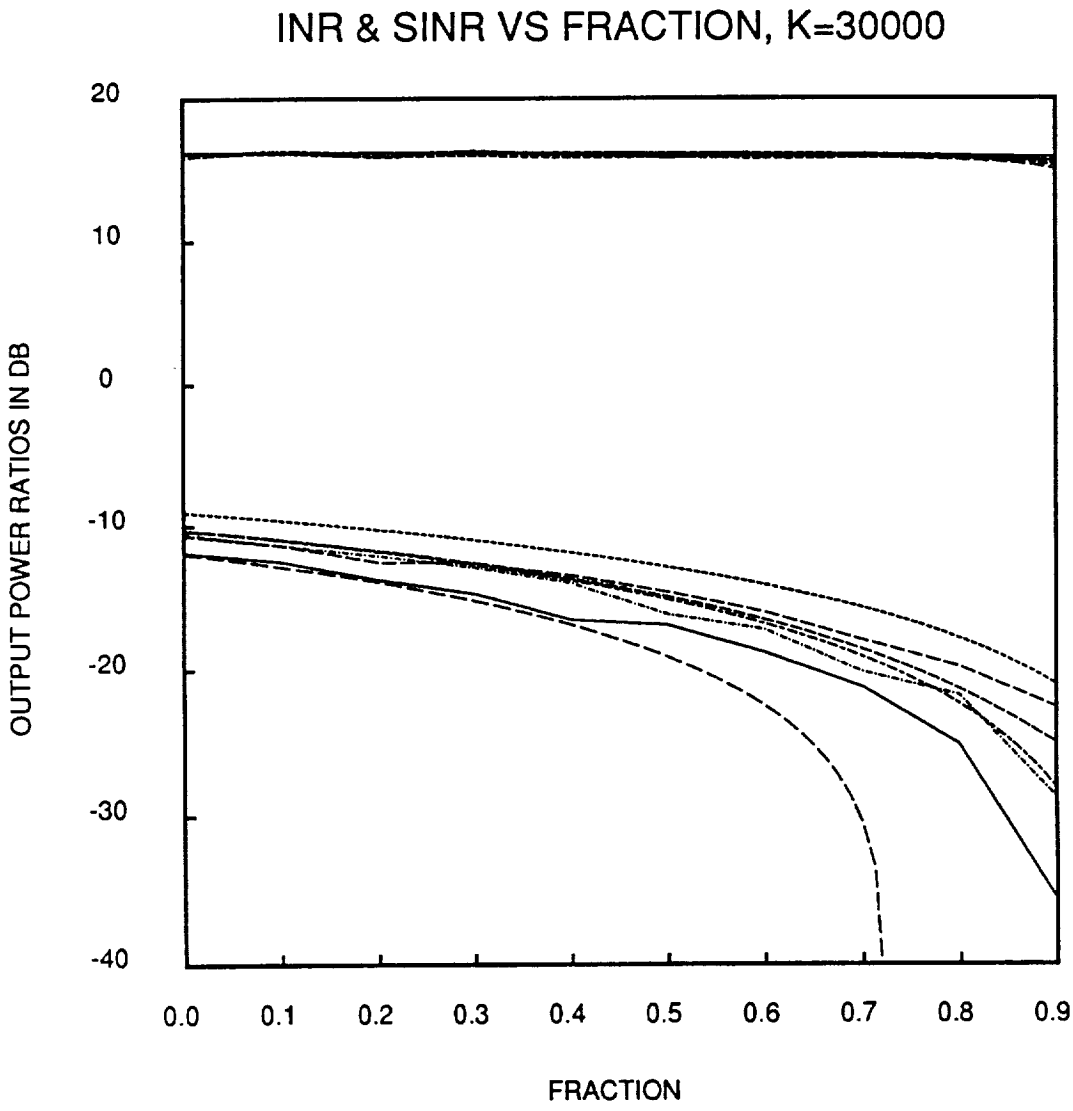

Figure 6.14: Output INR and SINR versus fraction F. The desired signal is present in the auxiliary channels. K = 30,000.

The degradation in the output SINR with an increase in F is very small. Thus, one can use the modified SMI algorithm to increase the interference suppression.

As pointed out before, in this experiment, a steering vector was used to avoid the cancellation of the desired signal.. During the experiment, it was observed that if a proper steering was not used, the weights were adjusted to cancel the desired signal. Thus, for the optimum performance, one should use a proper steering vector. The performance of the modified SMI algorithm with TVRO satellite signals is discussed next.

6.4 Performance with TVRO Satellite Signals

To test the performance of the modified SMI algorithm with TVRO satellite signals, the ground station described in Chapter 4 was used to receive TVRO satellite signals. Instead of using all seven feeds, only four feeds were used for these experiments. The four feeds were the prime feed and the three feed in the cluster #1. The signals received by the prime feed and the offset feed #1 were summed to form the main channel signal. The signal received by the other two feeds in the cluster #1 were used as the auxiliary channel signals. The prime feed was used to receive signal from the desired satellite; while the feeds in cluster #1 were used to receive signals from an interfering satellite. The signal received by offset feed #1 was attenuated before summing with the prime feed signal. A variable attenuator was used to control the amount of interference in the main channel. As pointed out

before, the prime feed and the Offset feed #1 also have a switch to turn off the DC power to their respective LNAs (low noise amplifiers). Thus, one can separate the desired and interference signal in the main channel. Due to the time constraints and some problems encountered with the equipment (the elevation control of the 30 foot parabolic dish was lost) only one series of experiments was performed. In this series of experiments, the main channel signal consists of only the interfering signal. Thus, the power to the prime feed LNA was turned off. In this case, the SMI algorithm updates the array weights such that the interference signal is suppressed.

In the case of TVRO satellite signals, one does not have much control on the noise in various channels. Since, it is not possible to measure the level of a weak signal in the presence of equal or larger amount of noise, the performance of the SMI algorithm, as for the modified feedback loops, is measured in terms of the quality of the TV picture before and after adaption.

Table 6.1 shows the results of a typical experiment. In the table, the auxiliary channel weights and picture quality after adaptive weights are applied is given for various values of the fraction F. The signal scenario consists of an interfering signal. To test the performance of the SMI algorithm in the presence of weak interfering signals, some noise was injected in all channel from the noise sources in the array simulator. The amount of noise injected in the various channels was adjusted so that the noise level in the various channels was approximately equal. The attenuator in the Offset feed #1 path was set at 15 dB. Thus, the amount of noise injected in the main channel was more than the auxiliary channels. After the adaptive

Table 6.1: Auxiliary channel weights and the output TV picture quality versus fraction F. No desired signal.

Fraction (F)	Auxiliary channel #1 weight	Auxiliary channel #2 weight	Quality of TV picture
0.	-0.178 + j 0.210	0.148 - j 0.0897	No color
0.1	-0.189 + j 0.223	0.156 - j 0.0947	No color
0.2	-0.202 + j 0.238	0.166 - j 0.100	faint B&W
0.3	-0.216 + j 0.254	0.177 - j 0.107	faint B&W
0.4	-0.232 + j 0.273	0.189 - j 114	No Synchro.
0.5	-0.250 + j 0.295	0.203 - j 0.123	Noise
0.6	-0.272 + j 0.321	0.220 - j 0.133	Noise
0.7	-0.297 + j 0.351	0.240 - j 0.145	Noise
0.8	-0.328 + j 0.388	0.264 - j 0.159	Noise
0.9	-0.367 + j 0.433	0.293 - j 0.176	Noise

weights were applied, the injected noise in the main channel was removed to judge the TV picture. With the injected noise, the INR in the main channel is approximately -6.94 dB; while the INR in the auxiliary channel #1 and the auxiliary channel #2 is, respectively, -3.5 dB and -9.6 dB. In the experiment, the number of samples used to estimate the covariance matrix is 30,000 and two eigenvectors are used to compute the array weights. Note that, as expected, the magnitude of the auxiliary channel weights increases with an increase in the value of the fraction F and the quality of the output TV picture deteriorates with an increase in F. Thus, the modified SMI algorithm can be used to increase the interference suppression.

In the above experiment, two eignevectors were used to compute the adaptive array weights while only one interfering signal was incident on the array. The adaptive array weights obtained using a single eigenvector

as well as all three eigenvectors were also tried. In the case of the single eigenvector it was found that the adaptive array weights did not vary with the fraction F. Thus, the modified SMI algorithm did not increase the interference suppression. When all the eigenvectors were used to calculate the adaptive array weights, the auxiliary channel weights became too large with an increase in the value of fraction F. As pointed out before, this is because of the large weight jitter. Thus, the number of eigenvectors that should be used in the weight computation is an important parameters and needs to be further studied. This is especially true for wideband signals where the signal eigenvectors are not well defined. A summary of this work and some general conclusions are given in the next chapter.

Chapter 7

Summary and General Conclusions

Under this project, the feasibility of using adaptive antenna arrays to reduce interference in satellite communication systems was studied. The particular signal scenario of interest involved weak interfering signals where interfering signals are well below (15 to 25 dB) the desired signal. The SNR in these communication systems is of the order of 15 – 20 dB. Thus, the interfering signal level can be below the thermal noise in the communication systems. The conventional adaptive antennas can not provide the required suppression of these interfering (weak interference) signals. To achieve the required interference suppression, some modifications to the feedback loops used to update the adaptive array weights were suggested. In situations, where the SMI algorithm is used to update the array weights, a modified SMI algorithm was developed to obtain the required interference suppression.

In theory, modified feedback loops as well as the modified SMI algorithm are suitable for the satellite communication systems under consideration. In practice, the modified SMI algorithm, however, can have some problems.

First, since it is an open loop system, one has to calibrate the system very carefully. Any error in the calibration can lead to significant degradation in the performance. Second, to control the large jitter in the array weights, one should exclude the noise eigenvectors from the weight calculations. Defining the noise eigenvectors, especially in wideband signal scenario, is non-trivial. Thus, the modified feedback loop system is the better choice for weight update.

Two types of modified feedback loops were suggested. One of the modified feedback loop decorrelates the internal noise; while the other modified feedback loop decorrelators internal as well as external noise. The first feedback loop uses two amplifiers to decorrelate the internal noise. The second feedback loop uses two spatially separated antennas followed by their individual amplifiers to decorrelate internal as well as external noise. These antennas should be located such that the phase of each directional signal received by one of the two antennas is the same as the phase of the corresponding signal received by the other antenna. Thus, the second modified feedback loop not only uses more antenna elements, the distribution of antenna elements should be done very carefully.

In the experimental system built under this project, feedback loops with two separate antennas were used. During the evaluation of the experimental system, it was observed that the internal noise is the dominent component of the noise in varius channels. Thus, one could have used feedback loops with a single antenna and two amplifiers (see Figure 2.2). In the experimental system, to satisfy the phase requirement, the two feeds used with an auxiliary channel were moved out of the geosynchronous plane. Thus,

the mainbeams corresponding to the two feeds were pointed away from the geosynchronous satellites, resulting in the reduced auxiliary antenna gain in the interfering satellite direction. With one feed for each feedback loop, the feed can be moved back in the geosynchronous plane; which in turn, will lead to more gain in the interfering signal direction. This increase in the gain will make up for any increase in the noise correlation (due to external noise) in the feedback loops. Therefore, for future systems, single antenna – two amplifier feedback loops are recommended.

The experimental system is a sidelobe canceller with two auxiliary channels. To avoid the cancellation of the desired signal, it uses a steering vector. The steering vector depends on the level of the desired signal incident on the system. The desired signal level in the satellite communication systems under consideration varies not only from one satellite to the other satellite and from one channel to the other channel but also with the video in the channel. Thus, one has to constantly update the steering vector, which may not be possible in real systems. Therefore, for future systems, a fully adaptive array with two amplifier feedback loops is suggested. A fully adaptive array also needs a steering vector to avoid the cancellation of the desired signal. The steering vector, however, is independent of the desired signal level at the receive site.

Finally, a word about the number of auxiliary channels. In the experimental system., two auxiliary channels are used to null two interfering signals. It is assumed that the two interfering satellites are on the two opposite sides of the desired satellite. Thus, the experimental system is not only fully constrained, but is also unable to suppress more than one inter-

fering signals originating from the satellites on the same side of the desired signal satellite. To avoid this situation, for future systems, a fully adaptive array with four auxiliary channels is recommended. In these systems, the five feeds (one for the main channel and one each for the four auxiliary channels) should be distributed such that up to two interfering signals originating from the same side of the desired signal can be nulled. The extra auxiliary channels will also provide some protection from additional interfering signals [16].

Bibliography

[1] I.J. Gupta, and A.A. Ksienski, "Adaptive Arrays for Satllite Communications," Technical Report 716111-1, The Ohio State Unviersity ElectroScience Laboratory, prepared under grant NAG3-536 for NASA, Lewis Research Center, Cleveland, Ohio, June 1984.

[2] I.J. Gupta and A.A. Ksienski, "Adaptive Arrays for Weak Interfering Signals," IEEE Transactions on Antennas and Propagation, Vol. AP-34, No. 3, pp. 420-426, March 1986.

[3] I.J. Gupta,"Adaptive Antenna Arrays for Weak Interfering Signals," Technical Report 716111-2, The Ohio State University ElectroScience Laboratory, prepared under grant NAG3-536 for NASA, Lewis Research Center, Cleveland, OH, January 1985.

[4] I.J. Gupta, W.G. Swarner and E.K. Walton, "Adaptive Antenna Arrays for Satellite Communications – Design and Testing," Technical Report 716111-3, The Ohio State University ElectroScience Laboratory prepared under grant NAG3-536 for NASA, Lewis Research Center, Cleveland, OH, September 1985.

[5] I.J. Gupta, "Subarray Utilization in Adaptive Suppression of Weak Interfering Signals," Technical Report 716111-4, The Ohio State University ElectroScience Laboratory, prepared under grand NAG3-536 for NASA, Lewis Research Center, Cleveland, OH, April 1986.

[6] J. Ward, " Adaptive Arrays for Weak Interfering Signals – An Experimental System," M.Sc. Thesis, The Ohio State University, Dept. of Electrical Engineering, Columbus, OH, 1987.

[7] J. Ward et al., " An experimental System to Suppress Weak Interfering Signals," IEEE Transactions on Antennas and Propagtion, Vol. AP-36, No. 11, pp. 1551-1559, November 1988.

[8] K. Steadman, "Adaptive Array for Weak Interfering Signals – Geostationary Satellite Experiment," M.Sc. Thesis, The Ohio State University, Dept. of Electrical Engineering, Columbus, OH, 1989.

[9] R.A. Mozingo and T.W. Miller, Introduction to Adaptive Arrays, John Wiley and Sons, New York, 1980.

[10] I.S. Reed, J.D. Mallet and L.E. Brennan, "Rapid Convergence Rate in Adaptive Arrays," IEEE Transaction on Aerospace and Electronic Systems, Vol. AES-10, No. 6, pp. 853-863, November 1974.

[11] I.J. Gupta, "SMI Adaptive Antenna Arrays for Weak Interfering Signals," IEEE Transactions on Antennas and Propagation, Vol. AP-34, No. 10, pp. 1237-1242, October 1986.

[12] I.J. Gupta, "SMI Adaptive Antenna Arrays for Weak Interfering Signals," Technical Report 716111-5, The Ohio State University ElectroScience Laboratory, prepared under grant NAG3-536 for NASA, Lewis Research Center, Cleveland, OH, September 1987.

[13] R.L. Dilsavor and R.L. Moses, "Analysis of Modified SMI Method for Adaptive Array Weight Control," Technical Report 716111-6, The Ohio State UniversityElectroScience Labortory, prepared under grant NAG3-536 for NASA, Lewis Research Center, Cleveland, OH, February 1989.

[14] R.L. Dilsavor, "Analysis of Modified SMI Method for Adaptive Array Weight Control," M. Sc. Thesis, The Ohio State University, Dept. of Electrical Engineering, Columbus, OH, 1989

[15] R.L. Dilsavor and I.J. Gupta, "An Experimental SMI Adaptive Antenna Array for Weak Intefering Signals," Technical Report 716111-7, The Ohio State University ElectroScience Laboratory, prepared under grant NAG3-536 for NASA, Lewis Research Center, Cleveland, OH, September 1989.

[16] R.L. Moses, "Effects of Additional Interfering Signals on Adaptive Array Performance," Technical Report 716111-8, The Ohio State University ElectroScience Laboratory, prepared under grant NAG3-536 for NASA, Lewis Research Center, Cleveland, OH, September 1989.

[17] R.T. Compton, Jr., Adaptive Antennas – Concept and Performance, Prentice-Hall, Englewood Cliffs, NJ, 1988.

[18] I.J. Gupta and E.K. Walton, "Qualitative Performance of the OSU Adaptive Antenna System," Technical Memo #1, Project #716111, The Ohio State University ElectroScience Laboratory, prepared under grant NAG3-536 for NASA, Lewis Research Center, Cleveland, OH, December 1987.

[19] J.W. Eberle, "High Gain Antenna Array Facilities at The Ohio State University," Technical Report 1072-3, The Ohio State University ElectroScience Laboratory, September 1961.

[20] Y.C. Chang and R.C. Rudduck, "Numerical Electromagnetic Code - Reflector Antenna Code, Part II: User's Manual (Version II)," Technical Report 712242-17 (713742), The Ohio State University ElectroScience Laboratory, December 1982.

[21] W.F. Gaberial, "Using Spectral Estimation Techniques in Adaptive Processing Antenna Systems," IEEE Transactions on Antennas and Propagtion, Vol. AP-34, No. 3, pp. 291-300, March 1986.